A HIGH-RESOLUTION MARINE $^{187}OS/^{188}OS$ RECORD FOR THE LATE MAASTRICHTIAN

A THESIS SUBMITTED TO THE GRADUATE DIVISION OF THE
UNIVERSITY OF HAWAI‘I AT MĀNOA
IN PARTIAL FULFILLMENT OF THE REQUIREMENTS FOR THE
DEGREE OF

MASTER OF SCIENCE

IN
GEOLOGY AND GEOPHYSICS
AUGUST 2016

By
Nicole Robinson

Thesis Committee:
Greg Ravizza, Chairperson
Craig Glenn
Steven Stanley

Keywords:
Osmium isotopes, Maastrichtian, K-Pg, Deccan, Large igneous provinces

Acknowledgements

I would like to thank my advisor Greg Ravizza for the guidance and encouragement he provided during the (prolonged) duration of this project. He was always willing to expand our conversations beyond the immediate topic, and his enthusiasm and breadth of knowledge was always appreciated. I would like to thank both Craig Glenn and Steve Stanley for their additions and comments throughout this process. Their experience and suggestions strengthened the final product. Thank you also to Christian Miller for his invaluable comments on the initial draft of this thesis, and his willingness to step in to help at the eleventh hour. Thank you to Denys VonderHaar for all the assistance in the lab.

Thank you to my family, who were supportive throughout this entire process, and especially to my daughter Petra, who is as yet too young to appreciate that she provided the critical motivation to finish what I started.

And finally, thank you to my grandfather Haagen Larsen, who let me constantly rearrange and play with the rocks lining his garden when I was a little girl, and to my grandmother Gerda Larsen, who returned each to its proper place at the end of the long, Danish summer day.

Abstract

The marine osmium (Os) isotope record can potentially act as an independent proxy indicator of major volcanic activity, marked by decreases in seawater $^{187}Os/^{188}Os$ to more mantle-like values. A composite late Maastrichtian (66 to 68.5 Ma) marine Os record, based on bulk sediment samples from the Southern Ocean (Ocean Drilling Program (ODP) Site 690), the Tropical Pacific Ocean (Deep Sea Drilling Project (DSDP) Site 577), the South Atlantic (DSDP Site 525) and the paleo-Tethys Ocean, provides robust evidence of a 20% decline in seawater $^{187}Os/^{188}Os$ over a period of about 200 ka early in magnetochron C29r, ending approximately 200 ka before the Cretaceous-Paleogene (K-Pg) boundary (Robinson et al., 2009). This shift in $^{187}Os/^{188}Os$ is interpreted as a chemostratigraphic marker of Deccan volcanism, and is temporally separate from the Os isotope excursion associated with the Chicxulub impact at the K-Pg boundary. Improved geochronologic data constraining the eruptive history of the Deccan (Renne et al., 2015; Schoene et al., 2015), as well as Os isotope records coinciding with other episodes of large igneous province (LIP) eruption (Duvivier et al., 2015; Bottini et al., 2012; Kuroda et al., 2010), provide a new and larger context for understanding the response of the marine Os record to LIP emplacement. Comparison of Os isotope records coinciding with other LIP events to the Deccan/K-Pg record reveal important differences in the structure and duration of shifts in the Os isotope record, and precludes a single interpretation of all LIP-associated Os isotope excursions.

Contents

List of Tables

List of Figures

List of Abbreviations

CAMP = Central Atlantic Magmatic Province

CCD = carbonate compensation depth

DSDP = Deep Sea Drilling Project

KBP = Cretaceous – Paleogene Boundary

K-Pg = Cretaceous – Paleogene Boundary

LIP = large igneous provinces

MAR = mass accumulation rate

mbsf = meters below seafloor

MORB = mid ocean ridge basalts

NAIP = North Atlantic Igneous Province

OAE1a = Oceanic Anoxic Event 1a

OAE2 = Oceanic Anoxic Event 2

ODP = Ocean Drilling Program

OJN = Ontong Java Nui Plateau

ppb = parts per billion

ppt = parts per trillion

P-E = Paleocene – Eocene

PETM = Paleocene – Eocene Thermal Maximum

PGE = platinum group element

T-J = Triassic – Jurassic

Note: This work uses a, ka, Ma, and Ga (year, thousand years, million years, and billion years respectively), to express both absolute ages and duration of time.

Preface

Chapter 1 presents an overview of the Rhenium-Osmium (Re-Os) isotope system, and is intended to introduce the reader to the characteristics of the Re-Os system that make it an important tool in the study of impact events and emplacement of large igneous provinces.

Chapter 2 (originally published as Robinson et al., 2009) presents a high-resolution $^{187}Os/^{188}Os$ record for the late Maastrichtian. It interprets the record in the context of the K-Pg impact event and main phase Deccan volcanism, showing that these events are temporally separate in the marine Os isotope record, and characterized by distinct geochemical fingerprints.

Chapter 3 presents the results from Robinson et al. (2009) with a revised age model and refined Deccan eruptive history, to allow the data to more readily be used in conjunction with recent and future Os isotope records from the time period. Chapter 3 also summarizes the Os isotope record from four (4) other LIP emplacement events (the Central Atlantic Magmatic Province, the North Atlantic Igneous Province, the Caribbean/Madagascar LIP eruptions, and Ontong Java Nui), and compares these records to that from the K-Pg and Deccan presented in Chapter 2 in order demonstrate that the marine Os isotope record does not have a consistent response to LIP emplacement.

Chapter One:
Introduction to the Use of the Re-Os Isotopic System as a Paleoceanographic Tracer

1.1 Re-Os Isotopic System

Study of rhenium-osmium (Re-Os) isotopic systematics have matured over the past 30+ years and are now used extensively in cosmochemistry, high-temperature geochemistry, and paleoceanographic research. The Re-Os isotope system has distinct characteristics that make it well suited to study continental weathering, the emplacement of large igneous provinces (LIPs), and large impacts of undifferentiated meteorites and iron meteorites. This thesis will interpret the temporal variation of the Os isotopic ratio of seawater as a record these events.

The Os isotopic variation central to this study is change in abundance of ^{187}Os. Rhenium has two naturally occurring isotopes, ^{185}Re and ^{187}Re, and it is ultimately the decay of ^{187}Re to ^{187}Os that creates natural variations in the abundance of ^{187}Os. Osmium is one of six platinum group elements (PGEs), which include ruthenium, rhodium, palladium, iridium, and platinum. Osmium has seven naturally occurring isotopes: ^{184}Os, ^{186}Os, ^{187}Os, ^{188}Os, ^{189}Os, ^{190}Os, and ^{192}Os. Osmium is one of the least abundant elements in the Earth's crust and, as such, Os concentrations in most crustal rocks are extremely low (parts per billion (ppb) and parts per trillion (ppt) concentrations, Table 1.1). Yet modern analytical techniques allow for sensitive enough measurements of Os concentrations to the extent that the abundance of ^{187}Os can be used for geochronology and as a tracer for a variety of geochemical processes. The relative abundances of each Os isotope in nature varies because both ^{186}Os and ^{187}Os are products of radioactive decay; ^{187}Os is produced from ^{187}Re by beta decay (β^-) with a half life 4.1×10^{10} a (Smoliar et al., 1996, Selby et al., 2007); ^{186}Os is produced from ^{190}Pt by alpha (α) emission with a half life of 4.69×10^{10} a (Begemann et al., 2001). ^{186}Os itself decays to ^{182}W by alpha (α) emission with a half life of 3.5×10^{16} a (Shirey & Walker, 1998), a half life so long that ^{186}Os is considered stable for geologic purposes. Early work in the Re-Os isotope system reported the abundance of ^{187}Os as $^{187}Os/^{186}Os$ ratios (e.g. Luck & Turekian, 1983); it is now standard practice to utilize $^{187}Os/^{188}Os$ ratios instead because ^{188}Os is unaffected by long-lived radioactive decay schemes.

The $^{187}Os/^{188}Os$ ratio of geologic materials varies due to 1) in-situ decay of ^{187}Re to ^{187}Os, and 2) the mixing of isotopically distinct sources of Os at the time of rock formation. In the first case, the older a material gets, the higher its $^{187}Os/^{188}Os$ becomes because there has been more time for whatever ^{187}Re is present to decay to ^{187}Os. Measuring the ratio of parent to daughter isotopes allows the Re-Os isotope system to be used for dating purposes. It is the second mechanism that is most important for this study: Different geologic reservoirs are characterized by different concentrations of Os and Re and different $^{187}Os/^{188}Os$ ratios, and as the contribution of Os from each reservoir to the marine Os budget changes, so will the $^{187}Os/^{188}Os$ ratio of seawater. High temperature and low temperature fractionation determine the compositions of the major Re and Os reservoirs. Table 1.1 summarizes the Re and Os concentrations and $^{187}Os/^{188}Os$ of these major reservoirs. The processes leading to the characteristics of each reservoir are discussed below.

1.2 High temperature Re-Os geochemistry

Rhenium and Os are both highly siderophile elements. This distinguishes the Re-Os isotope system from other isotope systems where pairs tend to be lithophile (such as Rb-Sr, Sm-Nd, or U-Pb). Osmium and Re likely accreted to the early Earth in their chondritic abundances (Carlson, 2005). Due to their siderophile nature almost all of the Os and Re originally accreted to the Earth was partitioned into the core during planetary differentiation, such that 98% of all terrestrial Os and Re is calculated to be in the core vs. 2% in all other reservoirs (Palme and O'Neill, 2005). Chondrites and iron meteorites are therefore strongly enriched in Os and Re relative to the remaining terrestrial reservoirs. During partial melting of the mantle, Re is moderately incompatible and enters the melt, whereas Os is highly compatible and is retained in the mantle source mineralogy (Carlson, 2005). Therefore, partial melting and fractional crystallization act to increase the Re/Os ratio of crustal rocks relative to the mantle. In the absence of native metal phases both Os and Re partition into sulfide phases. Re has a sulfide-melt partition coefficient of 43 - 325 (Burnham et al., 1998) and Os has a sulfide-melt partition coefficient of 10^3 - 10^5 (Roy-Barman et al., 1998). Consequently, the transfer of Re and Os from the mantle into crystalline rocks is sensitive to both the degree of melting and whether or not residual sulfide remains in the mantle source. The difference in the partitioning coefficients of Re and Os strongly influences the Re/Os ratio of a material, and ultimately the $^{187}Os/^{188}Os$ ratio.

As a result of their differing compatibilities during mantle melting, Re is enriched in oceanic and continental crustal rocks and depleted in ultramafic rocks relative to Os. As ^{187}Re decays to ^{187}Os, the ^{187}Os/^{188}Os of crustal rocks increases compared to that of mantle rocks (see Figure 1.1). For this reason, continental crust is often referred to as a source of radiogenic Os (high ^{187}Os/^{188}Os values) whereas mantle and extraterrestrial sources are called sources of unradiogenic Os (low ^{187}Os/^{188}Os values). Osmium is depleted in average continental crust relative to the Earth's mantle, with an average Os concentration of ≈ 30 pg/g (Table 1.1). However two continental lithologies have very high Os concentrations, and these may exert a disproportionate influence on the surficial cycle of Os: Ophiolites and black shales (Peucker-Ehrenbrink & Blum, 1998). Black shales will be discussed in the next section. Ophiolites are uplifted and exposed portions of the Earth's oceanic crust and upper mantle. These generally have high Os concentrations and low ^{187}Os/^{188}Os ratios (Luck & Allegre, 1991) due to the higher compatibility of Os relative to Re in mantle source mineralogies, which concentrates Os in the mantle and depletes Re relative to Os. Over time there is very little change in the ^{187}Os/^{188}Os ratio because the ratio of Re to Os is low (Figure 1.1). No other specific lithologies are both sufficiently common and Os-rich to warrant additional discussion. Consequently, continental sources of Os generally are considered as derived from average continental crust. Qualitatively, older silicic rocks are representative of upper continental crust. Therefore, although Precambrian granitoids have high ^{187}Os/^{188}Os ratios (the more time ^{187}Re has to decay to ^{187}Os, the higher the ^{187}Os/^{188}Os ratio of the rock), concentrations remain low relative to mantle sources. One exception to the low Os concentration of the upper continental crust might be basalts. Basalts are unradiogenic sources of Os with very low Os concentrations, yet very high Os concentrations have been documented in lateritic soils at Deccan (Wimpenny et al., 2007), which may suggest that some portions of basalts contain an Os inventory much larger than implied by published basalt analyses. Alternatively, these high Os concentrations may result from preferential Os retention in deeply weathered horizons, and argues that basalt weathering does not release substantial Os to seawater.

1.3 Surficial cycle of Re-Os and the aqueous fractionation of Re from Os

Osmium is one of the least abundant elements in seawater ([Os] ~0.01 pg Os/g seawater). Rhenium, on the other hand, occurs in much higher concentrations in seawater ([Re] ~8×10^6 pg

Re/g seawater), primarily due to the high solubility of its oxyanion (ReO_4^-) in oxic conditions (Colodner et al., 1993). In organic rich sediments and sedimentary rocks most Re is organically bound (Miller et al., 2011 sources therein), and is insoluble only in reducing conditions. Burial of Re in anoxic sediments removes an estimated 50% of the riverine flux of Re the oceans, which leads to Re having the highest degree of enrichment among all metals in reducing sediments (Colodner et al., 1993). The removal mechanisms of Re and Os in the ocean are not fully understood (Yamashita et al., 2007), although it is clear that while the major sink for Re in the oceans is reducing sediments such as organic rich black shales, Os is removed in a variety of redox conditions. Osmium can readily enter solid phases, such as ferromanganese crusts, even in oxic waters (Yamashita et al., 2007). For this reason, Re/Os ratios are low in oxic pelagic sediments but can be very high in reducing sediments (see Figure 1.2). Oxic sediments experience little to no ingrowth of ^{187}Os from ^{187}Re decay, whereas there will be rapid ingrowth of ^{187}Os in reducing sediments. Because Re and Os are reduced to insoluble forms in low oxygen environments they are concentrated in organic-rich muds and black shales (Georgiev et al., 2012, Yamashita et al., 2007). As ^{187}Re decays to ^{187}Os, black shales develop high $^{187}Os/^{188}Os$, along with very high Re and Os concentrations. When these reducing sediments are exposed to an oxygenated environment Re -- and to a lesser extent Os -- is mobilized (Peucker-Ehrenbrink & Hannigan, 2000).

1.4 Sources of Os to the oceans: Controls on the $^{187}Os/^{188}Os$ ratio of seawater

The Os isotopic composition of seawater is nearly homogenous, and reflects the average isotopic composition of the sources of Os to the oceans weighted by their fluxes. As previously described, each source is characterized by a different isotopic composition (see Table 1.1, Figures 1.2 and 1.3) and is broadly categorized as either radiogenic or unradiogenic. The contributions of Os to seawater can be considered as the weighted input (f = mole fraction of total ^{188}Os) from radiogenic (f_{radio}) and unradiogenic sources (f_{unrad}) after Levasseur et al. (1999):

Equation 1:

$$^{187}Os/^{188}Os_{SW} = (f_{radio})(^{187}Os/^{188}Os_{radio}) + (f_{unrad})(^{187}Os/^{188}Os_{unrad})$$

Radiogenic sources of Os to seawater are dominated by the continental run-off in rivers and dissolution of aoelian dust. Unradiogenic sources of Os to seawater include seafloor hydrothermal input resulting from the alteration of mantle-derived rocks, and extraterrestrial sources (cosmic dust and meteorites). The Os isotopic ratio of seawater ($^{187}Os/^{188}Os_{SW}$) can change over time for several reasons. First, the amount of radiogenic Os supplied to the oceans can vary through time (a change in f_{radio}) as a result of changes in the total riverine input and/or the amount of aolian dust delivered to the oceans. Second, the isotopic composition of the source of radiogenic Os can vary (a change in $^{187}Os/^{188}Os_{radio}$), reflecting a change in the average isotopic composition of the continental material being weathered. Third, the amount of unradiogenic Os supplied to the oceans could vary (a change in f_{unrad}), either from changes in seafloor hydrothermal input and/or the amount of extraterrestrial material delivered to the oceans. The degree to which the isotopic composition of unradiogenic sources changes ($^{187}Os/^{188}Os_{unrad}$) is negligible compared to the other terms in Equation 1, and is constrained by the mantle value of 0.13 (see Figure 1.1). Chapters 2 and 3 will argue that the observed variations in $^{187}Os/^{188}Os_{SW}$ in the late Maastrichtian result from changes in the isotopic composition of the weathered continental material and changes in flux of unradiogenic Os to the oceans as a result of Deccan volcanism.

Osmium has a short marine residence time of 10-40 ka (Peuker-Ehrenbrink & Ravizza, 2000 with further discussion below), which suggests that $^{187}Os/^{188}Os$ is able to capture high frequency changes in the fluxes of Os to the oceans. This makes the marine $^{187}Os/^{188}Os$ record an attractive tool in studying short-term changes in continental weathering. But there is a lack of agreement as to how climate variability affects the Os isotopic composition and fluxes of river waters, and by extension the marine Os isotopic record. Previous work suggests that the flux of ^{187}Os from the continents to the oceans is diminished during glacial episodes, yet the long-term evolution of $^{187}Os/^{188}Os$ over the Cenozoic is inconsistent with a simple association between a colder climate and a lowered seawater $^{187}Os/^{188}Os$ (Figure 1.4). The modern average $^{187}Os/^{188}Os$ of riverine input is ~1.45 (Sharma et al., 2011 references therein), which closely reflects the isotopic composition of average continental crust (~1.4, see Table 1.1 for references). Peucker-Ehrenbrink and Blum (1998) argued that rocks freshly exposed by deglaciation to chemical weathering rapidly (<1000 a) and incongruently lose their radiogenic Os, increasing the

$^{187}Os/^{188}Os$ of river water and sending a spike of radiogenic Os to the oceans which may have the ability to affect the isotopic composition of seawater on 10^3 - 10^4 a time scales. On the other hand, Oxburgh (1998), Oxburgh et al. (2007), and Burton et al. (2010) argued that an increase in total riverine flux of Os rather than a change in its isotopic composition drives change in seawater variation. However, results reported by Paquay and Ravizza (2012) show that the global change in marine $^{187}Os/^{188}Os$ does not reflect glacial-interglacial cycles, and if changes do occur as a result of glacial-interglacial cycles they are most likely localized. While it is widely assumed that changes in continental weathering are responsible for changes in the $^{187}Os/^{188}Os_{SW}$ record, the exact mechanisms responsible are not yet clear.

There are multiple sources of atmospheric Os that could affect the $^{187}Os/^{188}Os$ ratio of seawater: aoelian dust, cosmic dust, and magmatic degassing. For the focus of this work, extraterrestrial flux and magmatic degassing are likely most important. Only the fraction of the aeolian and cosmic dust delivered to the ocean that dissolves in seawater affects the marine $^{187}Os/^{188}Os$ ratio. As will be further discussed later, the undissolved fraction will instead affect the $^{187}Os/^{188}Os$ of bulk sediment. The dissolution of aeolian dust in seawater as a source of seawater Os has not been systematically studied. Assuming that Os concentrations of aoelian dust are similar to Os concentrations of loess (~30 ppt, Peucker-Ehrenbrink & Jahn, 1999), the modern annual dust flux carries only ~20 kg of elemental Os to the oceans, much too small to significantly affect the Os isotopic composition of seawater (Peucker-Ehrenbrink & Ravizza, 2000). Yet, this flux may be an order of magnitude higher during peak glacial conditions, and therefore may have significantly affected the Os budget of seawater at certain times in Earth's history (Peucker-Ehrenbrink & Ravizza, 2000). Osmium flux from the background supply of cosmic dust may be of a similar magnitude to the flux from aeolian dust, with between 7 - 60 kg elemental Os delivered annually (Sharma et al., 2007). These can reasonably be considered maximum estimates since it is likely very little Os from either aeolian dust or cosmic dust actually dissolves in seawater (Peucker-Ehrenbrink & Ravizza, 2000). This uncertainty in the flux of cosmic dust is the largest uncertainty in the modern Os budget for seawater. Nevertheless, cosmic dust flux during the Maastrichtian remained fairly constant (Mukhopadhyay et al., 2001), and what variation has been measured is not enough to account for the variability observed in marine $^{187}Os/^{188}Os$.

Recent work suggests the volcanic aerosols may provide an additional, if localized, atmospheric source of Os. Gannoun et al. (2015) present evidence that gas condensates degassed from mantle-plume sourced basalts may act as a non-trivial source of unradiogenic Os, at least at small spatial scales. Re and Os can be enriched in gas sublimates and aerosols relative to the source lava because their volatilities are enhanced in oxygenated environments. Gannoun et al. (2015) also provides evidence for the loss of Os during sub-aerial degassing. This flux of unradiogenic Os from volcanic degassing may be especially relevant to the late Maastrichtian because of the eruption of the main phase Deccan lavas at ~68 Ma.

Osmium flux from atmospheric sources is thought to have remained relatively constant through the Cenozoic, with the exception of two periods of sharply elevated cosmic dust flux (Figure 1.5, Farley et al., 2006, 2012). In contrast, the $^{187}Os/^{188}Os$ of seawater has large-scale variations through the Cenozoic, with a general trend towards more radiogenic values (Figure 1.4). This suggests either an increase in the amount of radiogenic Os entering the oceans, or a decrease in the amount of unradiogenic Os to the oceans. Since the flux of cosmic dust over this time period has remained generally constant, this argues that atmospheric input of unradiogenic Os is not a primary driver of changes to the marine Os isotope record (Peucker-Ehrenbrink & Ravizza, 2000). Equation 1 requires another unradiogenic source of Os to the oceans, which in combination with radiogenic Os delivered by rivers ($^{187}Os/^{188}Os_{radio} \approx 1.45$, see Table 1.1) produces the isotopic composition of seawater ($^{187}Os/^{188}Os_{SW} \approx 1.06$, see Table 1.1). The alteration of young, mantle-derived basalts is likely the major source of unradiogenic Os to the oceans. Yet the flux of Os to the oceans from seafloor hydrothermal input is very poorly constrained. Both high-temperature and low-temperature interactions with seawater have been invoked (Peucker-Ehrenbrink & Ravizza, 2000), although it is assumed that high temperature input from hydrothermal vents drives modern seawater to a lower $^{187}Os/^{188}Os$ than modern riverine water. Sharma et al. (2007) argued that the alteration of unradiogenic mid ocean ridge basalts (MORB) could account for less than half the unradiogenic Os in seawater. Therefore another source of unradiogenic Os to the oceans is required. While abyssal peridotites have high concentrations of unradiogenic Os, the exact mechanism for transfer of Os from these rocks to the ocean is lacking.

Osmium has generally been considered well mixed in the oceans, and consequently measurements of the $^{187}Os/^{188}Os$ of marine sediments should record a global signal. In the overwhelmingly oxygenated modern ocean Os has a short residence time of approximately 10 - 40 ka (Peuker-Ehrenbrink & Ravizza, 2000), which is longer than the ~1000 - 6000 a mixing time of the oceans (Broecker & Peng, 1982). But it should be noted that there is evidence for basin-to-basin heterogeneity in $^{187}Os/^{188}Os$ (Paquay & Ravizza, 2012). This is a consideration for studies that: 1) Use samples from a continental margin, which might be more influenced by localized continental run-off (i.e. a stream basin) and therefore do not reflect a whole ocean value of $^{187}Os/^{188}Os$; 2) Utilize a single $^{187}Os/^{188}Os$ record to extrapolate the isotopic composition of the whole ocean, where potentially localized signals might be misinterpreted as a global signal; 3) Use $^{187}Os/^{188}Os$ to argue for basin restriction or isolation (i.e. Dickson et al., 2015) on the assumption that spatial variations in $^{187}Os/^{188}Os$ demonstrate that it developed independently of the rest of the ocean at a certain location. Importantly, the magnitude of spatial variation in $^{187}Os/^{188}Os$ is small compared to temporal variation. Although the overall structure of an increase in the $^{187}Os/^{188}Os$ of seawater through the Cenozoic is clear, finer scale fluctuations in the record are increasingly open to interpretation as more and more high-resolution and multi-site records are generated. This emphasizes the importance of multiple records when establishing whether a measured signal is global in extent, and especially when arguing for a causal mechanism. Chapter 3 will further illustrate this point by exploring $^{187}Os/^{188}Os$ records of seawater coincident with the emplacement of different large igneous provinces. Although there are gross similarities between the shapes of the marine Os isotopic record from each event, fine scale structural differences in the records should not be ignored.

1.5 Measuring the marine Os isotope record: Do marine sediments record the $^{187}Os/^{188}Os$ of seawater?

Reconstructing the marine Os isotope record for use as a palaeoceanographic tracer requires that "the recovered signal is primary and global in extent" (Cohen et al., 2004). However when measuring bulk sediment samples we need to consider whether they actually record the $^{187}Os/^{188}Os$ of seawater. Where Equation 1 describes the isotopic composition of seawater, Equation 2 describes the isotopic composition of bulk sediment samples:

Equation 2:

$$^{187}Os/^{188}Os_{measured} = (f_{SW})(^{187}Os/^{188}Os_{SW}) + (f_{detritus})(^{187}Os/^{188}Os_{detritus}) + (f_{cosmic})(^{187}Os/^{188}O_{cosmic})$$

The $^{187}Os/^{188}Os$ measured in bulk sediment samples is modeled as a mixture of Os from three sources: The seawater in which the sediments formed (hydrogenous Os), detrital material incorporated into the sediment, and undissolved cosmic dust particles. f_{SW} is the mole fraction of ^{188}Os in the bulk sediment from seawater, and $f_{SW} = 1- (f_{detritus} + f_{cosmic})$. Therefore Equation 2 shows that when the detrital and cosmic dust contributions are small ($f_{SW} >> f_{detritus} + f_{cosmic}$), the $^{187}Os/^{188}Os$ of the bulk sediment closely approximates that of contemporaneous seawater ($^{187}Os/^{188}Os_{measured} \approx {}^{187}Os/^{188}Os_{SW}$). Estimates of $f_{detritus}$ and f_{cosmic} suggest that they are small compared to f_{SW} when measuring the bulk Os isotopic composition of pelagic carbonates. $f_{detritus}$ can be approximated using measurements of Al concentration as a proxy for detritus. The fraction from undissolved cosmic dust particles f_{cosmic} can be calculated from sedimentation rates assuming that the rate of cosmic dust influx is constant. Estimates of cosmic dust flux in the late Cretaceous demonstrate that this is a reasonable assumption (Ravizza, 2007). $^{187}Os/^{188}Os_{cosmic}$ is the isotopic composition of cosmic dust (0.13, see Table 1.1). $^{187}Os/^{188}Os_{detritus}$ is assumed to be the isotopic composition of average upper continental crust (≈1.4, see Table 1.1). As discussed previously, this assumption may be problematic as the average isotopic composition of continental crust can vary through time due to changes in the types of rocks exposed to weathering. As will be shown in Chapter 2, the Os budget of pelagic sediment is overwhelmingly dominated by hydrogenous Os, and removing the influence of detritus and cosmic dust is unnecessary. In short, for rapidly accumulating (≥ 1 cm/ka) pelagic carbonates such as those studied here, the contribution to the total Os budget from detrital material and cosmic dust can be considered negligible. Measurements of the $^{187}Os/^{188}Os$ of modern pelagic sediments yield values very close to the $^{187}Os/^{188}Os$ of modern seawater (Peucker-Ehrenbrink & Ravizza, 2000). It follows as a reasonable assumption that carbonates from the past also measure the $^{187}Os/^{188}Os$ of the contemporaneous seawater in which they formed.

The effects of diagenetic remobilization and ingrowth of ^{187}Os from the decay of ^{187}Re also needs to be examined to further demonstrate that measured $^{187}Os/^{188}Os$ are indeed dominated by the isotopic signature of seawater. Nonetheless, when analyzing samples with very low Re

concentrations, such as the pelagic carbonates used for this study, correcting for Re ingrowth is unnecessary (see Chapter 2, section 2.5 Results).

Table 1.1: Os and Re concentrations and $^{187}Os/^{188}Os$ of geologic reservoirs

	[Re] (pg/g)	[Os] (pg/g)	$^{187}Os/^{188}Os$	Source(s)
Chondrites, cosmic dust	$4.2 - 9.6 \times 10^4$	$\sim 5 \times 10^5$	0.12 - 0.13	Meisel et al. (1996) Horan et al. (2003)
Primitive mantle	250 - 300	3400	0.129	Meisel et al. (1996) Morgan (1986) McDonough & Sun (1995)
MORB	500 - 2000	150		Shirey & Walker (1998)
Average upper continental crust	230 - 370	31 - 50	1.4	Esser & Turekian (1993) Peucker-Ehrenbrink & Jahn (2001)
Pelagic carbonates	1.4 -100	7 - 74		Robinson et al. (2009)
Organic rich sediments	$2.8 - 4.5 \times 10^4$	450 - 750		Dubin & Peucker-Ehrenbrink (2015)
Riverine runoff	2.08	0.003 - 0.084	1.45	Miller et al. (2011) Sharma et al. (2011) and references therein
Deccan basalts	~300 - 900	15	0.129 *initial*	Allègre et al. (1999)
Modern seawater	7.5	0.006 - 0.014	1.05 - 1.09 *deep* <1.05 *surface*	Anbar et al. (1992) Colodner et al. (1993) Chen & Sharma (2011)

Figures

Figure 1.1 Schematic evolution of the $^{187}Os/^{188}Os$ ratio of meteorites, Earth's mantle and crust

After Koeberl & Shirey, 1998. The black dot on the right hand axis marks the estimated isotopic starting composition ($^{187}Os/^{188}Os_{4.56\ Ga}$ = 0.0965; Walker & Morgan, 1989) of the Earth's mantle and meteorites 4.56 Ga ago. Due to the relatively low Re/Os ratio of 0.1 the $^{187}Os/^{188}Os$ ratio increases only slightly with time, as indicated by the red line. The green line follows a hypothetical crustal extraction event 3 Ga ago. During most magmatic processes, Os is strongly retained in the mantle while Re partitions somewhat into the melt, leading to Re/Os ratios >>1 in many crustal rocks. Thus, the $^{187}Os/^{188}Os$ ratio of crustal rocks increases rapidly with time due to the production of radiogenic ^{187}Os by decay of ^{187}Re.

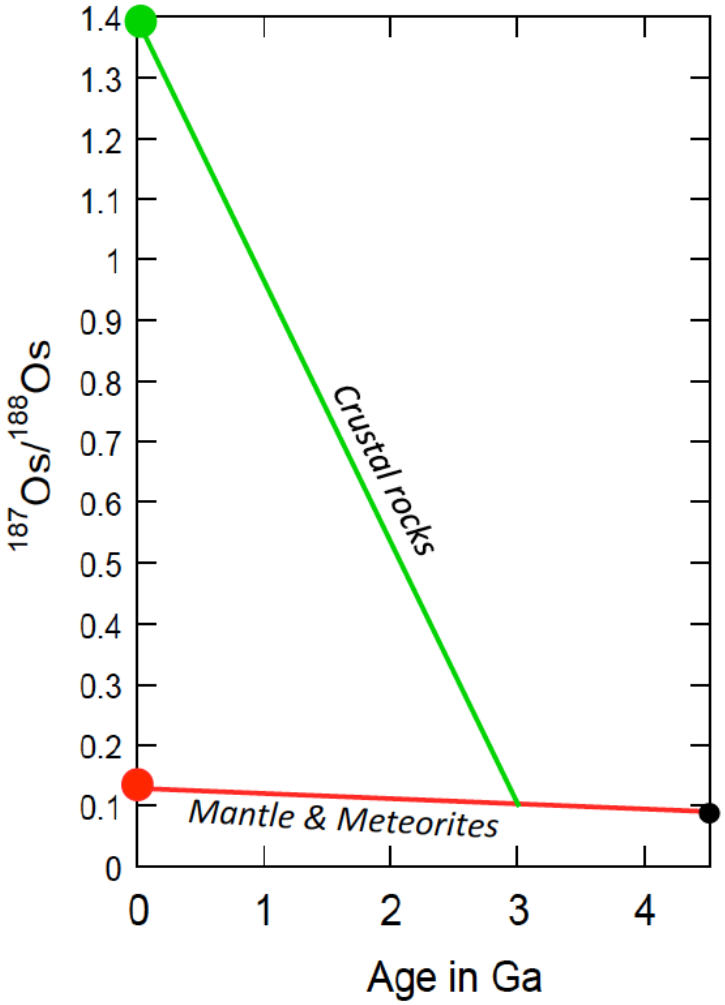

Figure 1.2 Re and Os Sources and Sinks

From Hannah & Stein (2013) and sources therein. See Table 1.1 for annual fluxes.

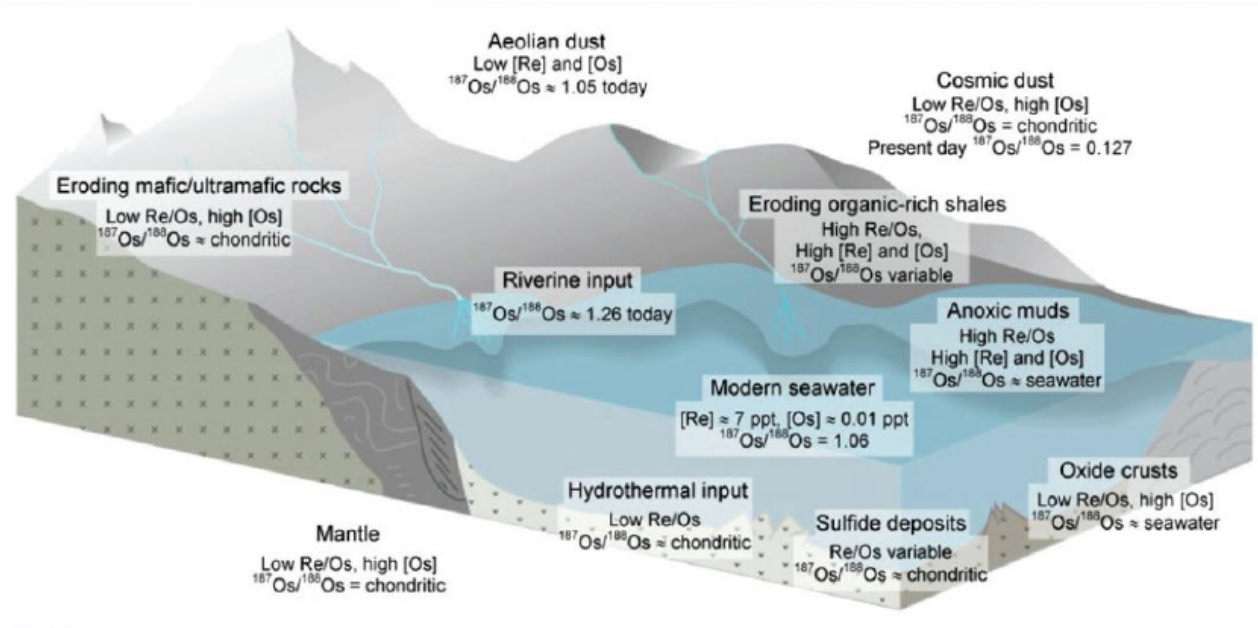

Figure 1.3: Sources of marine Os

Modified from Peucker-Ehrenbrink & Ravizza (2000). Red arrows indicate sources of unradiogenic Os to the oceans (low $^{187}Os/^{188}Os$), while the green arrow indicates sources of radiogenic Os (high $^{187}Os/^{188}Os$). The $^{187}Os/^{188}Os$ of seawater ($^{187}Os/^{188}Os_{SW}$) is a flux weighted average of these inputs:

$$^{187}Os/^{188}Os_{SW} = (f_{mantle})(^{187}Os/^{188}Os_{mantle}) + (f_{terr})(^{187}Os/^{188}Os_{terr}) + (f_{cosmic})(^{187}Os/^{188}Os_{cosmic})$$

Where f_{mantle} = the mole fraction of ^{188}Os from mantle sources (seafloor hydrothermal input), f_{terr} = the mole fraction of ^{188}Os from terrigenous sources (continental run-off), and f_{cosmic} = the mole fraction of ^{188}Os from extraterrestrial inputs

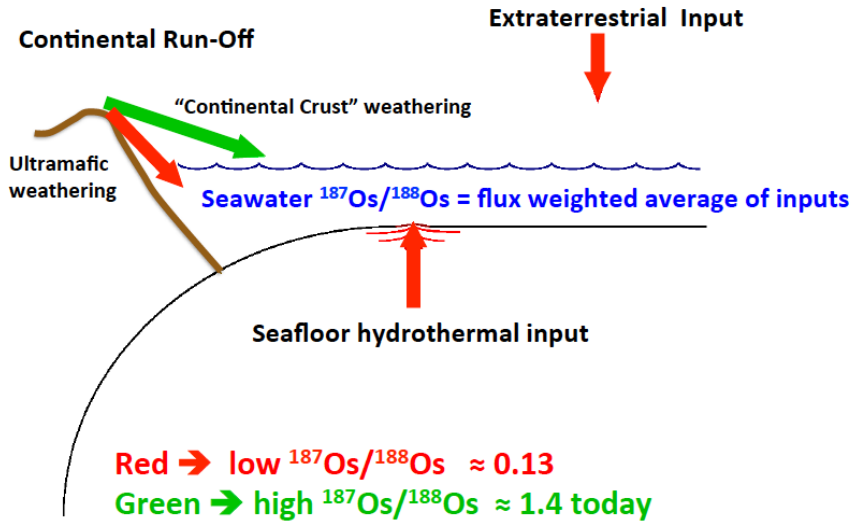

Figure 1.4: $^{187}Os/^{188}Os$ record of seawater for the past 75 Ma.

Record from a hydrogenous Fe-Mn crust (figure from Peucker-Ehrenbrink & Ravizza, 2012, data from references therein). These slowly accumulating crusts are difficult to accurately date, yet this record illustrates that the record of $^{187}Os/^{188}Os$ of seawater has trended to more radiogenic values since the Paleocene-Eocene Boundary (P-E Boundary). K-T Boundary = Cretaceous – Paleogene Boundary; E-O Boundary = Eocene – Oligocene Boundary.

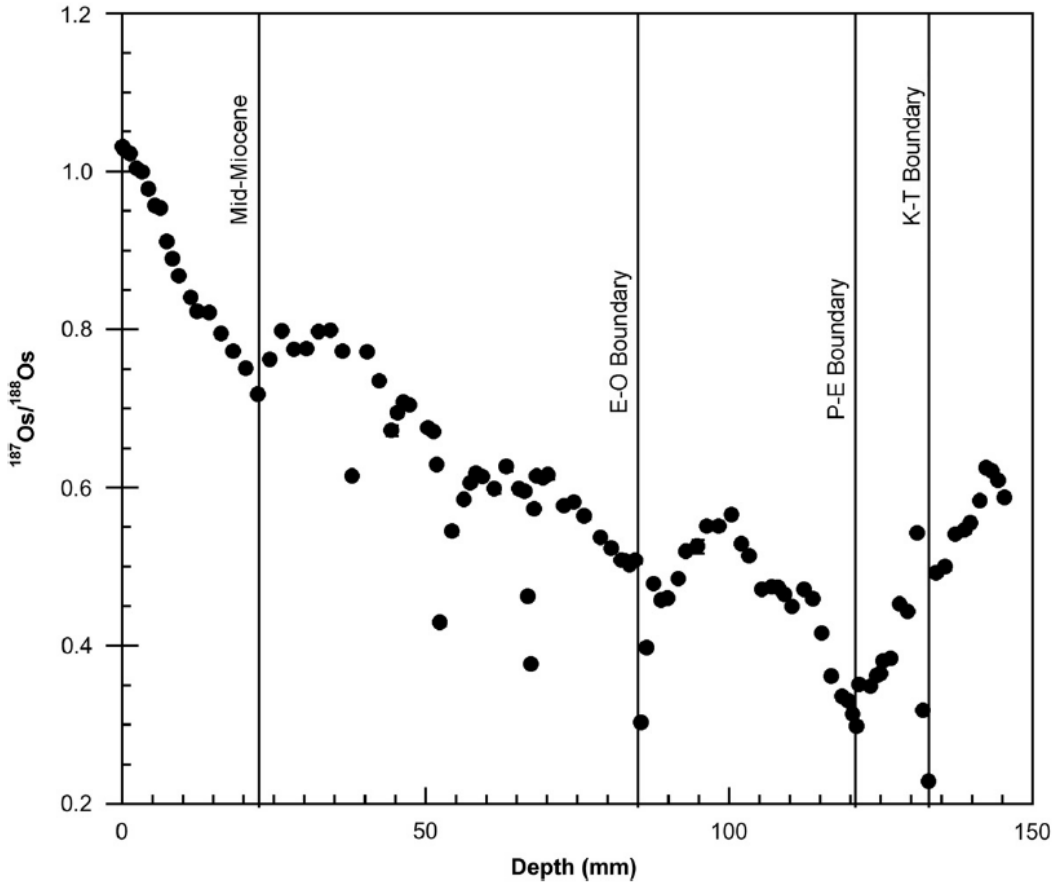

Figure 1.5: A 100 Ma record of extraterrestrial ^{3}He flux

^{3}He is used as a proxy for cosmic dust. Panel A (~2 Ma - 38 Ma): Data from ODP Site 757. Lines are 3-point running means from Farley et al., 2006. Panel B (~32 Ma - 100 Ma): Data from the Umbria-March Basin. Data are 5-point running means from Farley et al., 2012 (bold line), Mukhopadhyay et al., 2001 (dotted line), and Farley et al., 1998 (thin line).

Panel A

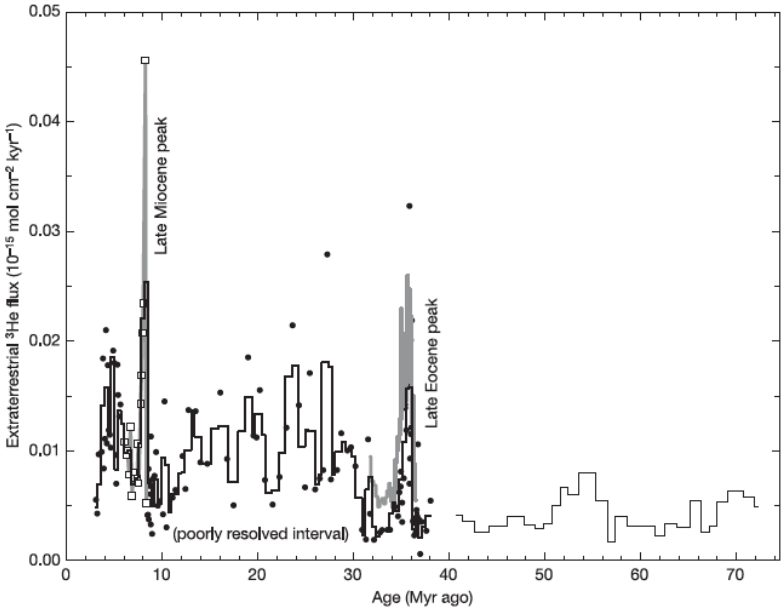

Panel B

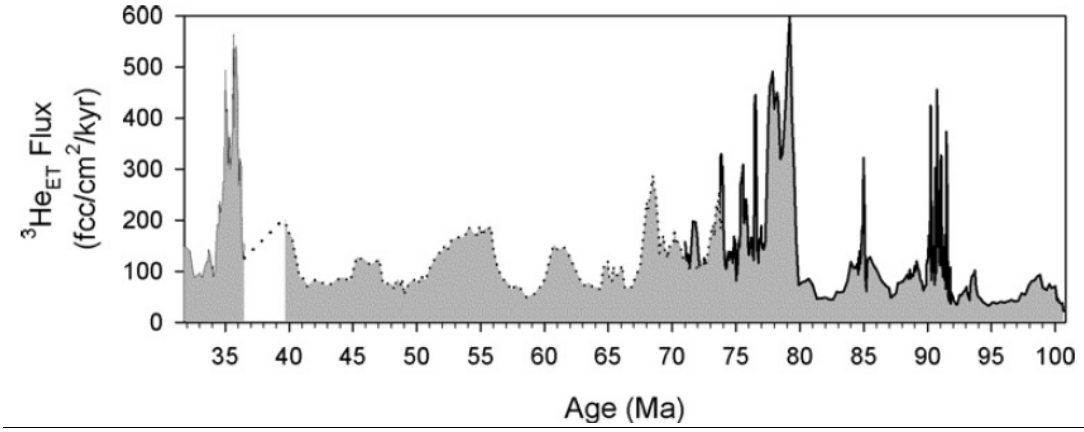

Chapter 2:

A High-Resolution Marine $^{187}Os/^{188}Os$ Record for the Late Maastrichtian: Distinguishing the Chemical Fingerprints of Deccan Volcanism and the KP Impact Event

This chapter was originally published as:

Robinson, N., Ravizza, G., Coccioni, R., Peucker-Ehrenbrink, B., Norris, R., 2009. A high-resolution marine $^{187}Os/^{188}Os$ record for the late Maastrichtian: Distinguishing the chemical fingerprints of Deccan volcanism and the KP impact event. Earth and Planetary Science Letters 281, 159-168.

Abstract

A composite late Maastrichtian (65.5 to 68.5 Ma) marine osmium (Os) isotope record, based on samples from the Southern Ocean (ODP Site 690), the Tropical Pacific Ocean (DSDP Site 577), the South Atlantic (DSDP Site 525) and the paleo-Tethys Ocean demonstrates that subaerially exposed pelagic carbonates can record seawater Os isotope variations with a fidelity comparable to sediments recovered from the seafloor. New results provide robust evidence of a 20% decline in seawater $^{187}Os/^{188}Os$ over a period of about 200 ka early in magnetochron C29r well below the Cretaceous-Paleogene Boundary (KPB), confirming previously reported low-resolution data from the South Atlantic Ocean. New results also confirm a second more rapid decline in $^{187}Os/^{188}Os$ associated with the KPB that is accompanied by a significant increase in Os concentrations. Complementary platinum (Pt) and iridium (Ir) concentration data indicate that the length scale of diagenetic remobilization of platinum group elements from the KPB is less than 1 m and does not obscure the pre-KPB decline in $^{187}Os/^{188}Os$. Increases in bulk sediment Ir concentrations and decreases in bulk carbonate content that coincide with the Os isotope shift suggest that carbonate burial flux may have been lower during the initial decline in $^{187}Os/^{188}Os$. We speculate that diminished carbonate burial rate may have been the result of ocean acidification caused by Deccan volcanism.

2.1 Introduction

There is substantial evidence the late Maastrichtian was punctuated by a transient warming event at ~66 Ma that terminated 100-200 ka prior to the KPB, which some workers have attributed to the influence of Deccan volcanism (Barrera & Savin, 1999; Li & Keller, 1999; Wilf et al., 2003). Reconstructions of Maastrichtian CO_2 levels based on paleosol data indicate abrupt increases in pCO_2 superimposed upon elevated background concentrations of 3-4 times present-day levels, and are interpreted in the context of the Deccan-induced warming hypothesis (Nordt et al., 2003). Ravizza and Peucker-Ehrenbrink (2003) show a decline in the marine $^{187}Os/^{188}Os$ record prior to that associated with the Cretaceous-Paleogene Boundary (KPB), which they attribute to Deccan volcanism. These initial results suggest that the marine osmium (Os) isotope record of the late Maastrichtian has a distinct and resolvable graphed shape that can be used to determine the relative timing of rapid and transient changes in osmium input to the oceans, specifically those resulting from Deccan volcanism. Studies of ferromanganese crusts (Burton, 2005; Klemm et al., 2005) and pelagic clays (Peucker-Ehrenbrink et al., 1995; Pegram & Turekian, 1999; Ravizza 2007) for the late Maastrichtian also record the decline to extremely unradiogenic, nearly chrondritic $^{187}Os/^{188}Os$ values ($\approx$ 0.127: Horan et al., 2003) at the KPB, but these records lack the temporal resolution and stratigraphic control needed to confirm or refute the seawater Os isotope evolution proposed by Ravizza and Peucker-Ehrenbrink (2003).

The motivation for this study is four-fold: (1) To better resolve the magnitude and timing of the late Maastrichtian decline in the marine $^{187}Os/^{188}Os$ record by comparing coeval records from sites distributed throughout the global ocean; (2) To explore the correlation between the structure of the marine Os isotope record and the transient warming event at ~66 Ma by comparing osmium isotope data with existing oxygen isotope analyses of well preserved foraminifera, and nannofosssil abundance patterns from the same cores; (3) To determine whether or not the marine osmium isotopic record of pelagic carbonates is adversely affected by uplift and exposure above sea level by comparing Os records obtained from the modern seafloor to a record obtained from analyses of pelagic carbonate now exposed on land; (4) To critically evaluate the length scale of osmium mobility during diagenesis and its potential influence on the marine osmium isotope record using complementary platinum group element (PGE: Pt, Ir, Os) data.

2.2 Sample Materials

The samples analyzed for this study are from the Deep Sea Drilling Program (DSDP) Site 525 on Walvis Ridge in the Atlantic (29°04.24'S, 2°59.12'E), DSDP Site 577 on Shatsky Rise in the Western Pacific (32°26.53'N, 157°43.39'E), the Ocean Drilling Program (ODP) Site 690 on Maud Rise in the Weddell Sea (65°9.629'S, 1°12.296'E), and the Scaglia Rossa Formation at Bottaccione in Gubbio, Italy (43°22'N, 12°35'E). Sample volumes from DSDP and ODP were typical 20 cm^3, while sample volumes from the Gubbio section were approximately 50 – 100 cm^3. The high latitude ODP Site 690 was selected for comparison to two previously studied lower latitude sites (DSDP 525 and 577) to evaluate whether the Os isotopic signal recovered is global in its extent. Additional samples from DSDP Sites 525 and 577 were analyzed to increase the temporal resolution available and compare leachate and Re data between sites. Benthic and planktonic foraminiferal stable isotope data from ODP Site 690 (See Wilf et al., 2003 and references therein) allow for a direct comparison of Os ratios to paleoclimate proxy records without the potential discrepancies in age models that might arise between sites. The Bottaccione section was chosen because as a rapidly accumulating pelagic limestone with well-developed age constraints it is well suited for a high-resolution comparison to the submarine records generated for this period. DSDP Sites 525, 577 and ODP Site 690 are submarine pelagic carbonate sections (calcareous nannofossil oozes). Over the interval studied DSDP Site 525 varies between 42.1 and 83.8 wt% $CaCO_3$ (Kucera et al., 1997), DSDP Site 577 sediments are generally > 90 wt% $CaCO_3$ (Zachos et al., 1985), and ODP Site 690 varies from 77 to 92 wt% $CaCO_3$ (this study). The Scaglia Rossa section of Bottaccione (Permoli Silva & Sliter, 1995) is a pink to reddish-brown bedded limestone that varies from 91.6 to 97.2 wt% $CaCO_3$ (Crocket et al., 1988; Alvarez et al., 1990; Rocchia et al., 1990).

2.3 Age Models

We elected to use magnetostratigraphy and the KPB as the sole basis for an integrated timescale in order to correlate temporally between different sites. Although this approach limits the number of age datums available for use in constructing the age models, we argue this approach is preferable when correlating such widely distributed sites because geomagnetic reversals and the KPB are very nearly globally synchronous, while other biostratigraphic datums may be slightly diachronous. The age models for DSDP Site 525, DSDP Site 577 and ODP Site 690 are based

on linear interpolation between age datums given by magnetostratigraphy and the KPB (Table A1). Note that we have retained the 65.5 Ma date for the KPB from Hicks et al. (2002), rather than the more recent date of 66.0 Ma based on 405 ka eccentricity cycles (Kuiper et al., 2008). This is because there is no comparable orbitally tuned age assignment for the base of C29r, placed at 65.843 Ma by Hicks et al. (2002), and thus adopting the 66.0 Ma KPB age in isolation would create a negative duration for the Cretaceous portion of C29r. For ODP Site 690 stratigraphic control is derived from the magnetostratigraphy of Hamilton (1990) and the depth of the KPB iridium (Ir) anomaly from Michel et al. (1990). It should be noted that in ODP Site 690 the C29r/C30n magnetic reversal is located at the break between cores 15 and 16. The break between cores 16 and 17 includes an estimated 4 m of unrecovered section and occurs within chron C30r. Hamilton (1990) does not assign a depth for the C30r/C30n reversal boundary, so we selected 255.0 mbsf based on the inclination data given (Figure 5 from Hamilton, 1990). The C30r/C31n reversal boundary is not used as a datum for ODP Site 690. At DSDP Sites 525 and 577 stratigraphic control is based on integrated magnetobiostratigraphy using the same datums as in Ravizza and Peucker-Ehrenbrink (2003). Previous work establishes the magnitude and location of the KPB Ir anomalies at DSDP Site 577 (Michel et al., 1985). In the Bottaccione section we use the integrated magnetobiostratigraphy of Coccioni et al. (2004), with the previously established location of the KPB anomaly from Alvarez et al. (1990). Using these age models the average temporal resolution of the new Os isotope records reported here is ≈ 85 ka for ODP 690, ≈100 ka for DSDP 577, and ≈ 40 ka for the Bottaccione section. In time interval of special interest samples were analyzed at temporal resolution as high as one sample each 15 ka.

2.4 Methods

Os isotope ratios and PGE concentrations were measured by isotope dilution using the nickel sulfide (NiS) fire assay preconcentration method followed by isotope ratio measurements using an Element2 ICP-MS (Ravizza & Pyle, 1997; Hassler et al., 2000). DSDP Site 577 and ODP Site 690 samples were hand-ground using a Pyrex mortar and pestle. Bottaccione samples were coarse crushed in a rock crusher with care taken that metal surfaces did not come in contact with sample material by covering the surfaces of the jaw crusher with disposable plastic sheets. The resulting coarse crush was then fine ground in a Rocklabs ceramic zirconia mill. For NiS fire

assay preconcentration a 1:1.5 sample to flux ratio was utilized, with 10 g of sample used except when not enough sample was available. Procedural fusion blanks accounted for approximately 1 in 6 analyses performed. Procedural gas blanks were analyzed between every five samples to monitor the amount of Os cross contamination which may come from carry-over in the Teflon vials used in sparging (Hassler et al., 2000). In cases where gas blanks accounted for more than 10% of the ^{188}Os signal intensity due to low count rates, results were not used. Procedural blanks accounted for 1- 2% of Os concentration measured in the Bottaccione Section, and 0.2% - 2% in ODP 690 and DSDP 577 samples. An in house Os standard prepared from a concentrated Johnson-Matthey standard solution was analyzed between every 5 samples, with a measured $^{187}Os/^{188}Os$ value of 0.1085 ± 0.0020 (2SD).

In order to better constrain the likely contribution of lithogenic Os to the sediment budget, a subset of samples from Site 690 were analyzed by XRF at Washington University in St. Louis, Missouri, for major and minor elements (Table A2). In order to better evaluate whether fluctuations in PGE concentrations resulted from differences in dilution, a subset of samples from ODP Site 690 were analyzed for bulk $CaCO_3$ content by elemental analyzer (EA) at the University of Hawaii. Bulk $CaCO_3$ content for selected samples from DSDP Site 577 were conducted at Woods Hole Oceanographic Institution. (Table A3)

To further assess the potential influence of non-hydrogenous Os on bulk sediment Os concentrations, leachable rhenium (Re) and Os were measured in separate powder splits in a subset of samples (8 from ODP Site 690, 5 from Bottaccione, and 4 from DSDP Site 525) using a modification of the method described in Ravizza (2007). One gram of sediment was allowed to react with a leach solution of ~5.3N HNO_3 and 0.8% H_2O_2 for about an hour, and then spiked with an enriched ^{190}Os and ^{185}Re isotope spike, prior to separation of the solution and sediment by centrifugation. After Os was measured, Re was separated from residual sample solutions using anion exchange columns prior to ICP-MS analysis (Peucker-Ehrenbrink et al., 1995). A general outline of the methods used in our lab for Re analysis by ICP-MS can be found in Ravizza and Paquay (2008).

2.5 Results

New $^{187}Os/^{188}Os$ data covering approximately the last 3 million years of the Maastrichtian (68.40 Ma to 65.51 Ma) together with complementary Pt, Ir and Os concentrations (Appendix A) are presented for DSDP Site 577 (Figure 2.1), ODP Site 690 (Figure 2.2), and Bottaccione (Figure 2.3). Previously reported $^{187}Os/^{188}Os$ and Os concentrations for DSDP Site 525 are re-plotted (Figure 2.4) with unpublished Pt and Ir data (Table A7). The composite $^{187}Os/^{188}Os$ record reconstructed using these new bulk sediment analyses agrees well with previously published values from DSDP Sites 577 and 525 as seen in Figure 2.5. All records show $^{187}Os/^{188}Os$ values close to 0.6 through magnetochron C30n (67.875 Ma to 65.843 Ma). In all records, a 2-stage decline leading up to the KPB is evident which begins at, or just before, the C29r/C30n magnetic reversal (Figure 2.5). After first declining from plateau values of approximately 0.59 to values of 0.42, $^{187}Os/^{188}Os$ values stabilize for 50–130 ka before decreasing again steeply approaching the KPB. Previous studies spanning the KPB have measured nearly chondritic values of $^{187}Os/^{188}Os$: ~ 0.13. For example the KPB at DSDP Site 577 has a $^{187}Os/^{188}Os$ of 0.157 (See Koeberl & Shirey, 1997 for additional KPB data).

The majority of Os concentrations fall between 10 and 50 pg/g, similar to values reported for other pelagic carbonates (Reusch et al., 1998; Ravizza et al., 2001) but lower than those reported for pelagic clays (Esser & Turekian, 1988; Ravizza, 2007). Ir concentrations remain low through C30n at all sites, not increasing above background levels (~8 to 20 pg/g) until just below the KPB. The maximum Ir concentrations are found in samples closest to the KPB. At Bottaccione and ODP Site 690 maximum Ir concentrations are below reported peak Ir concentrations (Bottaccione ≈ 3000 pg/g: Alvarez et al., 1990; ODP Site 690 ≈ 1500 pg/g: Michel et al., 1990) because the KPB clay was not analyzed. Pt concentrations remain stable through C30n at Bottaccione, and begin to rise steadily at the C29r/C30n reversal boundary from 100 pg/g to 382 pg/g just below the KPB. At ODP Site 690, Pt concentrations are higher and more variable in C30n. However, like Bottaccione, Pt concentration values at ODP Site 690 begin to increase steadily at the C29r/C30n reversal boundary, to a maximum concentration of 583 pg/g just below the KPB.

Approximately 30% of the sample powders were analyzed in duplicate. The average difference between replicate analyses was 2% for $^{187}Os/^{188}Os$, and 3.5% for Os concentration, with 2 notable exceptions. The first exception is that sets of duplicates from ODP Site 690 within the first declining limb after the $^{187}Os/^{188}Os$ plateau (249.9, 251.03, and 251.82 mbsf) had poor reproducibility of $^{187}Os/^{188}Os$ and Os concentration. Second, one sample from DSDP Site 577 (10.21 m below KPB) was analyzed in triplicate, and resulted in a $^{187}Os/^{188}Os$ range of 0.362 – 0.567 and a range in Os concentration of 7.8 – 14.8 pg/g. Given that the reproducibility of all other samples was very good, we consider the analyses that conform to the long-term trend in the $^{187}Os/^{188}Os$ record to be the best representation of the marine Os isotope record. Average reproducibility was also generally good for Pt and Ir with an average difference of 11% and 18% between replicate analyses for Pt and Ir concentrations, respectively. For clarity whenever replicate analyses were performed the resulting data are plotted separately, not averaged.

Results of Re and Os analyses of the 18 leach solutions (Table A8) yield two main results. First, the leachable Re concentration of nearly all samples is very low, often less than 10 pg/g. Total Re in these sample digestions was similar to the measured Re blanks. Blank corrected Re concentrations range from 2.6 pg/g to 6.3 pg/g at ODP Site 690 and from 1.5 to 3.0 pg/g at Bottaccione. DSDP Site 525 shows higher Re concentrations, from 4 - 100 pg/g. The single 577 sample analyzed had 3 pg/g Re, also barely distinguishable from procedural blanks. Consequently the late Maastrichtian $^{187}Os/^{188}Os$ records from DSDP Site 577, ODP Site 690 and Bottaccione sections show no indication of significant *in situ* decay of ^{187}Re as all age corrections were less than 1% of the measured $^{187}Os/^{188}Os$ ratio. Leach analyses of two samples from DSDP Site 525 indicate age corrections between 2 and 10% are required for these samples. However it should be noted that these corrections do not result in a better agreement with the osmium isotope data from other sites. Secondly, the $^{187}Os/^{188}Os$ of leachates agree with bulk values on average within 3%, with a range of variation of 0-12% (Table A8). Taken as a whole the leach data set does not display a systematic pattern of bulk-leach differences: Leachate values of ODP Site 690 samples were in all cases but one higher than bulk sediment values, leachate values of Bottaccione samples were in all cases but one lower than bulk sediment values, and leachate values of DSDP Site 525 samples were both higher and lower than bulk values. Leachable Os concentrations range from 10 - 70% of bulk Os concentrations, with an

average of 40% bulk osmium leached, while ^{188}Os count rates measured in leaches were usually less than 20% of those measured for bulk analyses. However calculated osmium concentrations should be regarded cautiously because it is difficult to assess whether or not sample and spike Os were isotopically equilibrated during the leaching procedure.

2.6 Discussion

2.6.1 Hydrogenous osmium dominates the sediment budget

There is good agreement of $^{187}Os/^{188}Os$ between the four sites when comparing bulk analyses directly (Figure 2.5) without corrections for contributions from terrigenous material or extraterrestrial matter (interplanetary dust particles). However, there are small offsets between the four sections corresponding to a total range in $^{187}Os/^{188}Os$ of ~10%. These offsets are most apparent throughout the plateau in $^{187}Os/^{188}Os$ that spans much of magnetochron C30n. In this interval measured $^{187}Os/^{188}Os$ ratios are generally lowest at DSDP Site 525 (≈ 0.55), while those measured at Bottaccione (≈ 0.61) are typically highest. The relatively good agreement between the various bulk sediment records is somewhat surprising because estimates of the terrigenous and extraterrestrial contributions to the bulk sediment Os inventory are non-trivial (Table 2.1). Systematic offsets in bulk sediment $^{187}Os/^{188}Os$ between coeval pelagic carbonate sequences have been reported previously and attributed to contributions of non-hydrogenous Os to the bulk sediment Os inventory (Ravizza et al., 2001; Dalai et al., 2006a). The bulk sediment osmium inventory is frequently considered to consist of three components: A hydrogenous component from seawater (Os_{SW}), undissolved particulate extraterrestrial material (Os_{ET}), and detrital material (Os_{det}) (See Esser & Turekian, 1988, Dalai & Ravizza, 2006 for details of such models). However, applying corrections to the bulk sediment analyses reported here based on this type of mixing model substantially increases the magnitude of offsets between records. In addition there are significant uncertainties associated with these corrections because the $^{187}Os/^{188}Os$ of the lithogenic component of the sediment is poorly constrained and the instantaneous sediment mass accumulation rate (MAR) need not be the same as the average sediment MAR used in the budget calculation. The agreement seen between the four sites presented here suggests that the hydrogenous component of the Os sediment inventory dominates the sediment budget, resulting in a measured bulk sediment $^{187}Os/^{188}Os$ that closely approximates that of seawater. The

generally good agreement between bulk sediment and leachable $^{187}Os/^{188}Os$ supports this interpretation (Table A8 and Results section).

2.6.2 Age Model & Offsets

As noted above, all sites are characterized by good magnetostratigraphy and accumulation rates that allowed for sampling resolution as high as 15 ka. However, incomplete core recovery between core breaks is commonplace in DSDP and ODP cores making it very likely that the ODP Site 690 record is incomplete. As noted above, the C29r/C30n magnetic reversal boundary is located at a core break and there is an estimated 4 m of unrecovered section in C30n. Although the overall agreement between the $^{187}Os/^{188}Os$ records presented here is good, the gaps in core recovery introduce uncertainty in age models and potential give rise to temporal aliasing when comparing records. While the initial decline in $^{187}Os/^{188}Os$ occurs at the C29r/C30n reversal boundary at DSDP Site 577 and ODP Site 690, it begins either at or just before the reversal boundary at Bottaccione. At DSDP Site 525 the $^{187}Os/^{188}Os$ values clearly begin to decline within C30n (Figure 2.5). The correspondence of a core break in ODP Site 690 to the C29r/C30n reversal boundary raises the possibility that $^{187}Os/^{188}Os$ began to decline prior to this boundary and that this section of the record was not preserved. However, Bottaccione is the most complete section in this study, and it shows only a minor decline prior to the reversal boundary. Therefore we proceed on the assumption that any time missing from ODP Site 690 at the C29r/C30n boundary is short, and that the initial decline in $^{187}Os/^{188}Os$ at DSDP Site 525 precedes the decline at the other three sites by as much as 400 ka.

Comparison of our new data to previously published data from DSDP 525 suggest that the $^{187}Os/^{188}Os$ of seawater during the Maastrichtian may not be homogeneous. During magnetochron C30n, the Os isotope and PGE signatures of DSDP Site 525 are distinct from the other three sites examined in this study. Also the highest measured Re concentrations were among these samples. $^{187}Os/^{188}Os$ values at DSDP Site 525 are consistently lower than values measured at the other three sites. Furthermore, Os/Ir ratios are much higher at DSDP Site 525 through C30n (averaging 2.6 compared to 1-1.4 at ODP Site 690, DSDP 577 and Bottaccione). Both Os/Ir and $^{187}Os/^{188}Os$ converge with the values measured at the other three sites after the C29r/C30n reversal boundary. These differences cannot be readily explained as the result of

variations in detrital and extraterrestrial contributions at these sites. Consequently we suggest that the lower $^{187}Os/^{188}Os$ ratios and elevated Os/Ir ratios and Re concentrations may indicate poorly ventilated intermediate waters at DSDP Site 525 during C30n.

Our suggestion of partial isolation of the South Atlantic during the late Maastrichtian is consistent with observed foraminifera fragmentation data presented in Kucera et al. (1997). That study examined sediments from Walvis Ridge during the late Maastrichtian, and saw no correspondence of dissolution signals between DSDP Sites 525 and 527. The authors interpreted this as evidence of a limited interaction between the deepwater masses on either side of the ridge. Although the residence time of Os in the modern oceans (10-40 ka: Peucker-Ehrenbrink & Ravizza, 2000) is longer than ocean mixing times, this does not preclude osmium isotopic heterogeneities at other times and spatial variation in the $^{187}Os/^{188}Os$ ratio of seawater may have occurred due to isolation of certain ocean basins.

In summary, several lines of evidence suggest that the offset between the $^{187}Os/^{188}Os$ ratios measured in DSDP Site 525 and the other cores may be the result of heterogeneous $^{187}Os/^{188}Os$ in the late Maastrichtian oceans. However, this offset may also result from contributions of non-hydrogenous Os to the bulk sediment $^{187}Os/^{188}Os$. Regardless of their cause, the offsets documented in this study provide empirical evidence that the bulk sediment $^{187}Os/^{188}Os$ records are not analogous to the $^{87}Sr/^{86}Sr$ records from marine carbonates. While the marine Os isotope record does have value as chemostratigraphic tool, it cannot be assumed to be "single-valued" function of time.

2.6.3 Diagenetic redistribution of PGE from the KPB

Analyses of $^{187}Os/^{188}Os$, Pt/Ir and Os/Ir ratios approaching the KPB horizon allow us to place empirical constraints on the extent of downward diagenetic remobilization of PGE from the KPB. Ir concentrations are the most commonly used indicator of extraterrestrial material in bulk sediment samples. However changes in Ir concentrations may also result from variations in the flux of other sedimentary components to the seafloor (Kyte et al., 1993; Evans et al., 1997) making it difficult to discern the full vertical extent of an Ir anomaly. In contrast, PGE ratios are less strongly influenced by variable dilution but are still sensitive indicators of the presence of

extraterrestrial material. The Pt/Ir and Os/Ir ratios of present day seawater are large compared to those of chondrites (Table 2.2). Therefore a large addition of chondritic PGE to seawater by an impact should shift the Pt/Ir and Os/Ir of marine sediments to values lower than pre-impact values as the pulse of meteoritic PGE is removed from seawater to the sediments.

Our low-resolution profile across the KPB at DSDP Site 577 (Pt/Ir = 1.7) confirms that Pt/Ir ratios vary as described above. High-resolution late Maastrichtian data from ODP Site 690 (Figure 2.2) and Bottaccione (Figure 2.3) demonstrate that Pt/Ir values begin to decline close to the KPB, much later than the decline in $^{187}Os/^{188}Os$ at the C30n/C29r boundary. At ODP Site 690 Ir and Os concentrations begin an irregular rise to higher concentrations roughly 3 m below the KPB, but Pt/Ir ratios begin to shift toward lower values only 0.65 m below the KPB. At Bottaccione the deepest indication of a significant decrease in Pt/Ir ratio occurs 0.80 m below the KPB. While the data set for DSDP Site 577 includes an analysis of the KPB, sample density close to the boundary is relatively low. Given this limitation we can safely conclude that Pt/Ir ratios give no indication of an extraterrestrial influence 1.6 m below the boundary, whereas such an influence is clear within 0.37 m of the boundary. There is a similar shift to Os/Ir ratios less than 1 approaching the KPB that is consistent with the influence of a limited redistribution of PGE at the KPB. We note that the very low, sub-chondritic Os/Ir ratios in ODP Site 690 and Bottaccione samples closest to the KPB support the model advanced by Paquay et al. (2008).

The constraints that PGE ratios place on the extent of diagenetic remobilization of the PGE have important implications for interpretation of marine sediment Os isotope data, both in general and in this study. With regard to this specific study, the PGE data confirm the initial inference, based mainly on previously reported data from DSDP Site 525, that there are two separate intervals of decreasing $^{187}Os/^{188}Os$ in the late Maastrichtian portion of the marine Os isotope record. The close correspondence between the shift to lower Pt/Ir ratios and the onset of the $^{187}Os/^{188}Os$ decline into the KPB provides strong evidence that this second decline is related to diagenetic redistribution of PGE from the KPB horizon. In the absence of diagenesis and physical mixing by bioturbation, we contend that this decline would be essentially instantaneous and correspond with the time of the impact event. An important corollary of this interpretation is that the initial decline in $^{187}Os/^{188}Os$ is unrelated to an impact event as there is only minor Ir enrichment and no

shift in PGE ratios towards chondritic values. More generally, these data place a robust upper limit on the length scale of diagenetic Os redistribution in ancient pelagic carbonate sequences. Even in the presence of strong concentration gradients (total KPB Os concentrations are elevated approximately 50-fold relative to background values at DSDP Site 577), diagenetic redistribution of Os is restricted to a length scale of 0.8 m over an approximately 65 Ma time span. This length scale is similar to that estimated by Lee et al. (2003) based on examining PGE concentration profiles across the KPB in a slowly accumulating pelagic clay sequence. Qualitatively we suspect that in more typical pelagic carbonate sequences, unaffected by large impact events and with modest concentration gradients, the typical length scale of diagenetic Os redistribution will be substantially reduced relative to the 0.8 m length scale estimated here.

2.6.4 Forcing of the marine Os record by Deccan volcanism

The refined late Maastrichtian Os isotope record presented here provides the impetus for a reassessment of Os isotope constraints on the timing of Deccan volcanism. Based mainly on data from DSDP Site 525, Ravizza and Peucker-Ehrenbrink (2003) concluded that the first major phase of Deccan volcanism straddled the C30n/C29r magnetic reversal boundary. This interpretation is consistent with more recent paleomagnetic (Chenet et al., 2008; Jay et al., 2008) and geochronologic results (Chenet et al., 2007; Widdowson & Kelly, 2008). This interpretation is predicated upon the assumption that the abrupt decline in the marine Os isotope record from $^{187}Os/^{188}Os$ of 0.6 to 0.4 was a direct consequence of Deccan volcanism. New data presented here show that the most significant portion of this decline occurs early in magnetochron C29r. During this initial $^{187}Os/^{188}Os$ decline the rate of change in $^{187}Os/^{188}Os$ in both the time and depth domain is less rapid than in the subsequent KPB-related decline. In the depth domain the decline spans between 2 to 3 m and there are no systematic changes in Os concentrations or PGE ratios during the decline. We argue that diagenetic remobilization cannot account for more than half the width of this feature, and likely much less. In the time domain the corresponding estimated duration of the decline is 200 ka, with a firm lower bound at 100 ka. It should be noted that because our age models are based upon the KPB and magnetic reversals C29r/C30n, changes to the assigned ages for these datums will adjust duration estimates accordingly.

Although there are other instances where large igneous province (LIP) formation is associated with excursions in the marine Os isotope record (Cohen & Coe, 2002; Tejada et al., 2006; Turgeon & Creaser, 2008), independent evidence of the timing of major volcanic activity is essential to fully exploiting the potential of the marine Os isotope record as a proxy indicator of LIP volcanism. For the late Maastrichtian, Ravizza and Peucker-Ehrenbrink (2003) suggested that much of the decline in the marine $^{187}Os/^{188}Os$ record was likely a consequence of Deccan volcanism eliminating a source of radiogenic Os from the Indian craton. Implicit in this interpretation is the idea that once weathering of radiogenic cratonic rocks is terminated by flood basalt emplacement, subsequent thickening of the pile of basaltic lavas need not further perturb the seawater $^{187}Os/^{188}Os$. This interpretation is motivated partly by the fact that the main Deccan province covered the Proterozoic and Archean Dharwar Province (Jerram & Widdowson, 2005). Additionally, Ravizza and Peucker-Ehrenbrink (2003) inferred that the Os inventory of Deccan lavas was too small to account for the observed change in seawater based on low Os concentrations of Deccan basalts (Allègre et al., 1999). Very high Os concentrations have been documented in lateritic soils from the Deccan (Wimpenny et al., 2007) but the significance of this finding to the present work is open to interpretation. These data may suggest that portions of the Deccan lava pile may contain an Os inventory much larger than implied by the published basalt analyses. Alternatively, if these high Os concentrations result from preferential Os retention in deeply weathered horizons, then one could argue the laterite Os data suggest basalt weathering does not release substantial Os to seawater.

In contrast, Cohen and Coe (2002, 2007) argue that in the case of the Central Atlantic Magmatic Province (CAMP), flood basalt emplacement and weathering added large amounts of unradiogenic Os to seawater, greatly increasing the flux of dissolved Os to the oceans. The distinction between the Deccan and CAMP interpretations has important implications for how the marine Os isotope record might be used to constrain the timing and duration of LIP volcanism. For the Deccan, Ravizza and Peucker-Ehrenbrink (2003) argued that the $^{187}Os/^{188}Os$ decline marked the onset of the initial major phase of volcanism. For the CAMP record, where emplacement and weathering of the volcanic pile is considered to be the primary cause of the Os isotope shift, the marine Os isotope record is interpreted as a more direct indicator of volcanic activity (Cohen & Coe, 2002, 2007). This comparison illustrates that even if one is willing to

accept the temporal coincidence of LIP emplacement with negative excursions in the marine Os isotope record as empirical evidence of a causal connection between the two, a more complete description of this connection is needed to understand in detail the relative timing of the Os isotope excursion and peak volcanism.

Two recent publications (Chenet et al., 2007; Keller et al., 2008) have renewed claims that Deccan volcanism may be a critical factor in the mass extinction at the end of the Maastrichtian. These arguments are based upon studies documenting large SO_2 fluxes associated with flood basalt eruption (Self et al., 2006; 2008) and putative Deccan eruption histories that concentrate eruptive volumes essentially at the KPB. While it is generally agreed that approximately 80% of the total thickness of Deccan erupted within magnetochron C29r, the distribution of volcanism within C29r prior to the KPB remains poorly constrained. Chenet et al. (2007) offer a fairly detailed description of Deccan eruptive history (summarized in Figure 2.6) based on K-Ar dating. This history draws upon biostratigraphic work demonstrating a KP age for intertrappen sediments within the Rajahmundry (Keller et al., 2008) and the proposed correlation of the upper and lower Rajahmandry outliers with the Mahabaleshwar and Ambenali formations, respectively. If correct this history places the most voluminous episode of the Deccan, the Ambenali formation, immediately prior to the KPB. Recent work (Chenet et al., 2008) argues for very rapid eruption rates (approximately 100 km^3/a) based on the stability of paleomagnetic poles within lavas up to 180 m thick with total volumes on the order of 20,000 km^3. Chenet et al. (2008) estimate fluxes of SO_2 from single eruption events within the Wai subgroup are comparable to the SO_2 flux estimated to have resulted from the Chicxulub impact event.

Even if we accept all the interpretations advanced in the preceding paragraph, the timing of the initial decline in the marine Os isotope record at the C29r/C30n reversal boundary is difficult to reconcile with the idea that SO_2 released by Deccan volcanism played an important role in the KPB extinction. Specifically we assert that it is likely that eruption rates and SO_2 fluxes associated with the flows emplaced early in C29r, presumably formations in the Kalsubai sub-group, were very similar to those emanating from the Ambenali. Note that recent direct measurements of sulfur in melt inclusions have confirmed the potential for large SO_2 fluxes from Kalsubai formations (Self et al., 2008) and rapid effusion is attributed to continental flood basalts

in general (Self et al., 2006). Consequently, it is difficult explain why an abrupt mass extinction should occur following emplacement of an eruptive unit that occurs in the upper third of the Deccan lava pile and represents less than 20% of it total eruptive volume, and not during the earlier phases of Deccan volcanism.

2.6.5 Possible link to Deccan volcanism & ocean acidification

As implied above, the marine Os isotope record suggests that the effects of Deccan volcanism should be more readily evident at the C29r/C30n reversal boundary, which we have interpreted as the onset of the main phase of Deccan volcanism. Evidence shows that extensive flood basalt volcanism, elevated atmospheric pCO_2 levels (Nordt et al., 2003) and global warmth (Thibault & Gardin, 2007; Wilf et al., 2003 and references therein) coincide within a time window of a few hundred thousand years. Comparison of Os isotope and foraminiferal oxygen isotope data show that the initial decline in $^{187}Os/^{188}Os$ is accompanied by a shift to oxygen isotope ratios indicative of warmer conditions (see Figure A1). The simplest interpretation of this coincidence is that Deccan volcanism played a causative role in increased atmospheric CO_2 levels and resulted in global warming, as previously suggested by Barrera and Savin (1999), Li and Keller (1999), Olsen et al. (2001) and Ravizza and Peucker-Ehrenbrink (2003). Although, the inferred magnitude and duration of warming cannot be readily explained as the result of the direct addition of volcanic CO_2 alone (Caldeira & Rampino, 1990; Self et al., 2006), significant shoaling of the lysocline and CCD are predictable consequences of this sort of perturbation to the global carbon cycle. This is illustrated clearly by study of carbonate dissolution associate with the Paleocene-Eocene Thermal Maximum (Zachos et al., 2005; Zeebe & Zachos, 2007). Results from several recent studies imply ocean acidification could reasonably result from Deccan volcanism. Self et al. (2006) estimates likely quantities of CO_2 to be 14 000 Gt and Self et al. (2008) estimate SO_2 released by Deccan volcanism to be 3500-5400 Gt. This large burden of carbon dioxide and sulfuric acid would significantly perturb ocean carbonate chemistry (D'Hondt et al., 1994; Sohsuke & Sujita, 2006). Model results aimed at assessing the impact of CAMP volcanism on ocean carbonate chemistry (Berner & Beerling, 2007) concluded that volcanic SO_2 would significantly enhance dissolution and that whole ocean undersaturation with respect to calcite was possible if the eruption interval was sufficiently brief.

Although pursuing a Deccan ocean acidification hypothesis is speculative, it is justified in the context of this work. The concentrations of Ir and $CaCO_3$ collected as part of this study suggest that the sedimentary signal of ocean acidification caused by Deccan volcanism may be preserved in these Maastrichtian pelagic carbonate sequences. Figures 2.1 - 2.4 show that Ir concentrations increase close to the C29r/C30n magnetic reversal at all sites except the shallow DSDP Site 525. If Ir is considered to be a quasi-constant flux tracer (Dalai & Ravizza, 2006) then increased Ir concentrations indicate diminished $CaCO_3$ burial flux. While it is possible Deccan volcanism provided a significant additional source of Ir to seawater (Zoller et al., 1993), Pt/Ir ratios do not support a change in PGE source prior to the decline in Pt/Ir ratios close to the KPB. For this reason we prefer to interpret the increase in bulk sediment Ir concentrations at Bottaccione, ODP Site 690 and DSDP Site 577 as evidence of a decrease in carbonate burial flux rather than an increase in Ir flux. Low-resolution $CaCO_3$ data from ODP Site 690 and DSDP Site 577 are grossly consistent with this interpretation (Figure 2.7). Together the Ir and $CaCO_3$ data are permissive evidence suggesting that a global episode of diminished carbonate production and/or seafloor carbonate dissolution began close to the C29r/C30n magnetic reversal. We speculate that decreased $CaCO_3$ burial fluxes may be a consequence of ocean acidification caused by Deccan volcanism. An unambiguous dissolution event very early in magnetochron C29r at DSDP Site 527 (paleodepth 2700 m) has been documented by careful study of fragmentation of foraminifera, but was interpreted as a consequence of a basin scale reorganization of deepwater circulation (Kucera et al., 1997) rather than the global phenomenon as we suggest here. Additionally, a recent examination of nannofossil assemblages at Site 525A (Thibault & Gardin, 2007) did not find evidence of varying levels of preservation. However, these workers did find evidence for pulses of what they termed high-stress environmental conditions, one of these they attribute to Deccan-induced warming. Using this conceptual framework we predict that significant deep-sea carbonate dissolution is associated with the initial rapid decline in the marine $^{187}Os/^{188}Os$ record. Confirmation of our prediction would constitute independent evidence supporting the interpretation that the abrupt shifts to lower seawater $^{187}Os/^{188}Os$ are caused by Deccan volcanism. Moreover if evidence of extensive dissolution persists into the $^{187}Os/^{188}Os$ plateau at ≈ 0.4 prior to the KPB, this will indicate that the marine Os isotope record may serve as a reliable indicator of the onset of major flood basalt volcanism, but not for eruptive duration or volume.

2.7 Conclusion

The osmium isotope record of the Maastrichtian has a coherent structure, characterized by two geochemically and temporally distinct declines leading up to the KPB. This pattern is seen in the four pelagic carbonate sections studied, and agrees well with previously published records. Additionally, the agreement between the subaerial carbonate section (Bottaccione) and the marine carbonate sections (DSDP and ODP Sites) demonstrates the robustness of bulk sediment osmium isotope analyses in recovering a global seawater signature. The initial decline in $^{187}Os/^{188}Os$ is coeval with an abrupt and transient warming event, an increase in atmospheric CO_2, and a potential suppression of carbonate burial, and is consistent with an interpretation of Deccan volcanism as the cause of this initial decline. $^{187}Os/^{188}Os$ records may be used to constrain the onset of Deccan volcanism, but may not constrain its duration.

Acknowledgements

We wish to thank the following individuals who assisted us during the course of this research. Denys VonderHaar (UH) and Tracy Atwood (WHOI) provided essential support in the lab. The Popp Lab (UH) and Steve Manganini (WHOI) assisted with carbonate analyses. The manuscript was improved by helpful comments from four reviewers: Martin Frank, Christian Koeberl, Cin-Ty Lee, and Troy Rasbury. This research used samples and data provided by the Integrated Ocean Drilling Program (IODP). Funding for this research was provided by NSF (EAR0309264 to GR and OCE0526559 to GR and BPE). This is SOEST Contribution # 7628. This is publication no. 32 of the Centro di Geobiologia of the Urbino University.

Tables

Table 2.1: Contributions of lithogenic and oceanic Os in pelagic carbonates

Calculated fractional contributions of lithogenic and cosmic Os to the total Os inventory of pelagic carbonates.

	f_{lith} Fraction lithogenic matter Based on [Al] $=[Al]_{sm}/[Al]_{ucc}$[d]	f_{lith} Fraction lithogenic matter Based on $CaCO_3$ $=1-f_{CaCO3}$	$f_{lith}Os$[a] Fraction lithogenic Os Based on [Al] $=f_{lith}*[0s]_{ucc}/[Os]_{sm}$	$f_{lith}Os$[a] Fraction lithogenic Os Based on $CaCO_3$ $=f_{lith}*[0s]_{ucc}/[Os]_{sm}$	Sediment MAR[b] Mass Accumulation Rate (g/cm^2*kyr) $=DBD*SR$	$f_{ET}Os$[c] Fraction cosmic Os Os_{ET} burial flux= 1.5 pg/cm^2kyr	$f_{ET}Os$[c] Fraction cosmic Os Os_{ET} burial flux= 3.5 pg/cm^2kyr
DSDP Site 525	0.27 to 0.51[e]	0.24 to 0.45[f]	0.159 to 0.393	0.139 to 0.432	0.44 to 2.82	0.014 to 0.074	0.034 to 0.173
DSDP Site 577	0.006 to 0.036[e]	0.005 to 0.074[f]	0.003 to 0.096	0.006 to 0.251	0.46 to 1.2	0.023 to 0.468	0.054 to 1.092
ODP Site 690	0.04 to 0.17[e]	0.03 to 0.19[f]	0.03 to 0.45	0.04 to 0.62	0.244 to 2.77	0.008 to 0.344	0.02 to 0.802
Bottacione, Gubbio, IT	–	0.028 to 0.084[f]	–	0.019 to 0.137	0.90 to 3.73	0.008 to 0.1	0.019 to 0.3

[a] $[Os]_{UCC}=30$ ppt, Peucker-Ehrenbrink and Jahn (2001).
[b] DBD = sediment dry bulk density (DBD) and SR = sedimentation rate.
[c] $f_{ET}Os = Os_{ET}$ burial flux / Os_{total} burial flux; Os_{total} burial flux $=[Os]_{total}$ * MAR.
[d] $[Al]_{UCC}=8$ wt.%, McLennan (1995).
[e] Al concentrations ranges: DSDP Site525, Chamley et al. (1984); DSDP Site 577, Michel et al., 1985; ODP 690, Supp. Table 3.
[f] Wt. fraction $CaCO_3$: DSDP Site 525, Kucera et al. (1997); DSDP Site 577, Supp. Table 3; ODP 690, Supp. Tables 2 and 3; Bottaccione, Alvarez et al., 1990.

Table 2.2: Characteristics of potential sources of PGEs to pelagic sediments.

	$^{187}Os/^{188}Os$	Os (pg/g)	Os/Ir	Pt/Ir
Modern seawater	1.06[a]	0.01[a]	≈100[b]	≈500[c]
Riverine runoff	1.4[a]	≈0.01[a]	≈5[b]	–
Eolian dust/loess	1.05[d]	30[d]	1.4[d]	23.2[d]
Chondrite/cosmic dust	0.12–0.13[e]	$\approx 5\times10^{5}$ [e]	1.08[e]	1.98[e]
Deccan basalts (initial)	0.129[f]	≈15[f]	≈0.5[g]	10–300[g]

[a] Peucker-Ehrenbrink and Ravizza (2000).
[b] Lee et al. (2003).
[c] Ravizza (2001).
[d] Peucker-Ehrenbrink and Ravizza (2000).
[e] Horan et al. (2003).
[f] Allègre et al. (1999), estimated initial ratio.
[g] Crocket and Paul (2004).

Figures

Figure 2.1 DSDP Site 577 Shatsky Rise

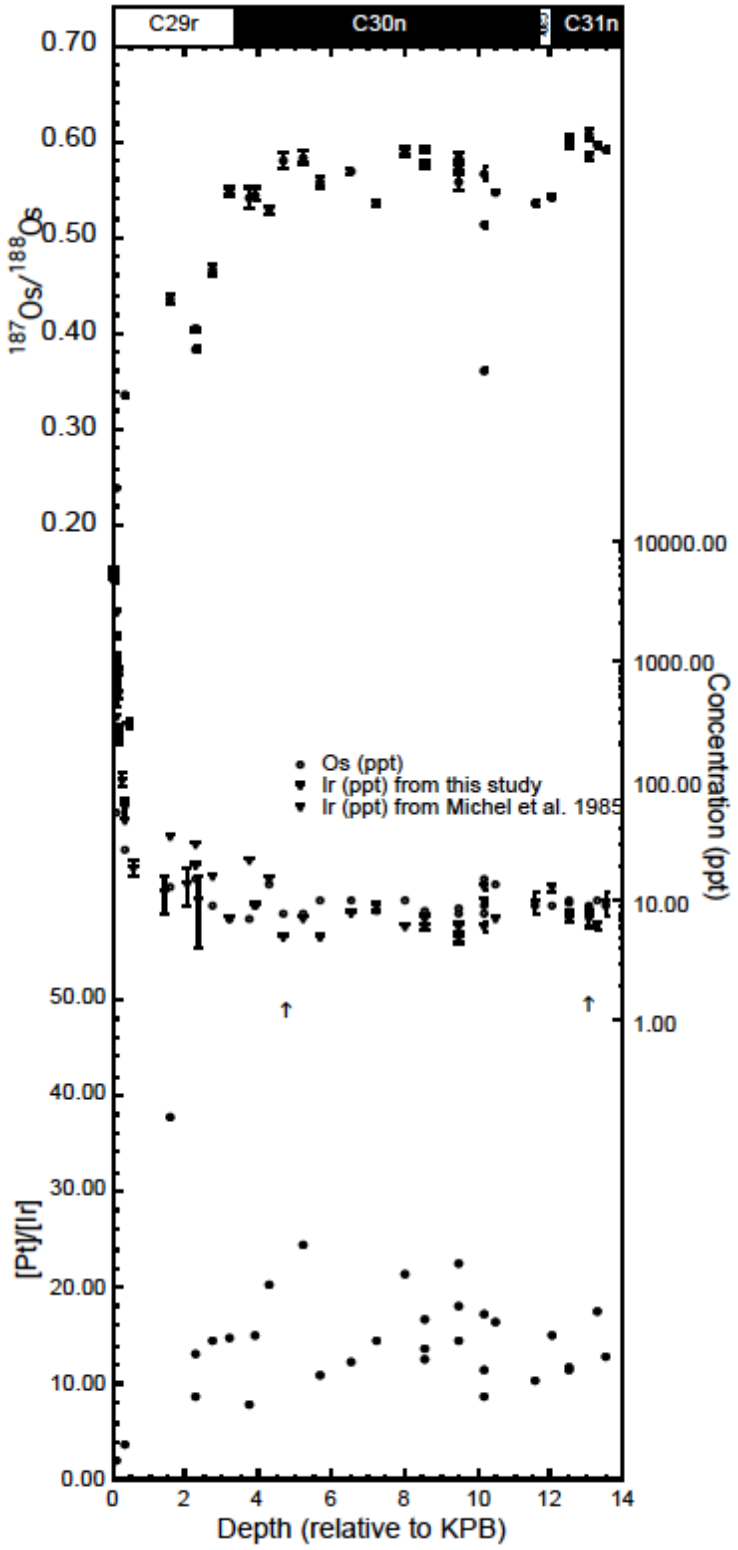

Figure 2.1 Depth view comparison of $^{187}Os/^{188}Os$, Os and Ir concentrations, and Pt/Ir ratios from DSDP Site 577. Depth is given in meters below KPB, which plots at left axis. Ir concentration data are from this study (■) and from Michel et al., 1985 (▼). Arrows indicate Pt/Ir ratios that plot above the axis range (Table A4). Two sigma standard error bars derived from counting statistics are plotted for $^{187}Os/^{188}Os$ data. Where error bars are not evident they are smaller than the symbols used.

Figure 2.2 ODP Site 690 Maud Rise

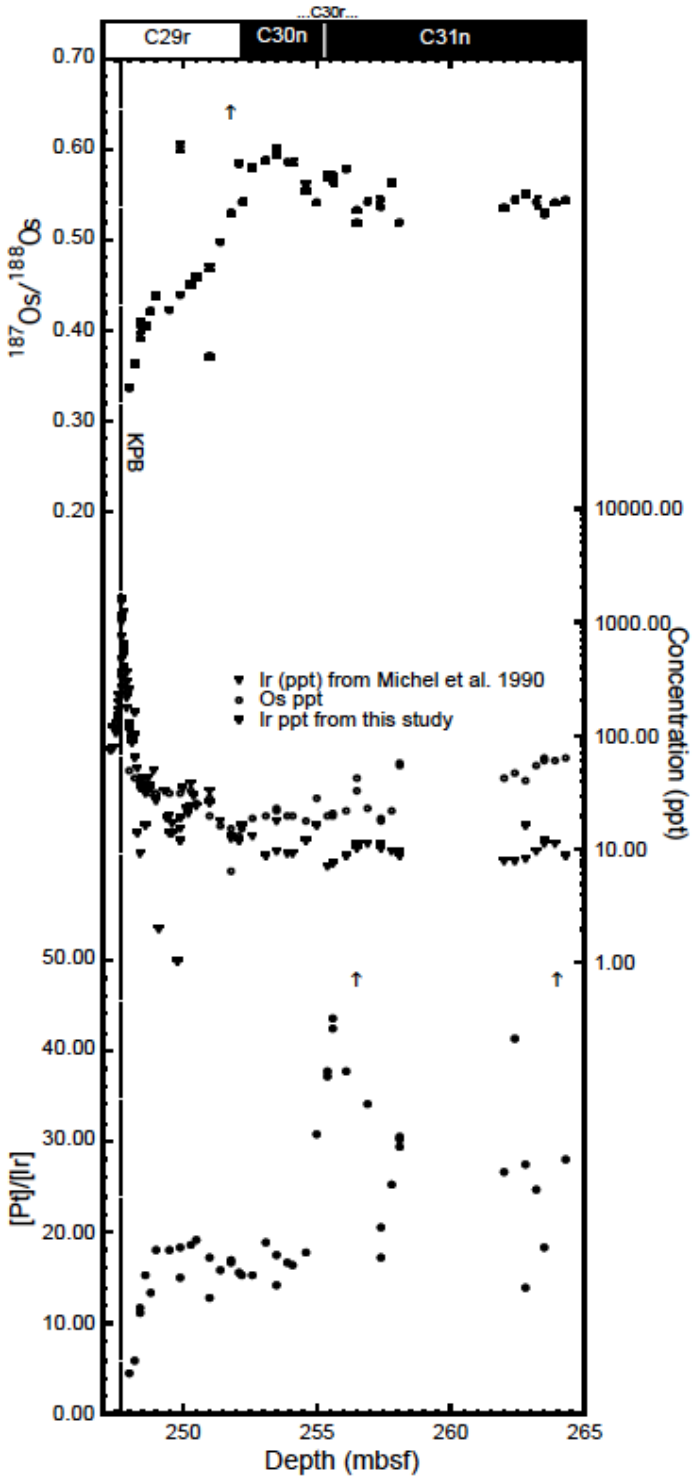

Figure 2.2 Depth view comparison of $^{187}Os/^{188}Os$, Os and Ir concentrations, and Pt/Ir ratios from ODP Site 690. Ir concentration data are from this study (■) and from Michel et al., 1990 (▼). Arrows indicate a replicate $^{187}Os/^{188}Os$ datum and Pt/Ir ratios that plot above the axis range (Table A5). The bottom of C30n was selected as 255 mbsf (Hamilton, 1990) while the depth of the top of C31n is not specified (Table A1). Therefore the location and duration of C30r is approximate. Two sigma standard error bars derived from counting statistics are plotted for $^{187}Os/^{188}Os$ data. Where error bars are not evident they are smaller than the symbols used.

Figure 2.3 Bottacione Gorge in Gubbio, Italy

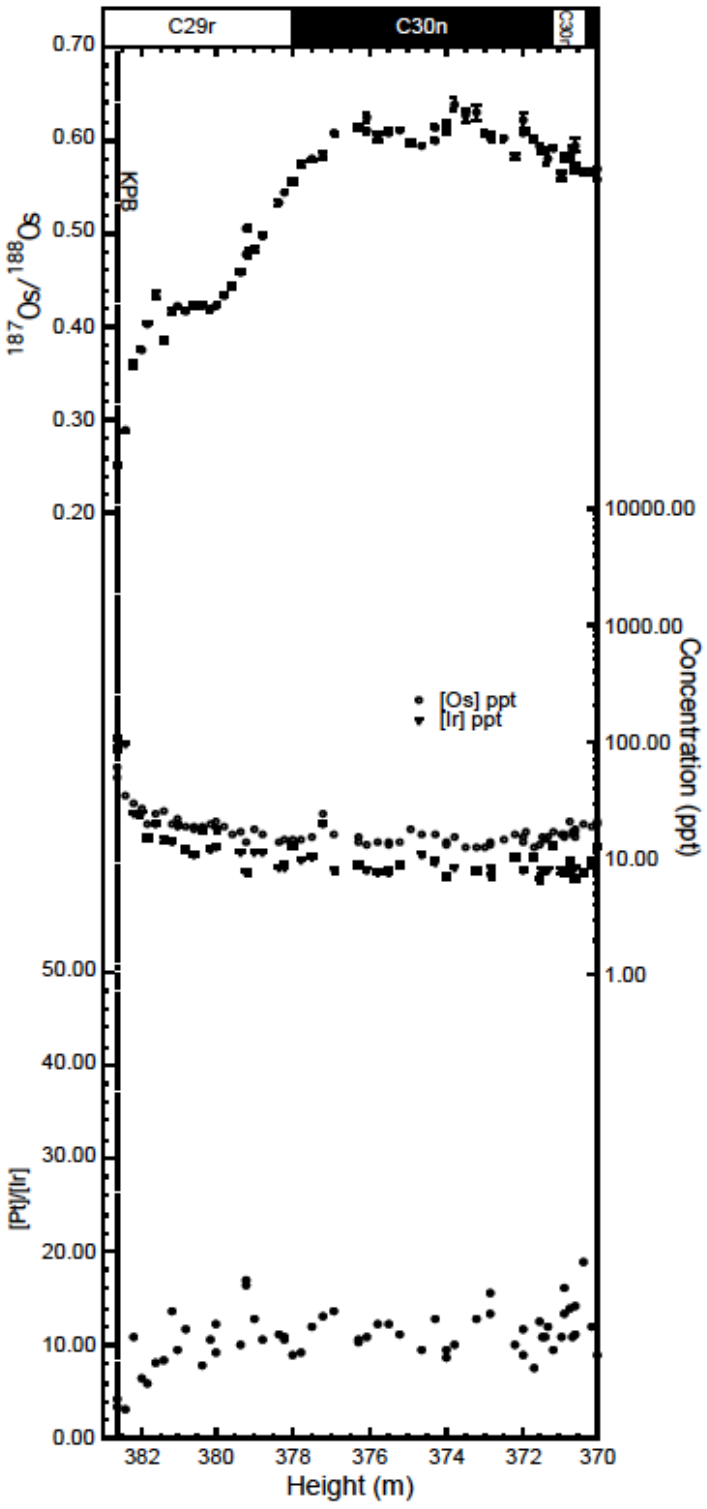

Figure 2.3 Depth view comparison of $^{187}Os/^{188}Os$, Os and Ir concentrations, and Pt/Ir ratios from Bottaccione Gorge in Gubbio, Italy. Two sigma standard error bars derived from counting statistics are plotted for $^{187}Os/^{188}Os$ data. Where error bars are not evident they are smaller than the symbols used.

Figure 2.4 DSDP Site 525 Walvis Ridge

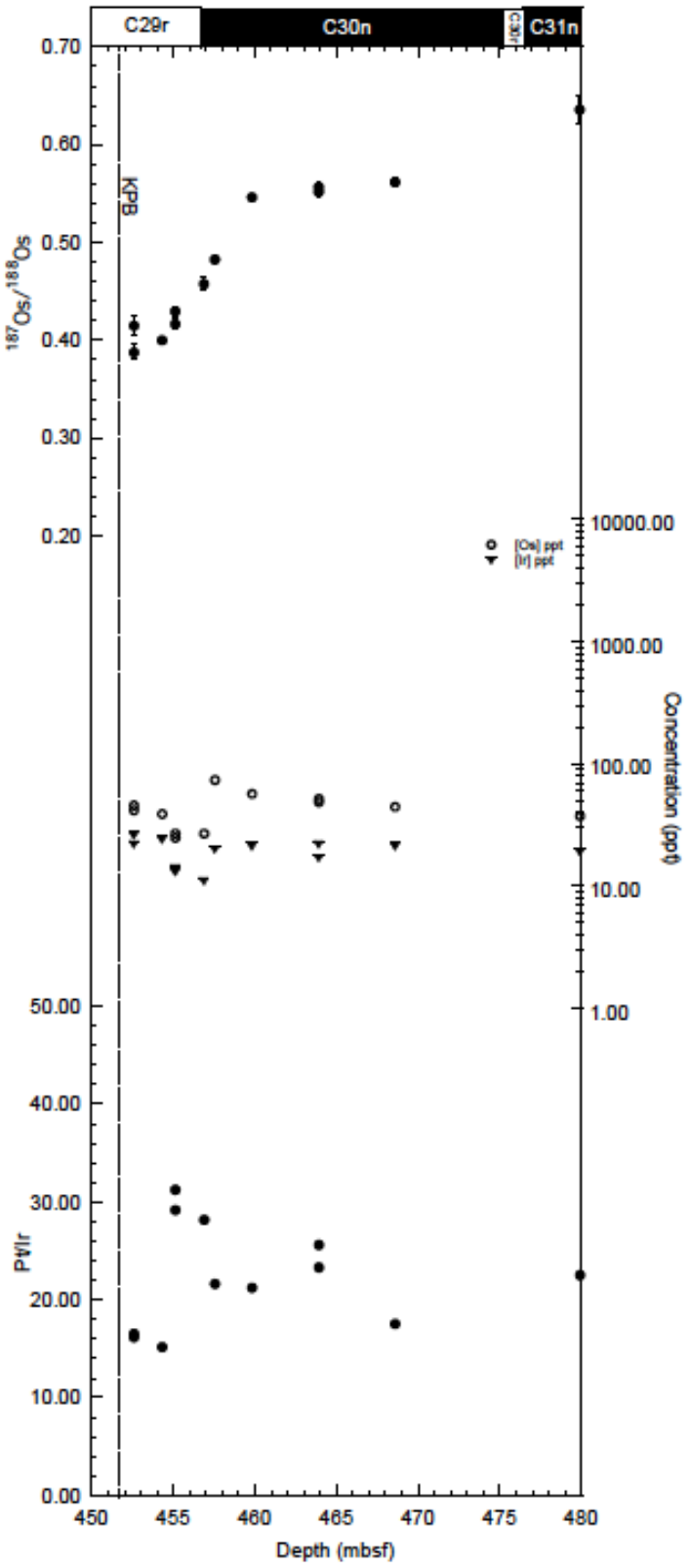

Figure 2.4 Depth view comparison of $^{187}Os/^{188}Os$, Os and Ir concentrations, and Pt/Ir ratios from DSDP Site 525. Two sigma standard error bars derived from counting statistics are plotted for $^{187}Os/^{188}Os$ data. Where error bars are not evident they are smaller than the symbols used.

Figure 2.5 Composite $^{187}Os/^{188}Os$ record for the late Maastrichtian

Age view comparison of $^{187}Os/^{188}Os$ from 4 study sites: DSDP Site 577 (▼), ODP Site 690 (●), Bottaccione Gorge, Gubbio (○) and DSDP Site 525(✠). The top of C31n is not used in the age model for ODP Site 690 (see text and Table A1). Where error bars are not evident, they are smaller than the symbols used.

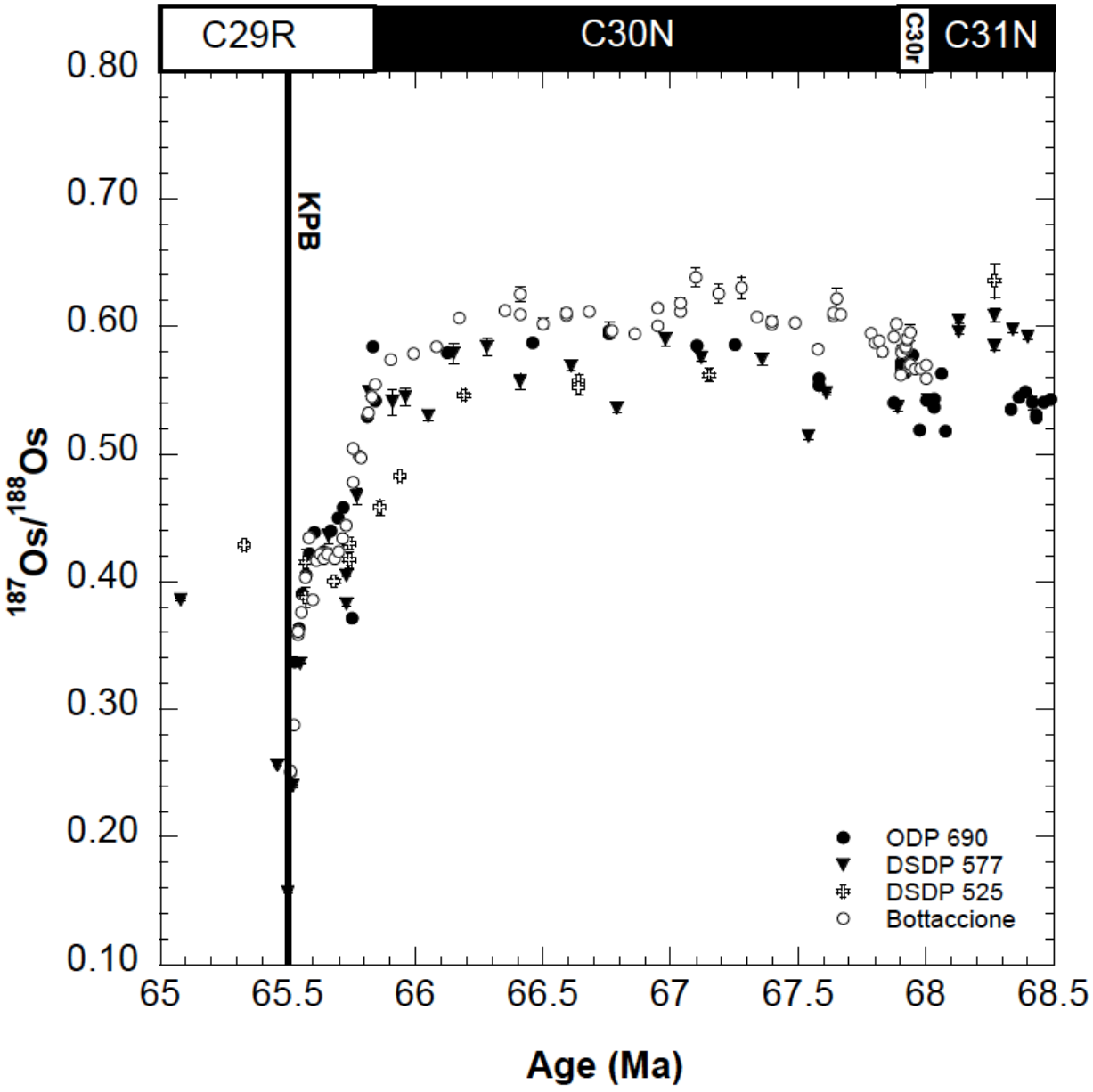

Figure 2.6 Stratigraphic sequence for the Deccan Basalt Group comparison with Bottaccione $^{187}Os/^{188}Os$ record.

A comparison of proposed stratigraphic sequence of Deccan Basalts with $^{187}Os/^{188}Os$ data from Bottaccione Gorge and proposed stages of volcanism from Chenet et al. (2007). Magnetochron and eruptive volume assignments are from Self et al. (2006). The eruptive stages from Chenet et al. (2007) are located as follows: Stage 1 occurred near the C30n/C30r reversal boundary; Stage 2 began somewhere in C29r and terminated precisely at the KPB; Stage 3 began in upper C29r and ended in C29n. The 2.5 Ma duration for the period of quiescence is from Chenet et al. (2007) and does not follow from the age model used here. Dates for magnetic reversals are from Hicks et al. (2002). Eruption rates and SO_2 fluxes associated with the flows emplaced early in C29r (Kalsubai) were similar to those emanating from the Ambenali. We question why an abrupt mass extinction would result from the emplacement of an eruptive unit in the upper third of the Deccan lava pile representing less than 20% of its total eruptive volume, and not elsewhere in Deccan.

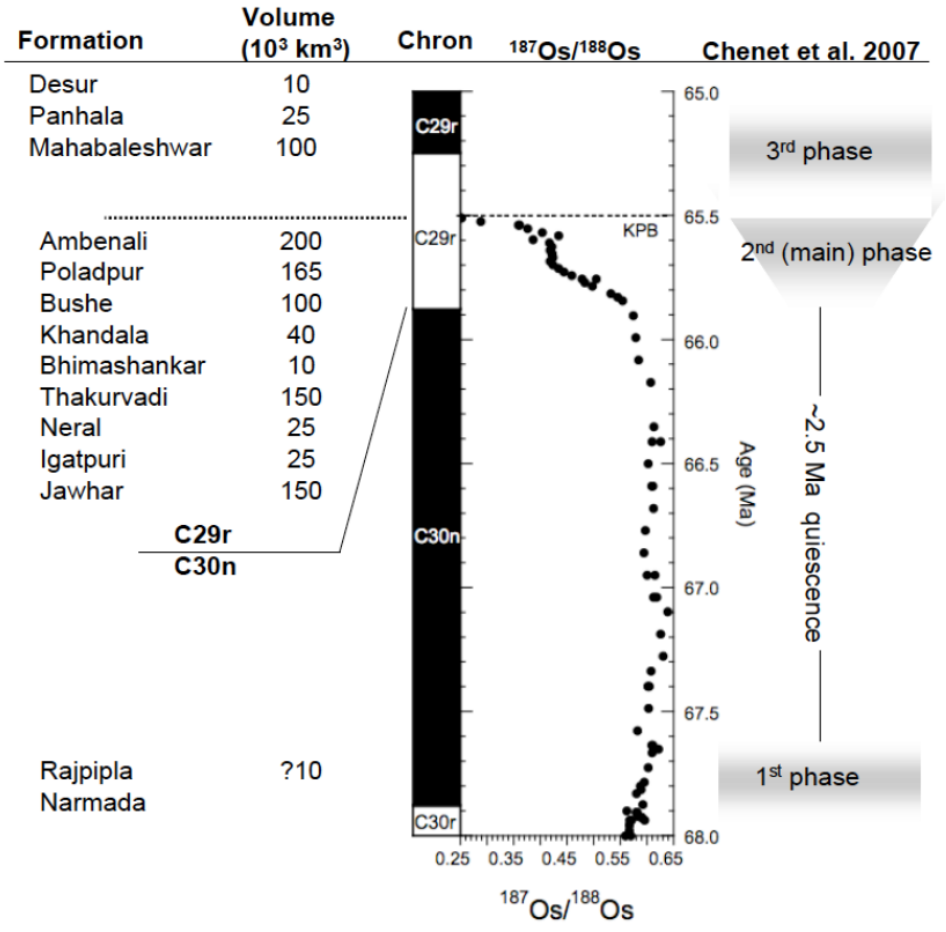

Figure 2.7 Weight % $CaCO_3$ from ODP Site 690C and DSDP Site 577

$CaCO_3$ (wt%) for DSDP Site 577 and ODP Site 690 plotted with Ir concentration. Spikes in Ir concentrations tend to coincide with decreases in wt% $CaCO_3$, and are interpreted here as potential evidence of suppressed calcium carbonate accumulation. We note a decrease from 97 to 94 wt% $CaCO_3$ could represent dissolution of half the original sediment present (doubling the fraction of the non-$CaCO_3$ component of the sediment). Calcium carbonate data for DSDP Site 577 (●) is previously unpublished elemental analyzer data from WHOI. Calcium carbonate data for ODP Site 690 (◆) is elemental analyzer data from this study.

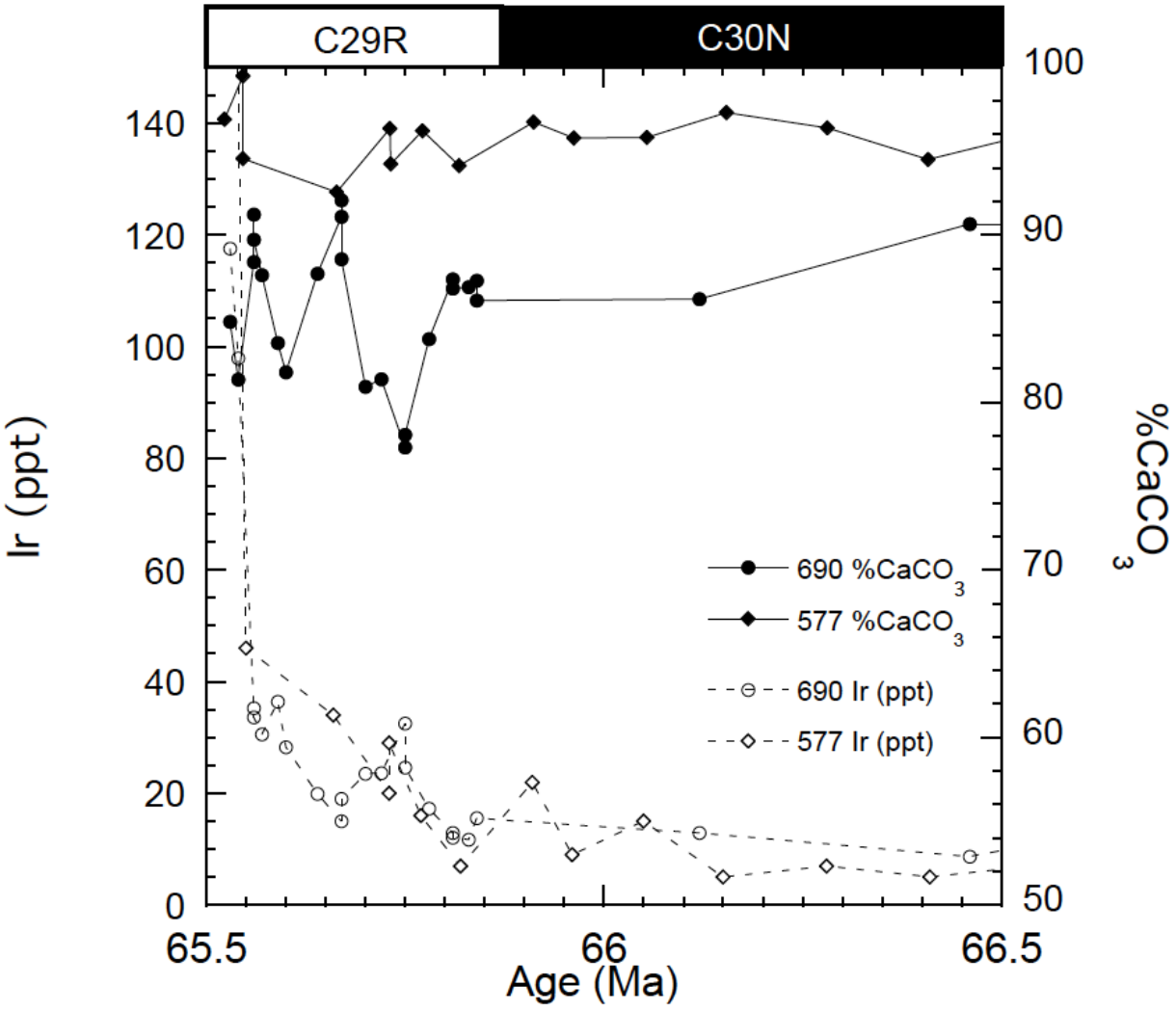

Chapter Three:
Reconsidering the Late Maastrichtian Marine Os Isotope Record: Revised Age Model and Timing of Deccan Eruptive Stages, and a Comparison to other LIP Events

Since the publication of Chapter 2 (Robinson et al., 2009) newer studies have revised the date of the Cretaceous-Paleogene Boundary (K-Pg) and the timing of the emplacement of major episodes of Deccan volcanism relative to the K-Pg. This chapter presents the data from Robinson et al. (2009) using a revised age model from Gradstein et al. (2012), and further discusses recent conclusions on the timing of eruptive episodes of the Deccan Traps (Renne et al., 2015; Schoene et al., 2015). These more recent studies are entirely consistent with the original interpretation presented in Robinson et al. (2009) that the initial decline in $^{187}Os/^{188}Os$ of global seawater primarily results from main phase Deccan volcanism that begins within C29r. In addition, these new studies have important implications for the duration of this decline, which are discussed further below.

As more and more studies measure $^{187}Os/^{188}Os$ in attempts to resolve the timing of large igneous provinces (LIP) emplacements relative to mass extinction events, it has become clear that the record of $^{187}Os/^{188}Os$ at the K-Pg and onset of main stage Deccan volcanism is very different from the $^{187}Os/^{188}Os$ records at the time other LIP events. Approximately 200 ka prior to the K-Pg, $^{187}Os/^{188}Os$ values drop from 0.6 down to 0.4 in a gradual decline from one relatively steady state to a new steady state, which Robinson et al. (2009) argued reflected the covering of radiogenic (high $^{187}Os/^{188}Os$) continental rock with unradiogenic Deccan basalts (low $^{187}Os/^{188}Os$). Records from other LIP events, such as the Central Atlantic Magmatic Province (CAMP), record transient excursions from radiogenic $^{187}Os/^{188}Os$ values down to extremely unradiogenic values of $^{187}Os/^{188}Os$ before recovering to pre-event or near pre-event values. A transient dip to unradiogenic $^{187}Os/^{188}Os$ values is generally interpreted as recording an increased flux of unradiogenic Os from a mantle source, while excursions to more radiogenic values are taken as an indication of increased flux from continental sources due to higher weathering rates, thought to be driven by increased temperatures. This chapter will compare and contrast the $^{187}Os/^{188}Os$ profiles from different LIP events and argue that interpretations to date of LIP related excursions in $^{187}Os/^{188}Os$ have been overly simplistic.

3.1 Revised Age Models

3.1.1 Gradstein et al. (2012)

The age model used in Robinson et al. (2009) was based on magnetostratigraphy (see section 2.3). A revised calibration of the magnetostratigraphy for the end Maastrichtian/early Danian is given in Gradstein et al. (2012), with a revised date for the K-Pg of 66.04 Ma, based on cyclostratigraphy and orbital tuning (Husson et al., 2011). Data from Robinson et al. (2009) presented using this updated age model can be found in Appendix B.

The motivation for presenting the data with an updated age model is primarily to allow the data to be easily compared to more recent studies using 66.04 Ma for the K-Pg, and continue to be utilized by future studies. Presenting the data with this refined age model notably does not change any of our original conclusions, and speaks to the robustness of the findings.

As shown in Table 3.1 revising the age model results in only minor changes in the duration of most important sections of the record: The time period spanning from the K-Pg to the C29r/C30n reversal becomes 8% longer, and the period from the C29r/C30n reversal to the C30n/C30r reversal becomes 12% shorter. The section of the record affected most by revising the age model is the period from C30n/C30r to C30r/C31n: This section becomes 38% longer, changing from a duration 125 ka to 173 ka. However, there are relatively few data points in this section compared to the rest of the record, and changing the duration of this section does not affect the conclusions of the original study. For example, Robinson et al. (2009) argued that the duration of the initial decline in $^{187}Os/^{188}Os$ of seawater from ~0.6 to ~0.4 was approximately 200 ka with a firm lower boundary of 100 ka. Adjusting these durations to account for the new age model results in an approximately 216 ka span with a lower boundary of 108 ka, demonstrating how small the affect of changing the age model is to our interpretation of the record. Essentially, age datums are shifted earlier with minimal changes to the length of each section (Figure 3.1). Likewise, changes to mass accumulation rates and calculations of the fraction of extraterrestrial Os within the overall Os budget are minimal (see Table 2.1 in Chapter 2 vs. Table A2).

3.1.2 Revised date for the C30n/C29r Reversal Boundary

Two recent studies have proposed a revised age for the C29r/C30n boundary that substantially shortens the duration of the Cretaceous portion of C29r and affecting all rate calculations in this period. Schoene et al. (2015) proposed a revised age of 66.288 ± 0.0277 Ma for C29r/C30n, based on U-Pb zircon geochronology. Using this date yields a 248 ka duration for the Cretaceous C29r, 26% shorter than the 333 ka used in Robinson et al. (2009), a significant shortening. Sprain et al. (2015) proposed an age of 66.195 ± 0.043 Ma for C29r/C30n using Ar-Ar dating. This date yields a duration of 155 ka for the Cretaceous C29r, 47% shorter than 333 ka. In other words, rates calculated for events in Cretaceous C29r would be almost twice as rapid. Yet even though both new radiometric dates have very low uncertainty, they are contradictory and uncertainties do not overlap (Thibault & Husson, 2016). Neither are these ages concordant with numerous other studies which use cyclostratigraphy to calculate the Cretaceous portion of C29r and yield an average age of 66.397 ± 0.036 Ma for C29r/C30n (Thibault & Husson, 2016). Thibault and Husson (2016) suggest reconciling these differences by revising the age for the K-Pg to the upper limit of the uncertainty provided by Renne et al. (2013). This would shift the age of the K-Pg from the currently accepted 66.043 Ma to 65.957 Ma. By doing so, the calculated duration of Cretaceous C29r using the 66.288 ± 0.0277 Ma age from Schoene et al. (2015) is 331 ka and in closer accordance with the durations yielded from cyclostratigraphy (Table 3.2).

Clearly the discrepancies surrounding the duration of Cretaceous C29r need to be further resolved before quantitative calculations of emplacement rates of Deccan eruptive events, emission rates and volumes of associated greenhouse gases, and calculated environmental affects can be definitively stated.

3.1.3 Robinson et al. (2009) in the context of refined ages of Deccan lava flows

Schoene et al. (2015) also presents new insights on the relative timing of various phases of Deccan emplacement using U-Pb dating, as does Renne et al. (2015) using Ar-Ar dating. Models of the timing of Deccan main phase eruption continue to be plagued by an inability to precisely locate the K-Pg within the flows. These models locate the K-Pg in the time domain using a calculated duration of C29r and an interpreted location of the C29r/C30n reversal

boundary. Where Chenet et al. (2007) argued the voluminous Ambenali formation occurred just prior to the K-Pg, both Renne et al. (2015) and Schoene et al. (2015) place it after the K-Pg (Figure 2.6 and Figure 3.2).

Importantly, Robinson et al. (2009) argued that it was not this peak of Deccan volcanism that caused the $^{187}Os/^{188}Os$ transition from 0.6 to 0.4, but instead the onset of main phase eruptions, and all three studies agree that main phase Deccan volcanism began at or just before the C29r/C30n reversal. Therefore these findings remain consistent with the interpretation of the Os record presented in Robinson et al. (2009): It was the covering of radiogenic continental crust rather than an increased flux of unradiogenic Os from mantle sourced magmas which most influenced the shape of the $^{187}Os/^{188}Os$ profile.

Shifting the timing of the emplacement of the Ambenali formation from before the K-Pg to after the K-Pg has a greater implication for the affects of volcanism on the atmosphere than it does for the interpretation of the Os record. If the majority of the main eruptive phase of Deccan occurs post K-Pg, then the climatic affects of CO_2 and SO_2 could not have contributed to the initial extinctions at the K-Pg. Alternately, shortening the duration of the Cretaceous section of C29r by ~26% following the age datum provided in Schoene et al. (2015) and Sprain et al. (2015) would compress the output of CO_2 and SO_2 to the atmosphere into a shorter timespan, presumably amplifying the environmental consequences of these emissions.

Robinson et al. (2009) speculated that decreased $CaCO_3$ burial fluxes early in C29r measured at ODP Site 690C and DSDP Site 577 were a consequence of ocean acidification caused by Deccan volcanism (see Chapter 2, section 2.6.5). Additional evidence for ocean acidification prior to the K-Pg is presented in Henehen et al. (2016). Proxy temperature records show a transient warming event within the Cretaceous portion of C29r previously interpreted as a result of Deccan volcanism (Barrera & Savin, 1999; Li & Keller, 1999; Wilf et al., 2003), coincident with evidence of decreased carbonate preservation from multiple locations (Henehen et al., 2016; Figure 3.3). So while recent dating of Deccan lava formations support the interpretation that the most voluminous Deccan flows were emplaced either shortly prior to or immediately after the K-Pg, evidence of decreased $CaCO_3$ preservation and transient warming coincident with the

decrease in $^{187}Os/^{188}Os$ early in C29r, strongly argues that the environmental affects of Deccan volcanism were felt ~400 ka prior to the K-Pg.

3.2 How the $^{187}Os/^{188}Os$ signature of Deccan differs from other LIP events

The relative timing of LIP eruptions is very important because they are often temporally associated with mass extinction events, and invoked as their cause (see Figure 3.4, Bond & Wignall, 2014). Osmium isotopes are increasingly used to determine the onset and duration of LIP emplacement: Simplistically, a large and rapid excursion from high (radiogenic) to low (unradiogenic) $^{187}Os/^{188}Os$ values is interpreted as the onset of an eruptive event, and a return to pre-excursion values is interpreted as the end of an eruption event and/or an increased weathering of radiogenic continental rock that results from volcanic-driven warming. If this scenario accurately describes the behavior of the Os isotopic record, then one would expect the shape of its curve to look the same at the onset of each LIP event, and behave roughly the same throughout the duration of the LIP emplacement. While this scenario is grossly consistent with existing records, there are significant differences in the structure and durations of LIP-associated $^{187}Os/^{188}Os$ excursions that cannot be ignored. By comparing the Os records from five large scale magmatic events, we will illustrate that there is not a consistent $^{187}Os/^{188}Os$ response to LIPs.

3.2.1 Deccan Traps across the Cretaceous-Paleogene Boundary

The complete record of the Os isotopic curve across the K-Pg revealed by combining the results from Robinson et al. (2009) and Ravizza and Vonderhaar (2012) clearly shows the initial decline from 0.6 to 0.4, the second K-Pg impact driven decline from 0.4 to 0.13, and the subsequent recovery after the K-Pg to 0.4 (Figure 3.5). Additional unpublished data from DSDP Site 524 show the post K-Pg steady state in $^{187}Os/^{188}Os$ persists for at least 2 Ma through C28r (Figure 3.6, Greg Ravizza, personal communication). Correlation with a transient warming at the C29r/C30n boundary recorded by oxygen isotopes, and evidence from [Pt]/[Os] and [Os]/[Ir] ratios strongly argues that the initial decline is caused by the emplacement and weathering of Deccan basalts, while [Ir] and [Os] show the second decline leading into the K-Pg records the K-Pg impact event (see Chapter 2, Robinson et al., 2009).

Deccan is the only LIP event discussed in this study with unambiguous evidence of a major extraterrestrial impact event during its emplacement. This complicates the understanding of the environmental consequences of the Deccan eruption and the interpretation of the Os isotope record.

3.2.2 Central Atlantic Magmatic Province (CAMP) at the Triassic-Jurassic Boundary

The mass extinction marking the Triassic-Jurassic boundary (T-J) at 201.3 Ma is counted among the "big five" extinction events of the Phanerozoic, with dramatic losses of both marine and terrestrial species (Figure 3.7). Major environmental changes include a destabilization of the carbon cycle, increased atmospheric CO_2 and 3°- 6° C warming (see Bond & Wignall, 2014 and sources therein). The rapidity and severity of the environmental changes recorded argue for extensive volcanism (Cohen & Coe, 2007). Blackburn et al. (2013) link the end-Triassic extinction event with emplacement of the Central Atlantic Magmatic Province (CAMP), extensive flood volcanism that is associated with the breakup of Pangea and initial rifting of the Central Atlantic. CAMP began in the latest Triassic, with peak extrusive activity occurring at ~201 Ma, erupting primarily in several intense pulses with most volcanism occurring in less than 20 ka (Bond & Wignall, 2014 and references therein).

Pacific and Atlantic records of the T-J Boundary both show decreased $^{187}Os/^{188}Os$, but the records do not agree in detail. Kuroda et al. (2010) show that $^{187}Os/^{188}Os$ begins to gradually decrease about ~3 Ma prior to the T-J, a decline they interpreted as caused by the gradual increased flux of unradiogenic Os to the oceans from the initial onset of CAMP volcanism (Figure 3.8). About 1 Ma prior to the T-J, $^{187}Os/^{188}Os$ reaches a minimum and then begins to gradually increase from ~0.2, reaching ~0.6, a result Kuroda et al. (2010) argue reflects the increased flux of radiogenic Os from enhanced continental weathering, presumably due to volcanism-induced warming. Cohen and Coe (2007) place the $^{187}Os/^{188}Os$ minimum measured at St. Audrie's Bay at the T-J, while Kuroda et al. (2010) place the $^{187}Os/^{188}Os$ minimum from Kurusu about ~1 Ma prior to the boundary, a difference Kuroda et al. (2010) attributes to the proximity of the St. Audrie's Bay samples to the CAMP: They argue that since St. Audrie's Bay is so close to CAMP, it would have continued to be dominated by the flux of unradiogenic Os from CAMP, and $^{187}Os/^{188}Os$ values would have continued to decline longer than in other areas,

and remove a portion of the total unradiogenic flux to the oceans before it had the chance to fully circulate. Therefore, the increase in radiogenic Os from enhanced weathering would be apparent earlier in the record at sites further from CAMP such as Kurusu.

The Os isotopic record from CAMP presented by Cohen and Coe (2007) and Kuroda et al. (2010) spans several million years, and therefore the structure in the record reflects a very different time scale than that of the Os record at Deccan presented in Robinson et al. (2009) and Ravizza and Vonderhaar (2012). Additionally Robinson et al. (2009) and Ravizza and Vonderhaar (2012) show multiple records with a well-correlated change in $^{187}Os/^{188}Os$, whereas the records from Kurusu and St. Audrie's Bay have a calculated 1 Ma offset in the $^{187}Os/^{188}Os$ minimum. Volumetrically CAMP was one of the largest LIPs of the Phanerozoic (Nomade et al., 2007) so it seems reasonable that its initial gradual emplacement would affect $^{187}Os/^{188}Os$ by gradually forcing it to lower values, before increased weathering drove $^{187}Os/^{188}Os$ values back up. Yet by the same reasoning, it seems very unlikely that $^{187}Os/^{188}Os$ values at St Audrie's Bay would reach its minimum $^{187}Os/^{188}Os$ value ~1 Ma later than sites elsewhere due to its proximity to CAMP eruptions. Larger fluxes of unradiogenic Os to the oceans coupled with the short marine residence time of Os should result in a global signal. While the presence of a minimum $^{187}Os/^{188}Os$ is expected, multiple coherent records are required to make a detailed interpretation of the Os record.

3.2.3 Oceanic Anoxic Event 2 (OAE2) at the Cenomanian-Turonian Boundary

The Cenomanian-Turonian Boundary (~93.5 My) is characterized by widespread deep-water anoxia and increased burial of organic matter, called the Oceanic Anoxic Event 2 (OAE2). OAE2 was the most extensive anoxic event of the half dozen that occurred during the Cretaceous (Jenkyns, 2010). Sinton and Duncan (1997) and Kerr (1998) proposed that these environmental changes were triggered by a large magmatic event, such as the emplacement of the Caribbean or Madagascar flood basalts (Figure 3.9). Massive outgassing of CO_2 would cause warming, elevating sea surface temperatures and interfering with the formation of deep water, thereby leading to ocean stratification and anoxia (Snow et al., 2005). The bulk of the Caribbean LIP erupted between 91 and 88 Ma ago, in a number of short, discrete pulses (Courtillot & Renne, 2003). The volumetrically smaller Madagascar flood basalts were emplaced at roughly the same

time (Courtillot & Renne, 2003), but establishing a causative relationship between volcanism and ocean anoxia necessitates that the causative magmatic event occurred immediately prior to the onset of OAE2.

Studies show that $^{187}Os/^{188}Os$ decreased dramatically just prior to the OAE2, rising gradually through its duration, and then stabilized post-OAE2 at a value lower than its pre-OAE2 value. Turgeon and Creaser (2008) measured a decline in $^{187}Os/^{188}Os$ from ~0.6 to 0.16 (Furlo, Italy) and from ~0.54 to 0.17 (ODP Site 1260B) just prior to the onset of the OAE2 (Figure 3.10). This excursion to low $^{187}Os/^{188}O$ persisted, suggesting a prolonged source of unradiogenic Os: A widespread magmatic event coincident with OAE2 would provide such a source. $^{187}Os/^{188}Os$ gradually rises throughout the OAE2, returning to ~0.46 after the carbon isotope excursion which defines the OAE2. Turgeon and Creaser (2008) calculate that the pulse of volcanism responsible for the sharp decline to unradiogenic values of $^{187}Os/^{188}Os$ precedes the carbon isotope excursion by ~9 ka (based a 220 ka duration for OAE2) to ~23 ka (based on a 550 ka duration for OAE2). Duvivier et al. (2014) refined this timing after measuring the $^{187}Os/^{188}Os$ at four additional sites, as well as additional samples at Furlo, Italy and ODP Site 1260B to increase the resolution of those records. They argue volcanism begins at least ~200 ka prior to the onset of OAE2 based on a precursor decline of $^{187}Os/^{188}Os$ of seawater seen at Portland Core #1, ODP Site 1260, Vocontian Basin, and DSDP Site 530. A larger, major pulse occurred ~30 ka prior to the onset of OAE2. These additional records clearly establish the $^{187}Os/^{188}Os$ decline just prior to OAE2 as global in extent. Further work has confirmed the structure of the $^{187}Os/^{188}Os$ record at the Cenomanian-Turonian Boundary as radiogenic and spatially heterogeneous (~0.55 – 0.85) prior to OAE2, abruptly shifting to unradiogenic and homogenous at the onset of OAE2 (~0.2 – 0.3), with a gradual return to a more radiogenic value (~0.7) towards the late OAE2 (Duvivier et al., 2015).

Robinson et al. (2009) argues that systematic offsets in coeval $^{187}Os/^{188}Os$ records from different sites provides empirical evidence that the marine Os record is not analogous to the $^{87}Sr/^{86}Sr$ record, which is a "single-valued" function of time, but rather it is the overall structure of the Os isotopic record that is most useful as a chemostratigraphic tool. The records from the Cenomanian-Turonian Boundary reaffirm that it is the shape of the $^{187}Os/^{188}Os$ curve that is most

important for correlating different records, and not the absolute values of $^{187}Os/^{188}Os$. At times of low flux from mantle sources the $^{187}Os/^{188}Os$ of marine basins may be locally influenced by terrigenous input of radiogenic Os, to the extent that seawater is not homogenous. Alternately, when there is a very high input from mantle sources, the affect of these localized differences between basins on the $^{187}Os/^{188}Os$ of seawater is minimized, and seawater becomes more homogenous globally.

3.2.4 North Atlantic Igneous Province (NAIP) and the Paleocene-Eocene Thermal Maximum (PETM)

The Paleocene-Eocene Thermal Maximum (PETM) at 55.9 Ma is characterized by a massive injection of isotopically light carbon into the oceans and atmosphere and sudden global warming, the causes of which are still debated. Storey et al. (2007) argue that volcanism in the North Atlantic Igneous Province (NAIP) triggered the PETM. Emplacement of the NAIP began ~61 Ma with intermittent volcanic activity occurring until ~56 Ma, and magma production remained low (~160 km^3/km/Ma), declining to little or none near the C25n/C24r reversal boundary (Storey et al., 2007). At ~56.5 Ma magma production abruptly increased 20-fold (see Figure 3.11) and remained high for ~1 Ma (Storey et al., 2007). It is the increased volcanism associated with the continental rifting of Greenland and Europe that Storey et al. (2007) link to the onset of the PETM, and one mechanism that has been proposed is that uplift resulting from the NAIP mantle plume depressurized marine sediments and destabilized methane hydrates (MacLennan & Jones, 2006).

Ravizza et al. (2001) first noted a transient increase from $^{187}Os/^{188}Os$ of ~0.34 to more radiogenic values during the PETM ($^{187}Os/^{188}Os$ ~0.44), followed by a return to pre-event values (Figure 3.12) coincident with the carbon isotope excursion that defines the PETM. They interpreted this transient excursion of $^{187}Os/^{188}Os$ to more radiogenic values as a result of an increased flux of radiogenic Os from continental rocks. This interpretation is consistent with records of increased global weathering rates due to extreme warming in the PETM (Zachos et al., 2005).

Although higher resolution work on continental margins has revealed fine structure in the marine Os record of the PETM, Dickson et al. (2015) confirmed a transient increase in $^{187}Os/^{188}Os$ during the PETM (Figure 3.13). However, just prior to this increase they note a brief excursion to more unradiogenic values (Figure 3.14). They ascribe this dip to an injection of unradiogenic Os into the oceans from a pulse of volcanism, and specifically the emplacement of the North Atlantic Igneous Province: "Volcanism caused a significant (though locally disproportionate) global shift in $^{187}Os/^{188}Os$" (Dickson et al., 2015), meaning that the signal was seen globally but to different extents. The volcanism-induced decline of $^{187}Os/^{188}Os$ in seawater is extremely brief and transient compared to the shift in $^{187}Os/^{188}Os$ recorded from the late Maastrictian to early Paleogene. In the late Maastrictian volcanism caused the $^{187}Os/^{188}Os$ of seawater to decline to ~0.4 and remain there; $^{187}Os/^{188}Os$ of seawater did not recover to pre-eruptive values. This is a fundamentally different response of the $^{187}Os/^{188}Os$ of seawater than what occurs at the PETM. It is also important to note that the NAIP provided a prolonged source of unradiogenic Os, yet appears to have only produced a brief, transient dip to low $^{187}Os/^{188}O$, whereas the extensive flood basalt emplacement coeval with OAE2 produced a prolonged excursion to unradiogenic values. This suggests that the presence of widespread oceanic anoxia contributed to the length of the $^{187}Os/^{188}O$ excursion during OAE2, although the mechanism remains unclear.

This eruptive pattern of the NAIP is grossly similar to that of the Deccan Traps, with an initial, low volume period followed by a second, main high volume phase. Why then do the osmium isotopic records look so different from one another? The main phase of the NAIP was emplaced at northern paleolatitudes of ~60° - 69° whereas Deccan was emplaced near the equator, and Deccan flows were predominantly subaerial, while NAIP was both subaerial and submarine (Storey et al., 2007). Additionally, main phase eruptions in NAIP are associated with continental rifting, which is not the case in main stage Deccan eruptions. Nonetheless, these differences do not sufficiently account for the fundamentally different shape of the $^{187}Os/^{188}Os$ curve of seawater seen in these two records. Considering the high volumes of magma production associated with NAIP it seems surprising that its effect on the $^{187}Os/^{188}Os$ would be so slight when compared to other LIP events. It is possible the perturbation to the carbon cycle at the PETM was so extreme that the increased weathering of high $^{187}Os/^{188}Os$ continental rocks overwhelmed the flux of unradiogenic Os from volcanism (Storey et al., 2007), or that the

isotopic signature of the old craton rock covered by NAIP is quite different from that which was covered by Deccan lavas.

3.2.5 Oceanic Anoxic Event 1a (OAE1a) and the Ontong Java Nui Plateau / Early Aptian

Oceanic Anoxic Event 1a (OAE1a) occurred in the early Aptian (~120 My), and like OAE2, is characterized by the presence of black shales. These globally distributed shales resulted from an anomalously high burial rate of marine organic carbon (Jenkyns, 2010). The eruption of the Ontong Java Nui Plateau (OJN) is implicated as the trigger for Oceanic Anoxic Event 1 (OAE1a) in the early Aptian (Tejada et al., 2009). The OJN is a predominantly submarine eruption often considered an order of magnitude larger than all other LIPs (Courtillot & Renne, 2003). No mass extinction is associated with OJN but it presumably released large amounts of CO_2 to the oceans and this could have led to ocean anoxia and a greenhouse period. Like OAE2, a preceding decline in $^{187}Os/^{188}Os$ of seawater is interpreted as evidence of a causative relationship between the emplacement of OJP and OAE1a.

Several records show an initial decline in $^{187}Os/^{188}Os$ of seawater (~0.8 down to 0.4) leading up to OAE1a. Just prior to the onset of OAE1a $^{187}Os/^{188}Os$ values increase to ~0.7 before declining rapidly to ~0.2. $^{187}Os/^{188}Os$ values then remain low (~0.20) through OAE1a (Figure 3.15). These swings in the $^{187}Os/^{188}Os$ of seawater are interpreted as reflecting the influence of two, distinct pulses of magmatism. The first pulse of OJN volcanism caused the initial dip in of $^{187}Os/^{188}Os$. A volcanism-induced greenhouse effect in turn led to an increase in weathering rates, and this increased the flux of radiogenic Os to the oceans, driving up $^{187}Os/^{188}Os$. Later a much larger and prolonged pulse of magma production drove $^{187}Os/^{188}Os$ to very low values, where they remained for the duration of OAE1a (Tejada et al., 2009; Bottini et al., 2012).

In both OAE1a and OAE2 there is evidence that the onset of anoxia was preceded by "a significant input of unradiogenic Os" (Bottini et al., 2012). There is no evidence at either time of an extraterrestrial source of Os, therefore the flux of unradiogenic Os is argued to be of volcanic origin (Tejada et al., 2012; Turgeon & Creaser, 2008). The persistence of low $^{187}Os/^{188}Os$ values throughout both OAE1a and OAE2 requires that a large flux of unradiogenic Os be supplied to the ocean for the duration of the OAEs. This supply of unradiogenic Os is interpreted to result

from ongoing magmatism and/or the hydrothermal alteration of young basalts. An important difference is that $^{187}Os/^{188}Os$ values stayed low until the cessation of OAE1a, suggesting that the flux of unradiogenic Os from the OJN remained intense until the end of OAE1a, while $^{187}Os/^{188}Os$ rose gradually through OAE2, suggesting that volcanic activity tapered off during the anoxic interval. Both the records of OAE1a and OAE2 differ significantly from the record of Deccan. At Deccan we argue that the $^{187}Os/^{188}Os$ record only reveals the onset of the main eruptive phase, not its duration.

3.3 Limitations of the marine $^{187}Os/^{188}Os$ record for timing of LIP emplacement

Figure 3.16 depicts idealized $^{187}Os/^{188}Os$ curves for the PETM, CAMP, Deccan, OAE1a and OAE2. It is immediately evident that the curves look very different, and there is enough Os data to show that the Os isotopic record does not have a consistent response to LIP events.

CAMP and Deccan are the most analogous events, both major LIP events without widely associated ocean anoxia. However, $^{187}Os/^{188}Os$ responds very differently to the increased flux of unradiogenic Os from the magmatic events: At the K-Pg $^{187}Os/^{188}Os$ values decline to a new, more unradiogenic steady state, while at the T-J Boundary $^{187}Os/^{188}Os$ recovers to pre-event LIP emplacement values, tracking the entire eruptive production rather than just its onset. So why does the Deccan record look so different from other LIP-associated Os profiles? The Deccan Traps were predominantly subaerial, rather than submarine, eruptions. As a result Deccan lavas would presumably cover rocks of a very different isotopic composition than lavas erupting on the sea floor. By removing a radiogenic source, rather than temporarily increasing an unradiogenic source, a transition from one steady state to another would occur, especially when the newly unradiogenic continental signal is strengthened by the assumed increased weathering following an extended magmatic event. A submarine eruption would not result in the same shift in $^{187}Os/^{188}Os$, since in that case unradiogenic flows are covering another unradiogenic source, and it is simply the flux that increases. When volcanism stops, the flux reverts to presumably pre-event levels or near to, and the previous state reasserts itself, returning $^{187}Os/^{188}Os$ to pre- or near pre-event levels. A slight increase or decrease would result from changes in weathering rates (from increased temperatures) or a continuation of elevated flux.

The previous scenario assumes that once the influence of the K-Pg impact is removed, the record from Deccan looks like simplified curve presented in panel A of Figure 3.16. An alternate possibility is that signal of the K-Pg impact is masking a similarly sharp decrease in $^{187}Os/^{188}Os$ values, driven to ~0.2 by Deccan, not only a bolide impact. Another way to consider this is: How much Deccan signal might the impact hide? The K-Pg excursion could easily hide a brief, PETM-like decrease in $^{187}Os/^{188}Os$. Perhaps Deccan does drive $^{187}Os/^{188}Os$ values to near mantle values, where it persists for a time until it recovers to 0.4. Schoene et al. (2015) and Renne et al. (2015) locate the voluminous Ambenali formation from before the K-Pg to after it, where it extends almost to the C29n/C28r boundary. Subsequently, the majority of the subsequent Mahabaleshwar formation erupts within C28r. These two formations represent a large volume of post K-Pg magma eruption. Figure 3.5 shows that the $^{187}Os/^{188}Os$ of seawater after the K-Pg recovers to 0.4 near the beginning of C29n. If the Os isotope record at the K-Pg behaved like the record at the T-J Boundary it would be expected that $^{187}Os/^{188}Os$ would remain low until the cessation of the magmatic event responsible for the increased flux of unradiogenic Os to the oceans, but this it not what occurs in the K-Pg record. Instead, $^{187}Os/^{188}Os$ rapidly stabilizes at 0.4 before the cessation of Deccan main stage eruptions. This argues that there is no "hidden Deccan" signal overlain by the K-Pg impact's influence on the $^{187}Os/^{188}Os$ record.

OAE1a and OAE2 are defined by global episodes of oceanic anoxia, and these two records also show the most prolonged $^{187}Os/^{188}Os$ excursions to unradiogenic values. Both OAEs recover from the excursion to lower than pre-event $^{187}Os/^{188}Os$ values. This likely reflects an increased flux of unradiogenic Os as young mid ocean ridge basalts (MORB) are weathered. In this they are similar to what occurs at Deccan, but a major difference is that at both OAE1a and OAE2 the $^{187}Os/^{188}Os$ excursion dips to ~0.2, whereas the Deccan induced excursion does not get that low (once the influence of the K-Pg impact is removed). The Os isotopic record seems to react differently to submarine LIP/oceanic plateaus (like those associated with OAE1a and OAE2) and to continental flood basalts (such as Deccan and CAMP).

There are currently numerous limitations to comparing these various $^{187}Os/^{188}Os$ records that hinder our ability to ascribe differences to a particular characteristic of the eruptive event. These limitations include uncertainty in the Os flux associated with hydrothermal alteration of oceanic

crust and oceanic plateaus, the effect of ocean circulation patterns on global and localized $^{187}Os/^{188}Os$ values of seawater, and the response of the marine Os cycle to ocean anoxia. These all warrant further study. Clearly a major limitation in comparing these records is the difference in resolution. What might appear a steady decline in one record may be revealed as a stepped decrease in a higher resolution record. Yet despite the difference in resolutions between the records, we can definitively say that they exhibit markedly different rates of decline leading into the excursion to unradiogenic values. Given that LIP events can manifest differently in the Os record, and that non-LIP events can produce curves that mimic LIP emplacement, caution must be used before assigning the cause of every decrease in the $^{187}Os/^{188}Os$ ratio to a volcanic event, and every increase to enhanced weathering. The late Eocene has a well-documented $^{187}Os/^{188}Os$ excursion to unradiogenic values with no known LIP association (Paquay et al., 2014; Dalai et al., 2006; Ravizza & Peucker-Ehrenbrink, 2003). Clearly processes other than LIPs can cause unradiogenic excursions in the $^{187}Os/^{188}Os$ record.

The above cautions notwithstanding, Os isotopic records are increasingly being used to link the emplacement of LIPs with major environmental changes and biotic crises. The record at the K-Pg presented in Robinson et al. (2009) establishes the temporal separation of the onset of main phase Deccan from the K-Pg, and the record remains robust despite changes in the accepted ages of the K-Pg and the C29r/C30n boundary. It contributes a high-resolution and robust record of LIP emplacement, as well as an impact signal, which can be used along with records from other LIP events to further characterize the behavior of Os isotopes during large magmatic events, and increased continental weathering. However, given wide variability in the shapes of the Os isotopic curves from what are grossly similar signals (increased unradiogenic flux), it is an over-simplification to attribute all decreases in $^{187}Os/^{188}Os$ to volcanism and all increases to weathering.

Tables

Table 3.1 Original age model vs. revised age model

	Age used in Robinson et al. 2009 (Ma)	Duration (Ma)	Revised Age from Gradstein et al. 2012	Duration (Ma)	Difference (Ma)	%
K-Pg	65.51		66.04			
		0.333		0.358	0.025	8%
C29R/C30N	65.843		66.398			
		2.032		1.798	-0.234	-12%
C30N/C30R	67.875		68.196			
		0.125		0.173	0.048	38%
C30R/C31N	68.000		68.369			

"Duration" column calculates time span between the age datums in the row directly above and below. "Difference" column calculates the difference in Duration between Robinson et al. (2009) and using Gradstein et al. (2012). The "%" column is the % change in duration from Robinson et al. (2009) and Gradstein et al. (2012). A positive value indicates that the revised duration using Gradstein et al. (2012) is longer.

Table 3.2 Comparison of ages for the base of C29r and calculated durations of Cretaceous portion of C29r

From Thibault & Husson, 2016. Ages obtained for the base of Chron C29r from radiometric dating and cyclostratigraphic evaluations. Ages derived from cyclostratigraphy are based on the La2004 precession model with two possible ages of the Cretaceous-Paleogene boundary (K-PgB) at 66.043 and 65.957 Ma when considering the average and youngest range of uncertainty of Renne et al. (2013). Duration uncertainties provided for radiometric dates take into account the uncertainty as given in the mentioned references as well as the total uncertainty of 0.086 Ma provided by Renne et al. (2013) for the K-Pg.

Site/section /study area	Oceanic basic/ Geographic area	Age (Ma), K-Pg at 66.043 Ma	Age (Ma), K-Pg at 65.957 Ma	Dating method	Precessional cycles from K-PgB	Duration (ka)	Duration (uncertainty)	Reference
Agost, Spain	NW Tethys	66.433	66.330	Cyclostratigraphy	19	390	10	Ten Kate & Sprenger (1993)
Relleu, Spain	NW Tethys	66.377	66.263	Cyclostratigraphy	16	334	10	Ten Kate & Sprenger (1993)
Zumaia, Spain	Basque-Cantabrian	66.414	66.310	Cyclostratigraphy	18	371	10	Ten Kate & Sprenger (1993)
Zumaia, Spain	Basque-Cantabrian	66.414	66.310	Cyclostratigraphy	18	371	10	Herbert et al. (1995,1999)
Zumaia, Spain	Basque-Cantabrian	66.414	66.310	Cyclostratigraphy	18	371	10	Westerhold et al. (2008)
Zumaia, Spain	Basque-Cantabrian	66.404	66.299	Cyclostratigraphy	17.5	361	10	Batenburg et al. (2012)
Bjala, Bulgaria	NE Tethys	66.361	66.241	Cyclostratigraphy	15 ± 1	318	20.5	Preisinger et al. (2002)
525A	South Atlantic	66.424	66.321	Cyclostratigraphy	18.5	381	10	Herbert et al. (1995, 1999)
1262 and 1267	South Atlantic	66.361	66.2411	Cyclostratigraphy	15 ± 1	318	20.5	Westerhold et al. (2008)
1267B	South Atlantic	66.361	66.241	Cyclostratigraphy	15	318	10	Husson et al. (2011)
516F	South Atlantic	66.424	66.321	Cyclostratigraphy	18.5	381	10	Herbert et al. (1995, 1999)
528	South Atlantic	66.424	66.321	Cyclostratigraphy	18.5	381	10	Herbert et al. (1995, 1999)
Bottaccione, Italy	Central W. Tethys	66.414	66.310	Cyclostratigraphy	18	371	10	Husson et al. (2014)
Western Ghats	West India	66.288 ± 0.027		$^{206}U/^{238}Pb$	-	245	±113	Schoene et al. (2015)
Hell Creek region	Montana, USA	66.195 ± 0.052		$^{40}Ar/^{39}Ar$	-	152	± 138	Sprain et al. (2015)

Figures

Figure 3.1 Updates to age model used in Robinson et al. (2009) presented in Chapter 2. Upper panel compares magnetic reversal and K-Pg ages used in Robinson et al., 2009 to ages from Gradstein et al., 2012 used to update the data (see Appendix B). Bottom panel compares the $^{187}Os/^{188}Os$ record from Gubbio, Italy using both age models. Although there are slight changes to the duration of each section, the overall result is a shifting of age datums earlier.

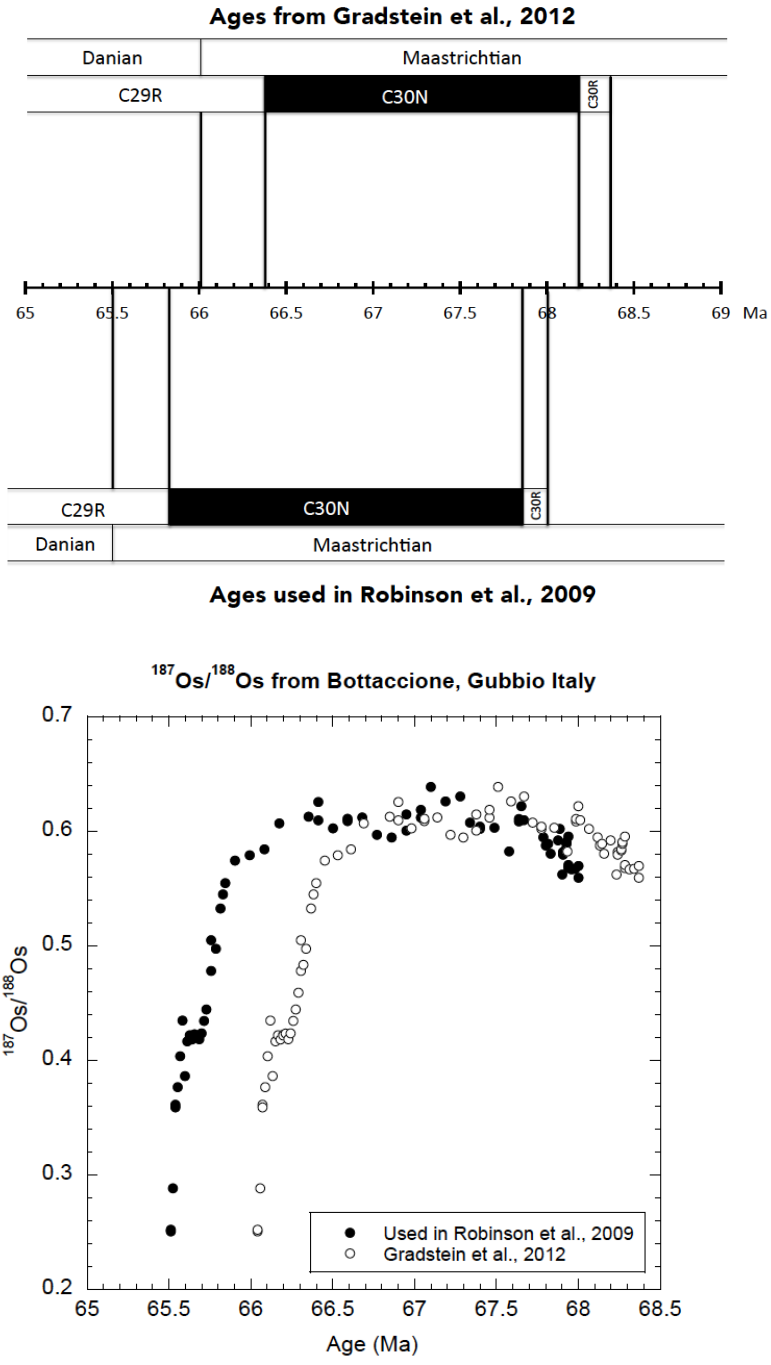

Figure 3.2 Revised Deccan eruptive histories

Locating the K-Pg in the Deccan lava pile. Both Schoene et al. 2015 (left panel) Renne et al. 2015 (right panel) locate the Ambenali Formation after the K-Pg. Compare these to Figure 2.6, showing the placement of the K-Pg after the Ambenali Formation from Chenet et al. (2007).

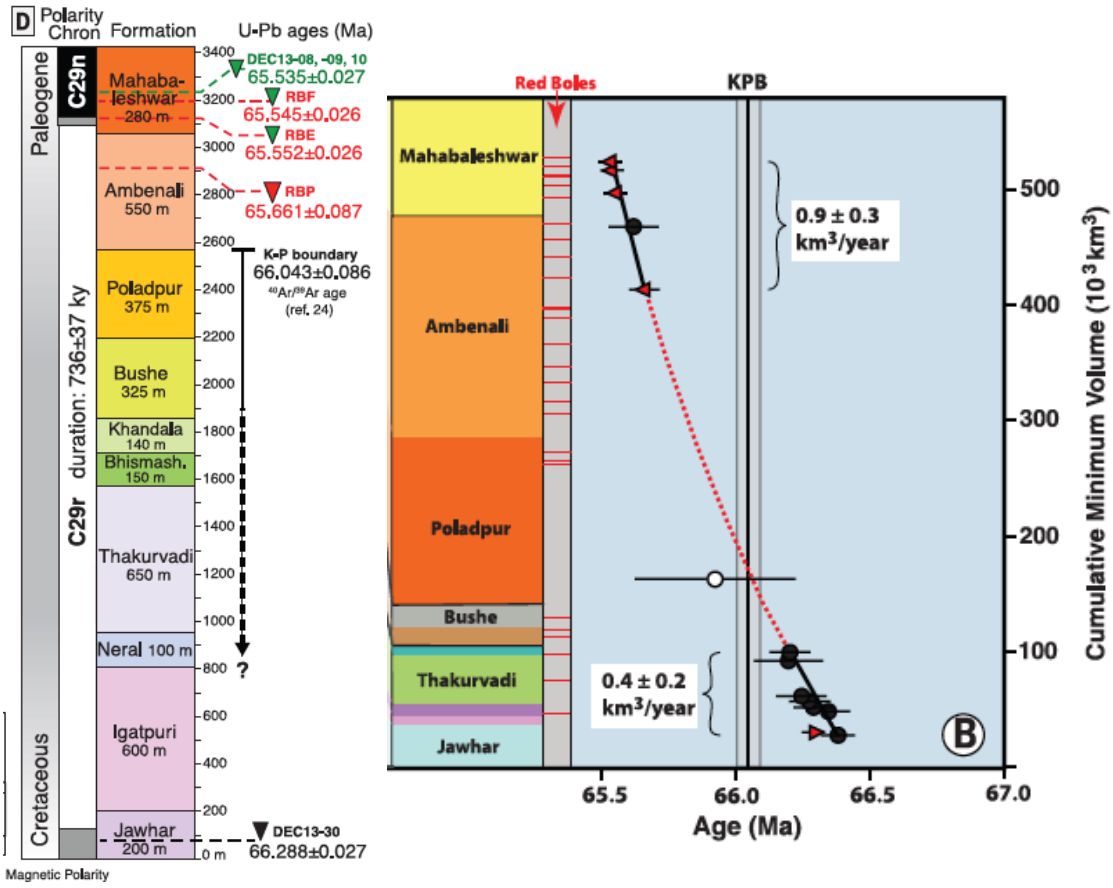

Figure 3.3: Environmental changes coincident with main phase Deccan volcanism.

Compilation of Os data (from Robinson et al., 2009) alongside $\delta^{18}O$ derived temperature records, and records of carbonate preservation (From Henehen et al., 2016 and references therein).

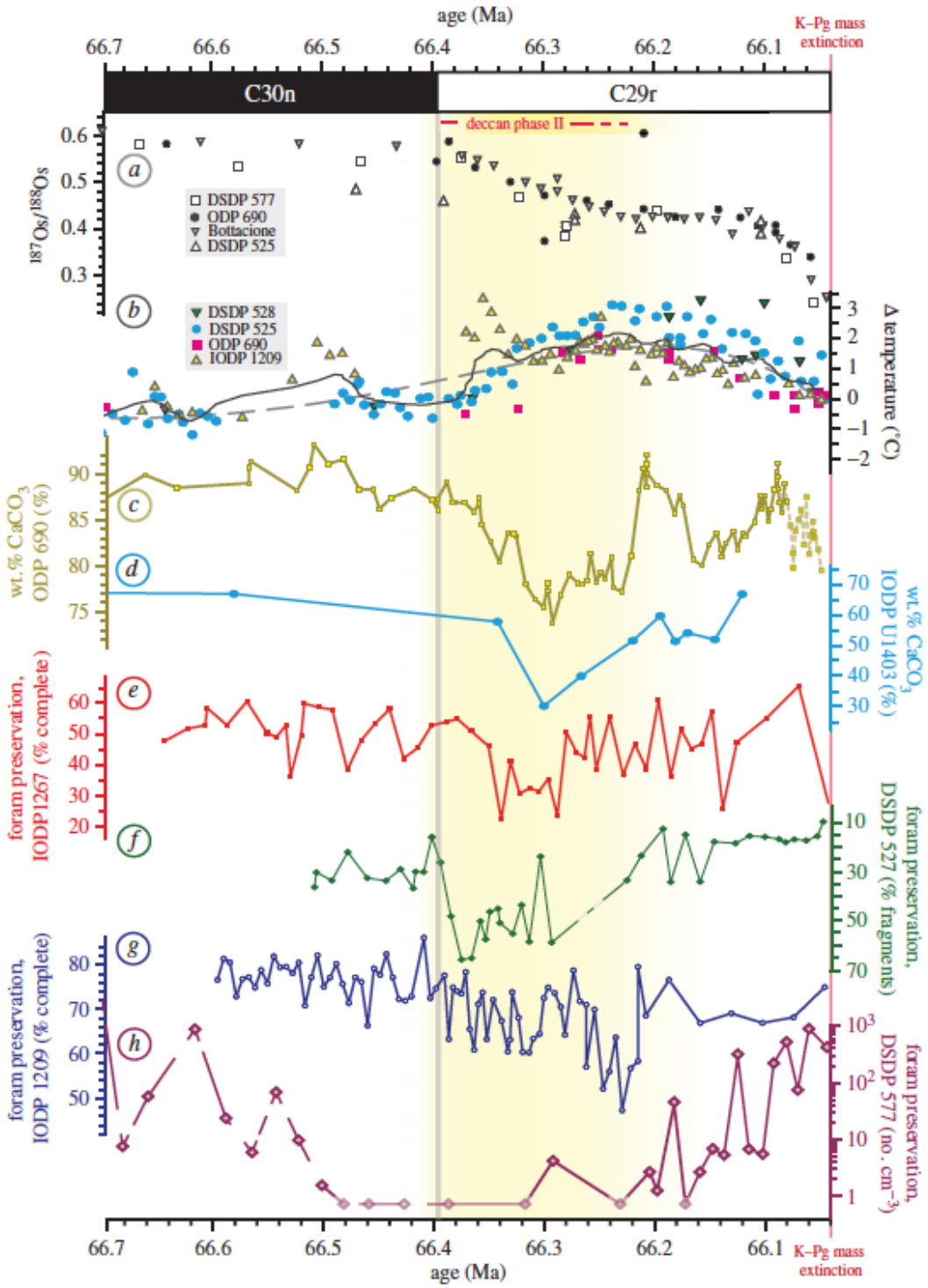

Figure 3.4: Age difference between LIP and stratigraphic boundary

From Kelley, 2007. Age difference between LIP and associated sudden environmental change vs. age of stratigraphic boundary associated with sudden environmental change. Top panel: Central Atlantic Magmatic Province (CAMP) associated with the mass extinction at the Triassic – Jurassic boundary; Caribbean-Madagascar eruptions associated with the Cenomanian-Turonian boundary (OAE 1a Bonarelli Event); Ontong Java II associated with end-early Aptian (OAE 2 Selli Event); Deccan Traps associated with the mass extinction at the Cretaceous-Paleogene boundary; North Atlantic Igneous Province associated with the Paleocene-Eocene Thermal Maximum (PETM).

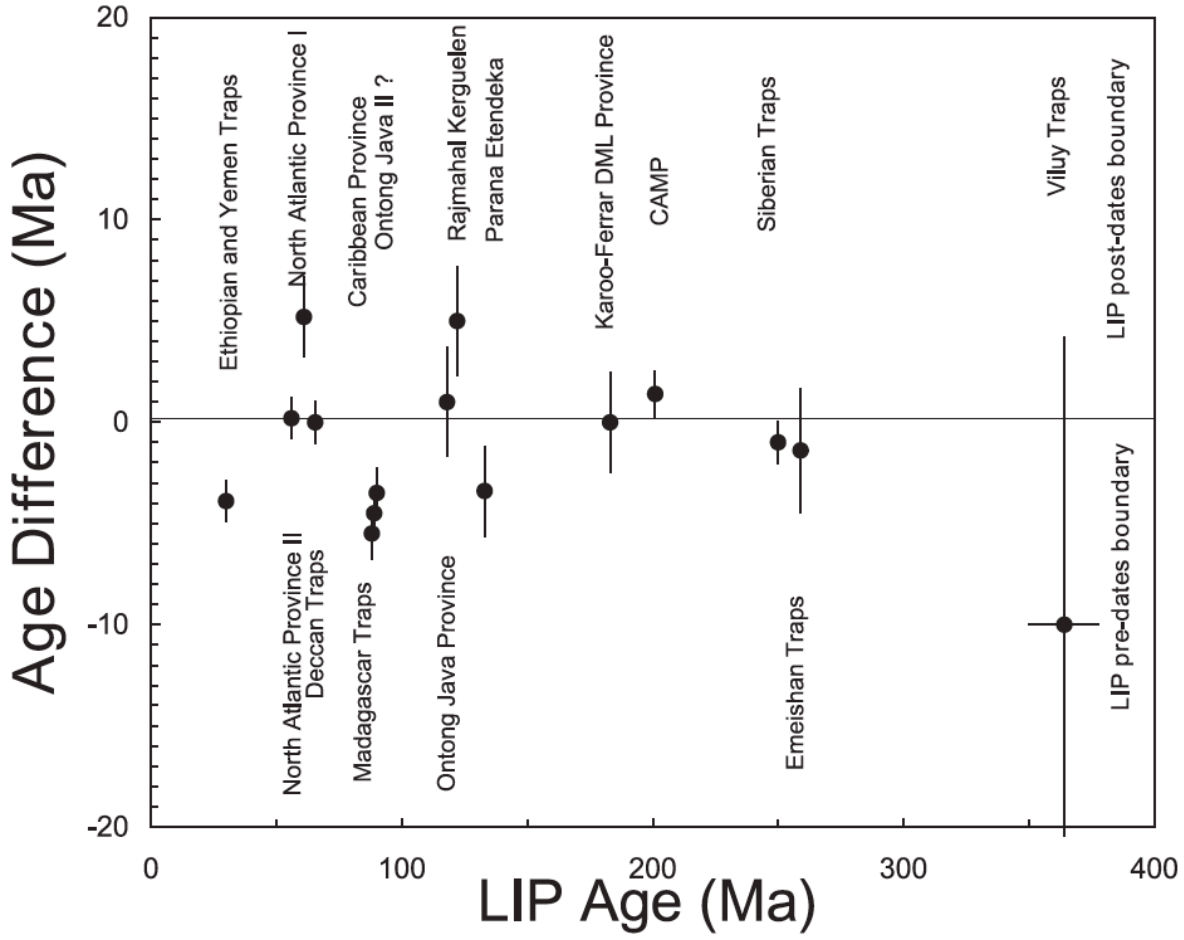

Figure 3.5: Complete $^{187}Os/^{188}Os$ from the late Maastrichtian to the early Paleogene. Data prior to the K-Pg are from Robinson et al. (2009). All other data are from Ravizza & VonderHaar (2012).

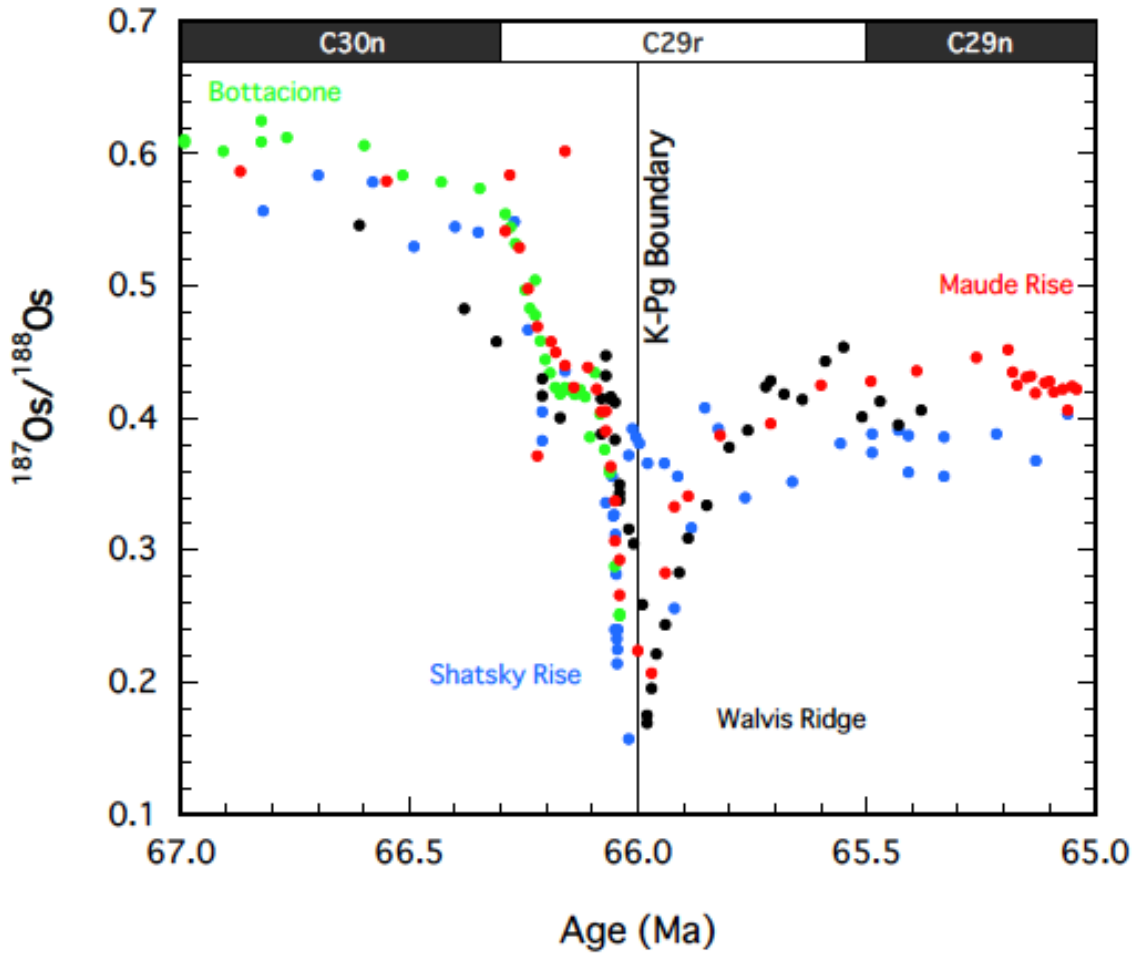

Figure 3.6: $^{187}Os/^{188}Os$ across the K-Pg at DSDP Site 524

Unpublished data from DSDP Site 524 Walvis Ridge show post-K-Pg $^{187}Os/^{188}Os$ values persisting at ~0.4 for at least 2 Ma through C28r (from Greg Ravizza, personal communication).

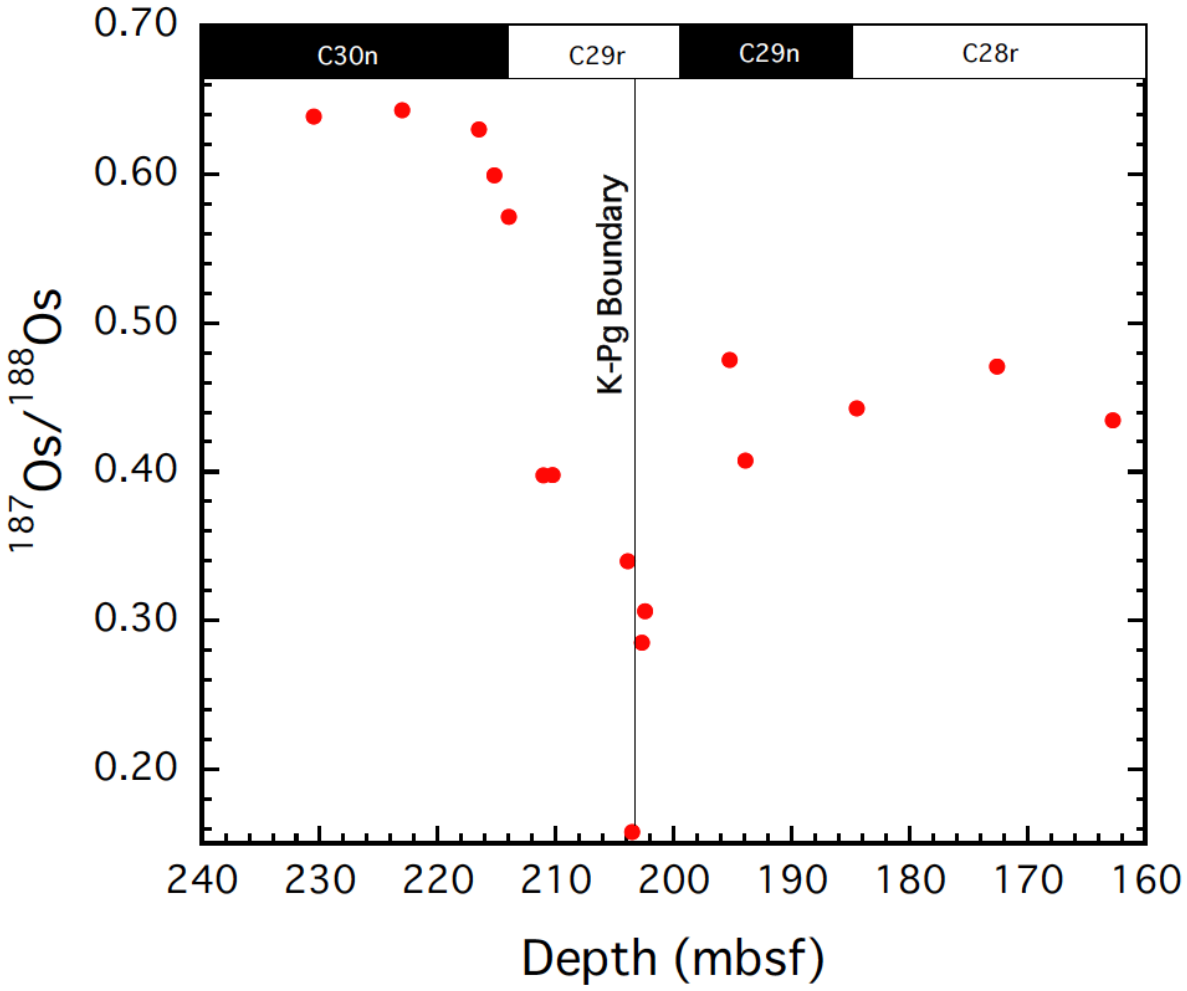

Figure 3.7: Percentages of extinction for genera of marine animals for stages of the Phanerozoic. Conspicuous peaks represent mass extinctions (From Stanley & Luczaj, 2015). The "big five" extinction events are marked: K-Pg = end Cretaceous; T-J = Triassic-Jurassic; Perm = end Permian; Dev = Late Devonian; O-S = Ordovician-Silurian.

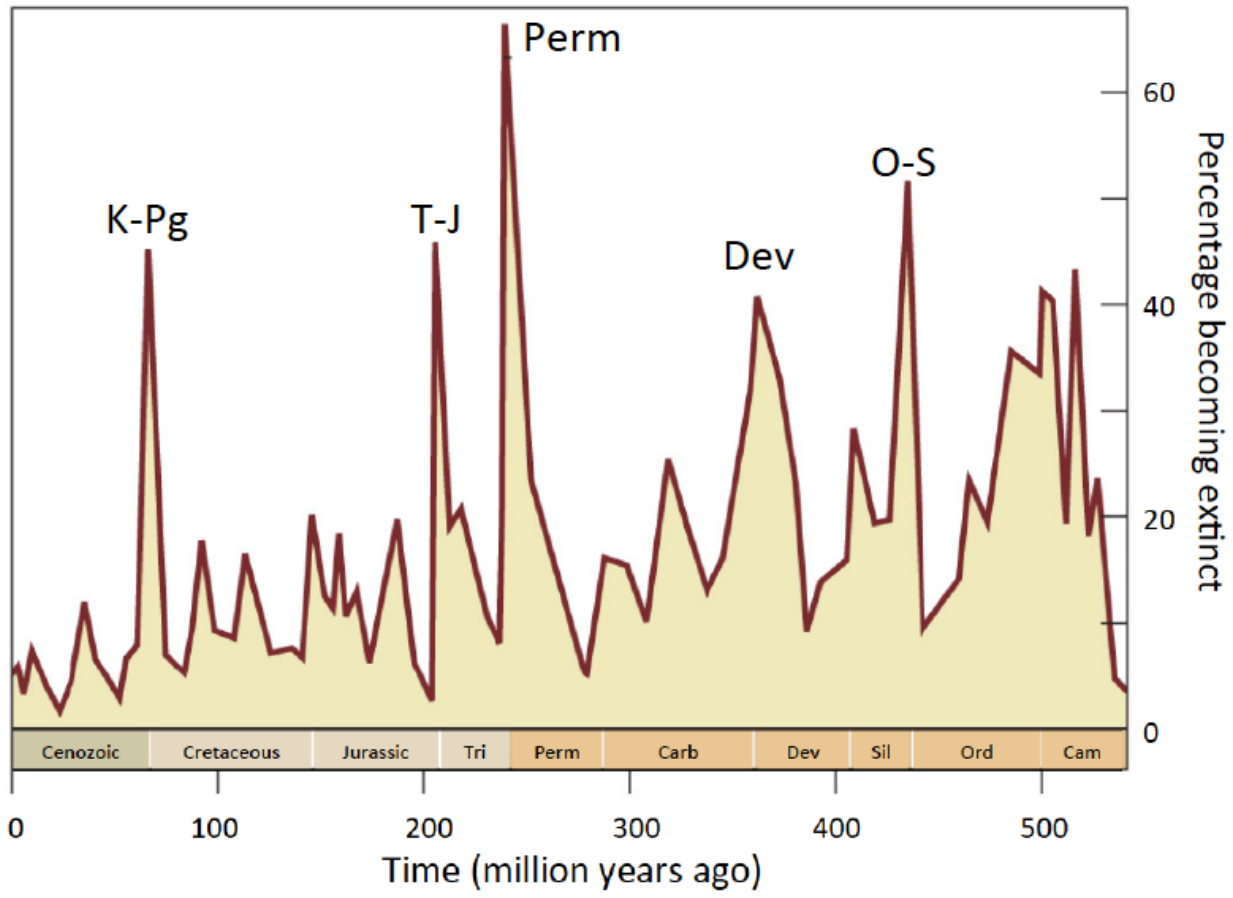

Figure 3.8: $^{187}Os/^{188}Os$ across the T-J Boundary from St Audrie's Bay, England and Kurusu section, Japan.

Grey band across Kurusu record marks the T-J Boundary. The initial negative excursion of $\delta^{13}C$ (INE) is used to correlate the two sections. From Kuroda et al., 2010.

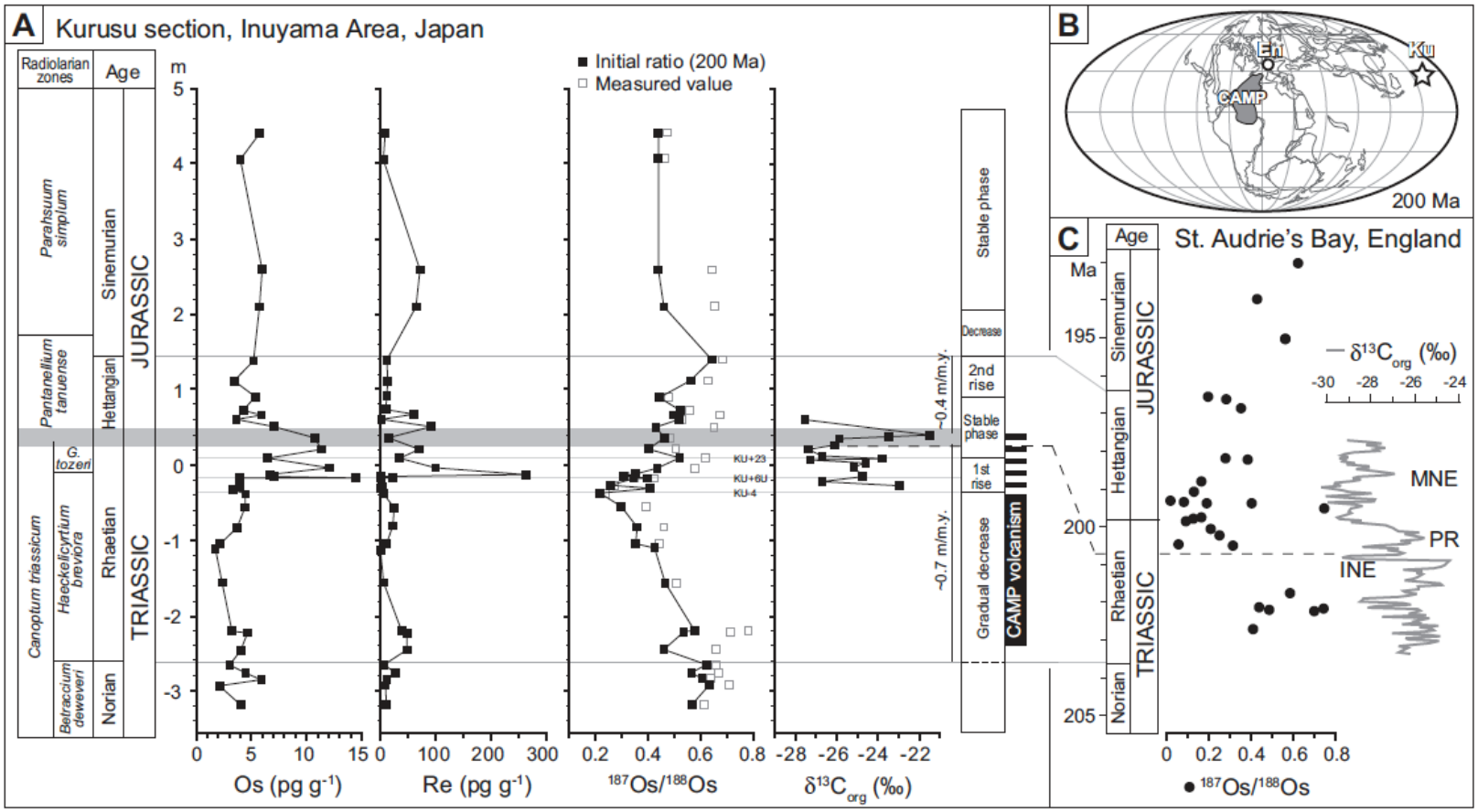

Figure 3.9: Palaeogeographic map at the time of the Cenomanian-Turonian Boundary. From Duvivier et al. (2014). P = Portland & Pueblo GSSP; 1260 = ODP Site 1260B Demerara Rise; W = Wunstof; VB = Vocontian Basin; F = Furlo, Italy; 530 = DSDP Site 530. The locations of the Caribbean and High Arctic Large Igneous Provinces are shown in red.

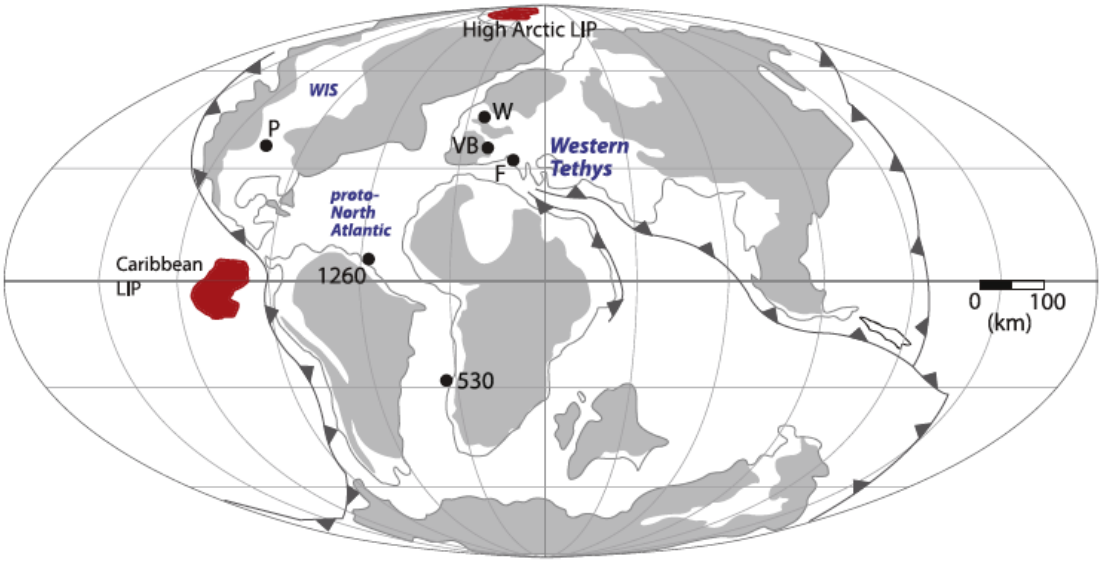

Figure 3.10: $\delta^{13}C_{org}$ and $^{187}Os/^{188}Os$ vs. stratigraphic height/depth during OAE2.

$\delta^{13}C_{org}$ (black) and $^{187}Os/^{188}Os$ (red) from six locations across OAE2. 'A' is the onset of OAE2, and 'C' is the last relatively enriched $\delta^{13}C_{org}$ value before the trend back to pre-excursion values. Figure from Duvivier et al., 2015.

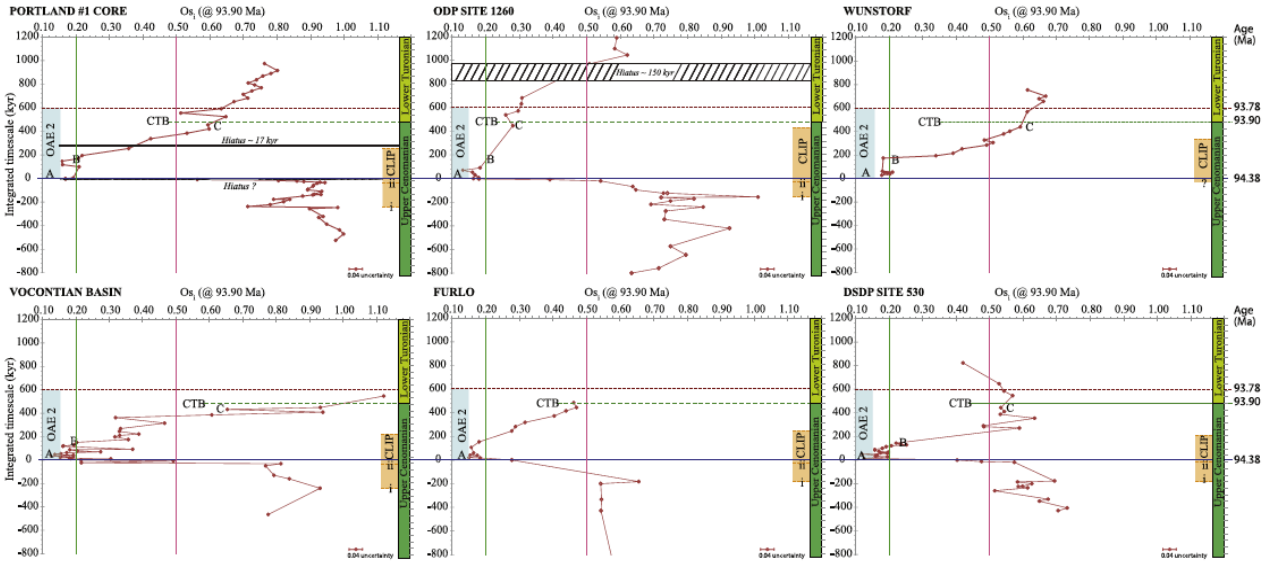

Figure 3.11: Estimated melt production rates for the Blosseville Kyst-Faeros Islands lavas.

From Storey et al. (2007)

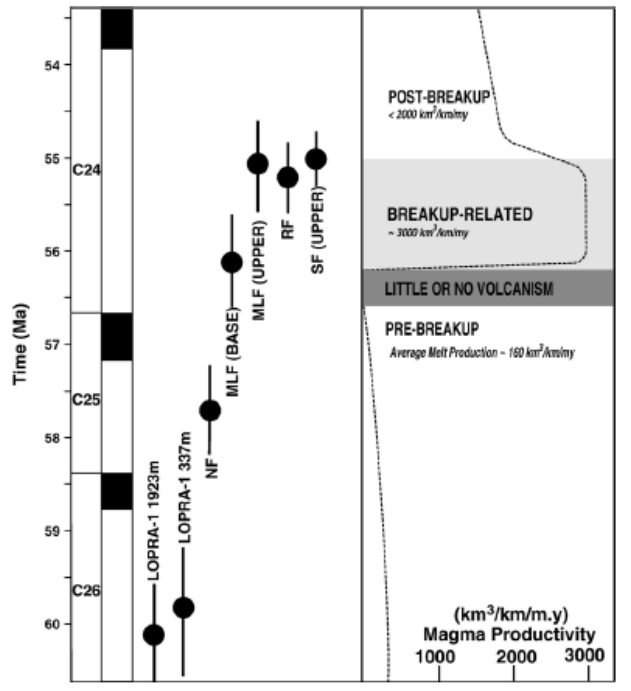

Figure 3.12: $^{187}Os/^{188}Os$ at DSDP Site 549 with carbon isotope data from bulk carbonate and planktonic foraminifera.

From Ravizza et al. (2001) with carbon isotopic data from Stott et al. (1996).

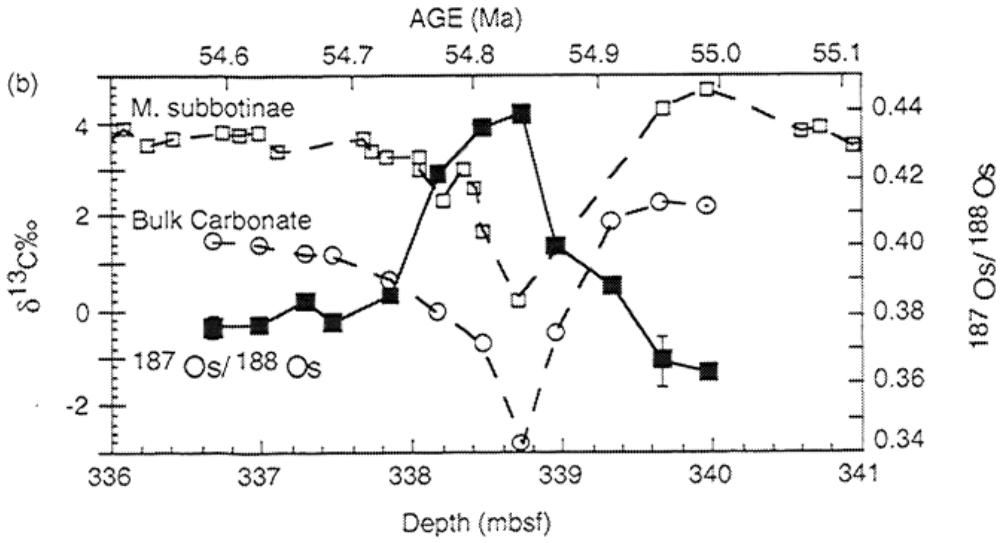

Figure 3.13: C- and Os-isotopes and osmium abundance from three Peri-Tethys sites at PETM. Grey shaded area denotes the PETM C-isotope negative excursion. Adapted from Dickson et al. (2015).

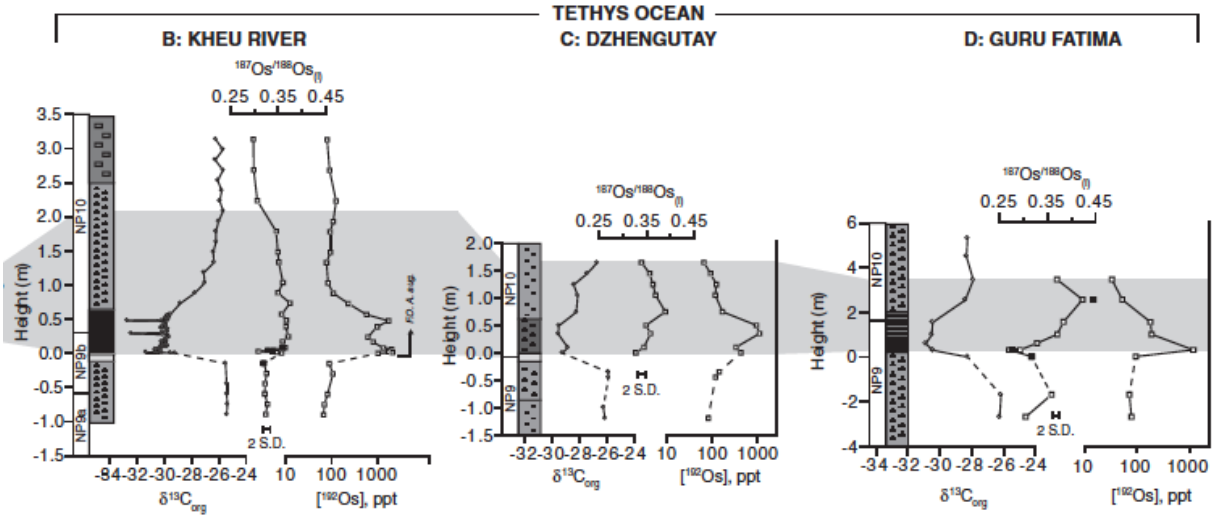

Figure 3.14: Expanded view of C- and Os-isotope data across the onset of the PETM. Kheu River and Guru-Fatima from Dickson et al. (2015), Zumaya from Schmitz et al. (2004) and Svalbard core BH9/05 from Wieczorek et al. (2013). All four sites record excursions of $^{187}Os/^{188}Os$ to more radiogenic values near the onset of the PETM. (Figure from Dickson et al., 2015). Gray shaded band marks the PETM C-isotope negative excursion.

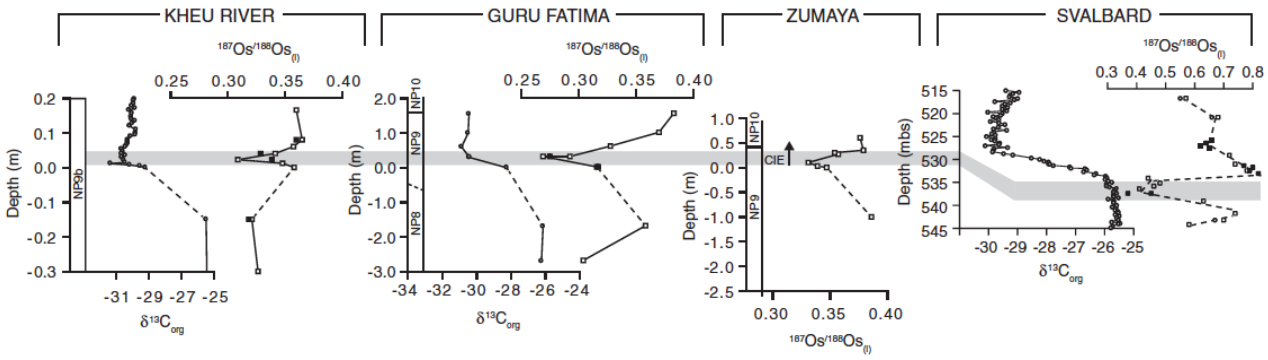

Figure 3.15: The $^{187}Os/^{188}Os$ values of seawater from OAE1a.

The $^{187}Os/^{188}Os$ values of seawater from OAE1a (grey shaded area in panels A and B, blue shaded area in panel C). $^{187}Os/^{188}Os$ are shown in red. Panel A and B adapted from Bottini et al. (2016) and panel C from Tejada et al. (2009).

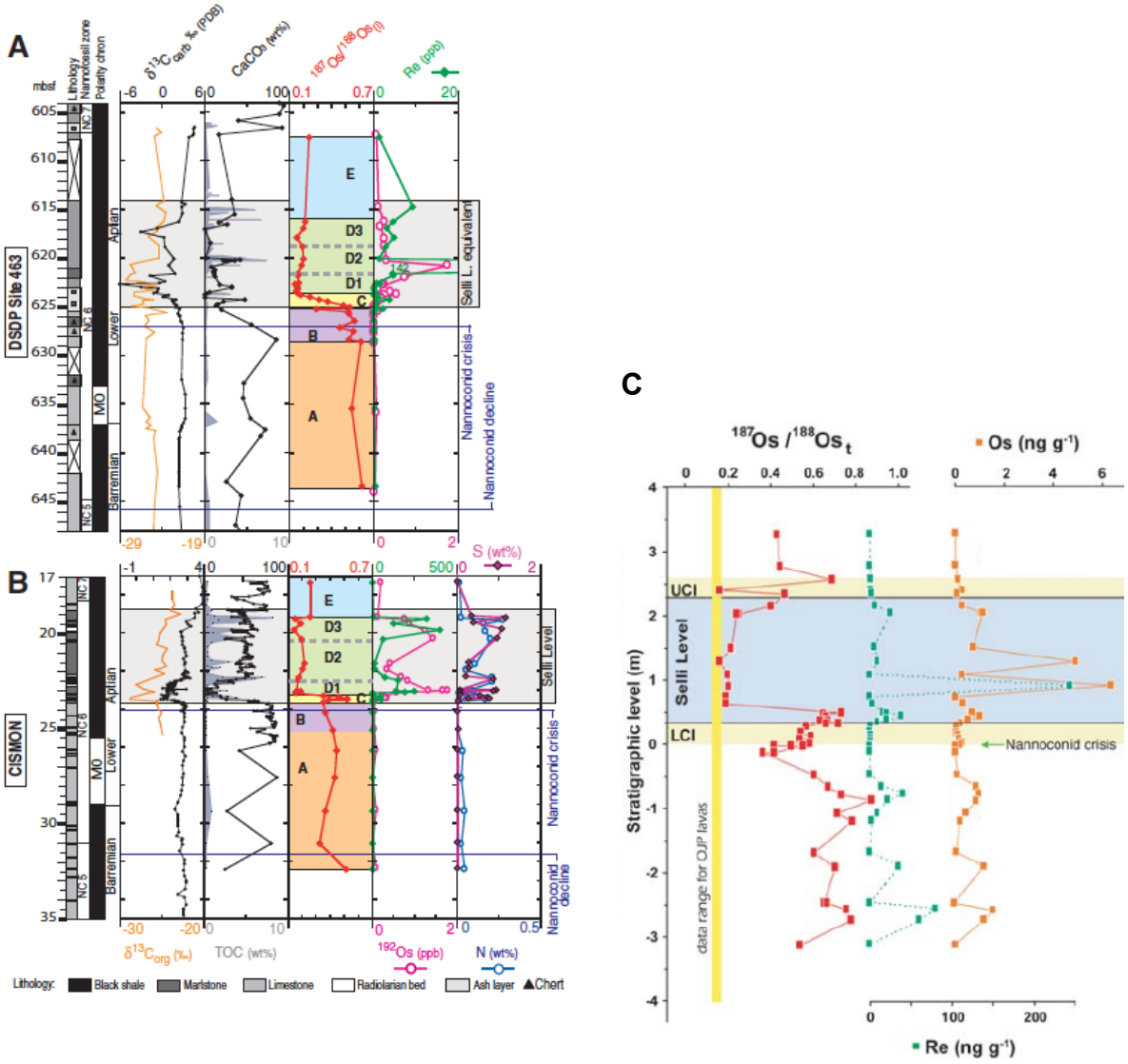

Figure 3.16: Simplified $^{187}Os/^{188}Os$ curves from major LIP events.

Simplified $^{187}Os/^{188}Os$ curves from the Cretaceous-Paleogene Boundary, the Triassic-Jurassic Boundary, the Paleocene-Eocene Thermal Maximum, OAE2, and OAE1a. Time moves forward from left to right. The dashed line in Panel A shows the influence of the K-Pg impact on $^{187}Os/^{188}Os$.

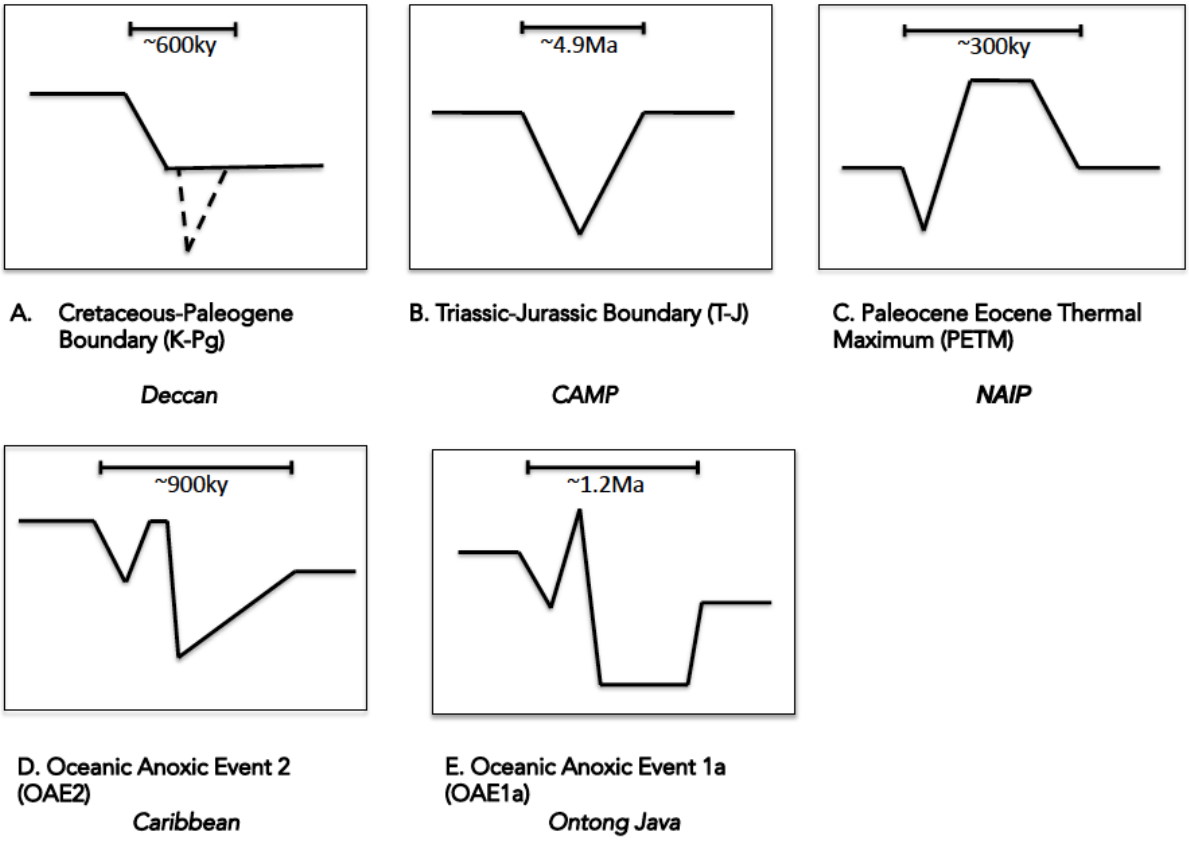

APPENDIX A

Supplemental Data from Chapter 2: Robinson et al. (2009)

Note: Appendix A contains the supplemental material that originally accompanied Robinson et al. (2009). Appendix B presents the same data with revised ages after Gradstein et al. (2012).

Table A1: Age model datums

	Age (Ma)[a]	Site 525 (mbsf)[b]	Site 577 (m, below KPB)[b]	Site 690 (mbsf)[c]	Bottaccione (height)[d]
KPB	65.51	451.71	0	247.82	382.60
C30n top	65.843	456.69	3.46	252.28	378.00
C30n bottom	67.875	475.15	11.55	255.00	371.20
C31n top	68.00	476.5	12.02	*missing*	370.20

References:

[a]Hicks et al., 2002

[b]Ravizza and Peucker-Ehrenbrink, 2003

[c]Hamilton, 1990

[d]Coccioni et al., 2004

Table A2: Major element XRF analyses for ODP Leg 113 Site 690C

Samle ID is as follows: core.section.midpoint of sample interval
Weight % of dry samples

Sample ID	Depth	SiO_2	TiO_2	Al_2O_3	Fe as Fe_2O_3	MnO	MgO	CaO	Na_2O	K_2O	P_2O_5	Loss on Ignition CO_2	TOTAL
015.04W.60	248.00	8.00	0.08	1.85	0.89	0.05	0.76	47.51	0.78	0.43	0.11	39.23	99.69
015.04W.140	248.80	7.97	0.08	1.92	0.94	0.06	0.70	47.52	0.70	0.42	0.11	38.90	99.32
015.05W.140	250.30	10.31	0.11	2.51	1.25	0.05	0.93	45.10	1.15	0.53	0.13	37.79	99.86
015.05W.140	250.30	10.20	0.11	2.47	1.23	0.06	0.92	45.32	0.94	0.53	0.14	38.00	99.89
015.06W.142	251.82	6.29	0.07	1.48	0.74	0.04	0.59	48.93	0.80	0.32	0.11	40.46	99.81
015.06W.142	251.82	6.29	0.07	1.48	0.74	0.04	0.59	48.93	0.80	0.32	0.11	40.46	99.81
015.07W.22	252.12	6.05	0.06	1.40	0.73	0.03	0.52	49.11	0.77	0.32	0.08	40.53	99.60
015.CCW.0	252.26	6.26	0.07	1.41	0.73	0.04	0.57	49.12	0.66	0.32	0.09	40.28	99.53
016.01W.15	252.65	6.35	0.07	1.44	0.75	0.06	0.63	49.22	0.54	0.31	0.25	40.04	99.64
016.01W.100	253.50	5.22	0.06	1.17	0.51	0.06	0.58	50.28	0.70	0.22	0.11	41.83	100.74
016.01W.100	253.50	4.60	0.05	1.08	0.52	0.05	0.50	50.56	0.74	0.22	0.11	41.64	100.07
016.01W.146	253.96	5.10	0.05	1.20	0.57	0.04	0.56	50.12	0.76	0.22	0.10	40.89	99.60
016.02W.16	254.16	4.75	0.05	1.14	0.56	0.04	0.54	50.61	0.68	0.22	0.11	41.12	99.82
016.02W.60	254.60	7.07	0.08	1.60	0.85	0.04	0.69	48.61	0.69	0.35	0.11	39.80	99.88
016.02W.100	255.00	6.25	0.07	1.44	0.74	0.06	0.59	49.21	0.72	0.31	0.11	40.40	99.87
016.02W.140	255.40	2.96	0.04	0.67	0.27	0.05	0.39	51.78	0.75	0.16	0.09	42.55	99.70
016.03W.15	255.65	3.62	0.04	0.82	0.36	0.05	0.42	51.68	0.56	0.18	0.08	41.89	99.70
016.03W.60	256.10	3.21	0.04	0.73	0.29	0.04	0.36	51.84	0.66	0.17	0.08	42.32	99.73
016.03W.60	256.10	3.10	0.04	0.71	0.30	0.05	0.45	52.09	0.66	0.17	0.06	42.44	100.06
016.03W.100	256.10	2.91	0.04	0.69	0.25	0.06	0.36	52.27	0.66	0.17	0.08	42.50	99.98
016.03W.144	256.94	5.82	0.07	1.33	0.69	0.06	0.59	49.30	0.82	0.30	0.08	40.65	99.70
016.04W.36	257.36	6.95	0.07	1.56	0.88	0.06	0.66	48.88	0.61	0.33	0.09	39.76	99.84
016.04W.80	257.80	5.41	0.06	1.21	0.65	0.05	0.61	49.62	0.78	0.26	0.13	40.81	99.57
016.CCW.15	258.05	4.95	0.05	1.25	0.56	0.05	0.49	50.57	0.49	0.20	0.09	40.93	99.63
017.01W.142	263.22	6.57	0.08	1.50	0.81	0.06	0.66	48.84	0.71	0.31	0.11	40.15	99.79
017.02W.100	264.30	5.93	0.05	1.45	0.61	0.08	0.64	49.33	0.76	0.21	0.10	40.37	99.52
017.03W.15	264.95	6.46	0.07	1.53	0.79	0.07	0.60	49.39	0.46	0.23	0.10	39.87	99.56
017.04W.5	266.35	6.16	0.06	1.32	0.70	0.05	0.58	49.71	0.55	0.27	0.12	40.28	99.79
018.01W.15	271.55	5.81	0.06	1.31	0.66	0.06	0.57	49.79	0.47	0.23	0.10	40.51	99.56
018.01W.100	272.40	5.31	0.05	1.19	0.52	0.07	0.54	50.33	0.41	0.22	0.14	40.66	99.43
018.02W.140	274.30	8.83	0.08	1.97	1.05	0.08	0.82	46.92	0.76	0.35	0.16	38.61	99.62
018.03W.100	275.40	9.73	0.09	2.18	1.08	0.08	0.86	46.47	0.72	0.41	0.12	38.15	99.89
018.04W.140	277.30	9.56	0.09	2.22	1.12	0.07	0.91	46.34	0.96	0.37	0.13	38.12	99.88
018.04W.140	277.30	9.50	0.09	2.15	1.10	0.09	0.90	46.25	0.79	0.37	0.15	38.20	99.57

Table A3: Weight percent calcium carbonate in DSDP 577 and ODP 690C

Leg 113 Site 690C[1] Sample	Depth (mbsf)	%$CaCO_3$
690C-015 04W 60-65cm	248.00	85%
690C-015 04W 83-88cm	248.23	81%
690C-015 04W 100-105cm	248.40	88%
	248.40	91%
	248.40	90%
690C-015 04W 120-125cm	248.60	88%
690C-015 04W 140-145cm	248.80	84%
690C-015 05W 15-20cm	249.05	82%
690C-015 05W 64-66cm	249.54	88%
690C-015 05W 100-105cm	249.90	91%
	249.90	92%
	249.90	89%
690C-015 05W 140-145cm	250.30	81%
690C-015 06W 15-18cm	250.55	81%
690C-015 06W 63-67cm	251.03	77%
	251.03	78%
690C-015 06W 102-105cm	251.42	84%
690C-015 06W 142-145cm	251.82	87%
	251.82	87%
690C-015 07W 22-25cm	252.12	87%
690C-015 CCW 0-7cm	252.26	87%
	252.26	86%
690C-016 01W 15-19cm	252.65	86%
690C-016 01W 60-65cm	253.10	91%
690C-016 01W 100-103cm	253.50	91%
	253.50	89%
690C-016 01W 146-149m	253.96	88%
690C-016 02W 16-20cm	254.16	90%
690C-016 02W 60-65cm	254.60	85%
	254.60	84%
	254.60	85%
690C-016 02W 100-105cm	255.00	86%

[1]Analysis at University of Hawai`i at Manoa

Leg 86 Site 577[2] Sample	Depth relative to KTB (m)	%$CaCO_3$
577B-001-01 93-95cm	-4.28	92%
577B-001-03 62-64cm	-1.56	95%
577B-001-04 53-54cm	-0.19	96%
577B-001-04 69-70cm	-0.03	89%
		90%
		89%
577B-001-04 85-86cm	0.13	97%
577B-001-04 109-110cm	0.37	99%
	0.37	95%
577A-012-05 73-76cm	1.60	93%
577A-012-06 1-3cm	2.30	96%
577B-001-06 2-4cm	2.31	94%
577A-012-06 42-46cm	2.72	96%
577A-012-06 90-95cm	3.21	94%
577A-012-06 144-147cm	3.74	97%
577A-012-07 13-16cm	3.94	96%
577A-013-01 0-3cm	4.30	96%
577A-013-01 40-43cm	4.70	97%
577A-013-01 90-94cm	5.21	96%
577A-013-01 140-145cm	5.71	95%
577A-013-02 70-75cm	6.51	97%
577A-013-03 69-72cm	7.99	97%
577A-013-04 141-145cm	10.21	97%

[2]Analysis at WHOI

Table A4: Os isotope and PGE data from DSDP Leg 86 Sites 577A and 577B.

Sample		Depth (mcd)	Depth relative to KTB (m)	Age (Ma)	$^{187}Os/^{188}Os$	error (2σ)	[Os] pg/g	error (pg/g)	[Ir] pg/g	error (pg/g)	[Pt] pg/g	error (pg/g)	[Os] / [Ir]	[Pt] / [Ir]
577B-001-04 85-86cm	*	109.73	0.13	65.52	0.240	0.001	54.0		348		726		0.16	2.09
577B-001-04 109-110cm	*	109.97	0.37	65.55	0.336	0.001	26.0		46		165		0.57	3.59
577A-012-05 73-76cm	*	111.20	1.60	65.66	0.436	0.006	13.0		34		1303		0.38	37.81
577A-012-06 1-3cm	*	111.90	2.30	65.73	0.405	0.001	15.0		20		255		0.77	13.01
577B-001-06 2-4cm	*	111.91	2.31	65.73	0.383	0.002	15.0		29		249		0.52	8.65
577A-012-06 42-46cm	#	112.32	2.72	65.77	0.467	0.006	9.0		16		231		0.57	14.55
577A-012-06 90-95cm	#	112.81	3.21	65.82	0.549	0.004	7.0		7		110		0.94	14.66
577A-012-06 144-147cm	#	113.34	3.74	65.91	0.541	0.010	7.0		22		173		0.31	7.74
577A-012-07 13-16cm	#	113.54	3.94	65.96	0.545	0.007	9.0		9		143		0.95	15.07
577A-013-01 0-3cm	#	113.90	4.30	66.05	0.530	0.004	14.0		15		312		0.91	20.20
577A-013-01 40-43cm	#	114.30	4.70	66.15	0.579	0.008	8.0		5		640		1.65	####
577A-013-01 90-94cm	#	114.81	5.21	66.28	0.584	0.007	8.0		7		163		1.20	24.38
577A-013-01 140-145cm	#	115.31	5.71	66.41	0.557	0.006	10.0		5		57		1.92	10.94
577A-013-02 70-75cm	#	116.11	6.51	66.61	0.569	0.004	10.0		8		92		1.33	12.20
577A-013-02 143-147cm		116.83	7.23	66.79	0.5360	0.0033	8.3	0.03	9	0.65	123	3.33	0.98	14.46
577A-013-03 69-72cm	#	117.59	7.99	66.98	0.590	0.005	10.0		6		122		1.75	21.36
577A-013-03 126-130cm		118.16	8.56	67.12	0.5757	0.0030	8.4	0.02	7	0.50	126	2.50	1.11	16.78
577A-013-03 126-130cm		118.16	8.56	67.12	0.5915	0.0035	8.1	0.02	7	0.67	90	10.07	1.12	12.54
577A-013-03 126-130cm		118.16	8.56	67.12	0.5756	0.0035	8.1	0.03	6	0.24	86	12.68	1.29	13.78
577A-013-04 70-74cm		119.10	9.50	67.36	0.5743	0.0047	8.0	0.06	6	0.66	113	5.08	1.28	18.12
577A-013-04 70-74cm		119.10	9.50	67.36	0.5581	0.0079	8.9	0.06	6	0.60	91	15.95	1.40	14.37
577A-013-04 70-74cm		119.10	9.50	67.36	0.5825	0.0048	8.6	0.05	5	0.61	112	14.12	1.73	22.51
577A-013-04 141-145cm		119.81	10.21	67.54	0.5140	0.0029	9.0	0.02	10	0.26	120	3.31	0.86	11.46
577A-013-04 141-145cm		119.81	10.21	67.54	0.5672	0.0061	7.8	0.04	6	0.60	99	16.67	1.37	17.33
577A-013-04 141-145cm		119.81	10.21	67.54	0.3618	0.0014	14.8	0.17	13	0.64	115	13.08	1.13	8.73
577A-013-05 84-86cm	*	120.1	10.50	67.61	0.548	0.001	14.0		7		111		2.06	16.32
577A-013-05 131-135cm		121.21	11.61	67.89	0.5366	0.0029	9.0	0.02	9.7	1.87	99.7	5.32	0.93	10.30

Table A4: Os isotope and PGE data from DSDP Leg 86 Sites 577A and 577B.

Sample	Depth (mcd)	Depth relative to KTB (m)	Age (Ma)	$^{187}Os/^{188}Os$	error (2σ)	[Os] pg/g	error (pg/g)	[Ir] pg/g	error (pg/g)	[Pt] pg/g	error (pg/g)	[Os] / [Ir]	[Pt] / [Ir]
577A-013-06 24-27cm	121.64	12.04	68.01	0.5423	0.0019	9.2	0.02	12.8	0.86	194.7	8.23	0.71	15.17
577A-013-06 72-76cm	122.12	12.52	68.13	0.5960	0.0022	9.7	0.02	7.0	0.29	81.0	2.07	1.38	11.62
577A-013-06 72-76cm	122.12	12.52	68.13	0.6048	0.0024	10.2	0.02	7.3	0.74	84.8	10.90	1.38	11.54
577A-013-06 123-127cm	122.63	13.03	68.27	0.5844	0.0037	9.0	0.04	7.1	1.09	652.6	8.43	1.27	91.96
577A-013-06 123-127cm	122.63	13.03	68.27	0.6088	0.0056	8.6	0.03						
577A-013-07 1-5cm	122.91	13.31	68.34	0.5977	0.0030	9.9	0.02	6.2	0.47	109.3	2.13	1.59	17.51
577A-013-CC 16-20cm	123.14	13.54	68.40	0.5919	0.0025	9.0	0.02	9.6	2.18	122.9	1.14	0.93	12.79

*Previously published Os data (Ravizza and Peucker-Ehrenbrink, 2003), except for [Pt] and some [Ir] which is previously unreported data from WHOI

#This study. Analyses at WHOI

Table A5: Os isotope and PGE data from ODP Leg 113 Site 690C

Sample	Depth (mbsf)	Age (Ma)	$^{187}Os/^{188}Os$	error (2σ)	[Os] pg/g	error (pg/g)	[Ir] pg/g	error (pg/g)	[Pt] pg/g	error (pg/g)	[Os] / [Ir]	[Pt] / [Ir]
690C-015 04W 60-65cm	248.00	65.53	0.3374	0.0014	49.9	1.1	117.6	0.9	526.2	3.3	0.42	4.48
690C-015 04W 83-88cm	248.23	65.54	0.3635	0.0030	43.0	0.2	98.0	1.6	583.2	2.3	0.44	5.95
690C-015 04W 100-105cm	248.40	65.56	0.4055	0.0069	40.3	0.4	35.3	0.7	409.9	5.2	1.14	11.61
	248.40	65.56	0.3905	0.0015	41.1	0.1	33.6	0.6	372.3	3.7	1.22	11.08
690C-015 04W 120-125cm	248.60	65.57	0.4052	0.0028	34.9	0.1	30.5	0.6	470.9	9.4	1.14	15.42
690C-015 04W 140-145cm	248.80	65.59	0.4220	0.0014	31.1	0.2	36.4	0.4	484.2	3.0	0.85	13.29
690C-015 05W 15-20cm	249.05	65.60	0.4386	0.0021	30.7	0.1	28.3	0.3	510.1	2.5	1.09	18.03
690C-015 05W 64-66cm	249.54	65.64	0.4234	0.0014	30.6	0.1	19.9	0.3	357.3	3.8	1.54	17.97
690C-015 05W 100-105cm	249.90	65.67	0.6022	0.0048	31.1	0.1	15.0	0.3	275.5	8.4	2.08	18.37
	249.90	65.67	0.4399	0.0014	30.7	0.1	19.0	0.0	286.9	0.0	1.61	15.11
690C-015 05W 140-145cm	250.30	65.70	0.4499	0.0020	32.9	0.1	23.5	0.4	440.8	3.3	1.40	18.77
690C-015 06W 15-18cm	250.55	65.72	0.4582	0.0022	25.9	0.1	23.6	1.1	450.2	6.4	1.10	19.07
690C-015 06W 63-67cm	251.03	65.75	0.3716	0.0016	27.7	0.1	32.5	0.7	418.9	1.8	0.85	12.88
	251.03	65.75	0.4693	0.0031	19.9	0.1	24.7	1.2	424.1	6.0	0.81	17.20
690C-015 06W 102-105cm	251.42	65.78	0.4982	0.0025	15.7	0.0	17.3	0.3	274.7	1.5	0.90	15.88
690C-015 06W 142-145cm	251.82	65.81	0.5294	0.0022	15.1	0.1	12.9	0.3	216.9	2.4	1.17	16.81
	251.82	65.81	0.8126	0.0093	6.4	0.0	12.1	0.5	205.0	3.5	0.53	16.98
690C-015 07W 22-25cm	252.12	65.83	0.5842	0.0026	13.1	0.0	11.7	0.4	181.3	0.9	1.12	15.45
690C-015 CCW 0-7cm	252.26	65.84	0.5418	0.0029	15.2	0.0	15.6	0.4	240.7	2.8	0.97	15.43
690C-016 01W 15-19cm	252.65	66.12	0.5796	0.0023	18.5	0.1	12.9	0.2	197.2	1.2	1.43	15.25
690C-016 01W 60-65cm	253.10	66.46	0.5872	0.0025	19.7	0.0	8.7	0.3	163.3	2.6	2.28	18.88
690C-016 01W 100-103cm	253.50	66.76	0.5942	0.0017	22.1	0.0	17.3	0.4	244.9	2.9	1.28	14.16

Table A5: Os isotope and PGE data from ODP Leg 113 Site 690C

Sample	Depth (mbsf)	Age (Ma)	$^{187}Os/^{188}Os$	error (2σ)	[Os] pg/g	error (pg/g)	[Ir] pg/g	error (pg/g)	[Pt] pg/g	error (pg/g)	[Os] / [Ir]	[Pt] / [Ir]
	253.50	66.76	0.5968	0.0063	22.2	0.3	9.6	0.4	169.4	5.0	2.32	17.66
690C-016 01W 146-149m	253.96	67.10	0.5850	0.0019	19.6	0.1	8.9	0.2	149.0	1.9	2.21	16.77
690C-016 02W 16-20cm	254.16	67.25	0.5858	0.0019	19.4	0.0	8.9	0.1	147.1	1.2	2.17	16.48
690C-016 02W 60-65cm	254.60	67.58	0.5539	0.0025	18.0	0.1	11.9	0.1	209.9	1.3	1.51	17.68
	254.60	67.58	0.5594	0.0030	17.9	0.1	12.0	0.2	215.0	5.4	1.49	17.91
690C-016 02W 100-105cm	255.00	67.88	0.5401	0.0017	28.6	0.1	16.3	0.4	504.0	4.3	1.75	30.83
690C-016 02W 140-145cm	255.40	67.90	0.5678	0.0022	19.3	0.0	7.1	0.2	266.5	2.9	2.73	37.70
	255.40	67.90	0.5718	0.0029	19.1	0.0	7.1	0.2	264.4	6.3	2.69	37.27
690C-016 03W 15-20cm	255.65	67.92	0.5640	0.0020	20.4	0.0	7.4	0.4	315.1	2.2	2.74	42.36
	255.65	67.92	0.5704	0.0024	19.8	0.1	7.4	0.2	321.6	2.5	2.68	43.54
690C-016 03W 60-65cm	256.10	67.95	0.5777	0.0017	21.6	0.0	8.5	0.3	322.3	1.5	2.54	37.84
690C-016 03W 100-105cm	256.50	67.97	0.5187	0.0013	31.9	0.0	9.9	0.3	2296.9	57.3	3.23	232.31
	256.50	67.97	0.5318	0.0022	41.2	0.2	11.1	0.3	2350.8	9.2	3.70	210.93
690C-016 03W 144-145cm	256.94	68.00	0.5422	0.0020	22.4	0.1	11.0	0.2	375.2	1.6	2.04	34.05
690C-016 04W 36-40cm	257.36	68.03	0.5369	0.0023	18.5	0.0	11.2	0.3	192.7	2.7	1.65	17.16
	257.36	68.03	0.5434	0.0030	18.1	0.1	10.0	0.1	206.1	1.7	1.82	20.66
690C-016 04W 80-85cm	257.80	68.06	0.5634	0.0020	21.4	0.1	9.6	0.4	240.4	2.2	2.24	25.15
690C-016 CCW 15-20cm	258.05	68.08	0.5181	0.0014	54.6	0.1	8.8	0.1	266.6	1.7	6.19	30.22
	258.05	68.08	0.5181	0.0014	54.6	0.1	8.4	0.0	248.5	0.0	6.47	29.43
	258.05	68.08	0.5187	0.0011	55.6	0.1	9.7	0.2	296.7	4.7	5.72	30.49
690C-017 01W 16-20cm	261.96	68.33	0.5350	0.0017	42.2	0.1	8.0	0.1	214.3	0.9	5.28	26.80
690C-017 01W 62-65cm	262.42	68.36	0.5447	0.0021	46.0	0.2	8.0	0.3	328.4	1.9	5.77	41.24

Table A5: Os isotope and PGE data from ODP Leg 113 Site 690C

Sample	Depth (mbsf)	Age (Ma)	$^{187}Os/^{188}Os$	error (2σ)	[Os] pg/g	error (pg/g)	[Ir] pg/g	error (pg/g)	[Pt] pg/g	error (pg/g)	[Os]/[Ir]	[Pt]/[Ir]
690C-017 01W 100-104cm	262.80	68.39	0.5490	0.0021	39.7	0.4	8.3	0.2	228.4	3.8	4.78	27.50
	262.80	68.39					16.0	0.8	224.7	6.3		14.00
690C-017 01W 142-144cm	263.22	68.42	0.5404	0.0052	54.3	0.5	9.4	0.2	232.2	2.9	5.78	24.72
690C-017 02W 16-20cm	263.46	68.43	0.5284	0.0016	61.6	0.2	12.0	0.3	218.3	2.1	5.15	18.26
	263.46	68.43	0.5309	0.0033	61.5	1.2	11.0	0.3	203.6	3.2	5.58	18.49
690C-017 02W 60-65cm	263.90	68.46	0.5404	0.0014	60.5	0.2	11.1	0.2	562.6	1.8	5.45	50.67
690C-017 02W 100-104cm	264.30	68.49	0.5430	0.0015	64.1	0.1	8.9	0.2	248.6	1.7	7.22	28.01

Table A6: Os isotope and PGE data from the Bottaccione Section, Gubbio, Italy.

Height (m)	Age (Ma)	$^{187}Os/^{188}Os$	error (2σ)	[Os] pg/g	error (pg/g)	[Ir] pg/g	error (pg/g)	[Pt] pg/g	error (pg/g)	[Os]/[Ir]	[Pt]/[Ir]
382.60	65.510	0.2505	0.0010	59.0	0.5	106.5	1.3	375.1	8.5	0.55	3.52
382.60	65.510	0.2519	0.0017	49.5	0.5	85.0	1.6	356.9	5.2	0.58	4.20
382.40	65.524	0.2881	0.0012	34.5	0.1	95.7	0.9	305.6	7.5	0.36	3.19
382.20	65.539	0.3610	0.0041	28.9	0.3	24.1	0.5	258.9	3.5	1.20	10.76
382.20	65.539	0.3588	0.0008	28.8	0.0	23.8	0.2	259.3	4.9	1.21	10.87
382.00	65.553	0.3763	0.0011	26.1	0.1	23.5	0.4	152.3	2.4	1.11	6.47
381.80	65.568	0.4034	0.0013	19.8	0.0	14.9	0.3	88.3	3.9	1.33	5.92
381.60	65.582	0.4345	0.0037	24.5	0.2	19.9	0.2	160.6	3.9	1.23	8.09
381.40	65.597	0.3860	0.0034	24.6	0.1	14.4	0.7	119.7	3.2	1.71	8.29
381.20	65.611	0.4164	0.0029	20.0	0.1	13.5	0.1	185.0	2.8	1.48	13.70
381.00	65.626	0.4217	0.0014	22.2	0.1	18.9	0.3	181.4	2.6	1.17	9.59
380.80	65.640	0.4181	0.0019	18.9	0.1	11.5	0.4	135.8	3.5	1.64	11.79
380.60	65.655	0.4223	0.0041	18.2	0.1						
380.60	65.655					10.6	0.2	97.8	0.8		
380.60	65.655	0.4215	0.0015	17.6	0.0						
380.40	65.669	0.4232	0.0016	18.4	0.0	17.6	0.8	139.6	2.7	1.05	7.94
380.20	65.684	0.4183	0.0020	19.2	0.0	12.0	0.3	127.1	1.4	1.60	10.59
380.00	65.698	0.4234	0.0019	20.3	0.1	17.6	0.6	163.4	4.1	1.15	9.26
380.00	65.698					12.4	0.2	151.9	2.8		12.24

Table A6: Os isotope and PGE data from the Bottaccione Section, Gubbio, Italy.

Height (m)	Age (Ma)	$^{187}Os/^{188}Os$	error (2σ)	[Os] pg/g	error (pg/g)	[Ir] pg/g	error (pg/g)	[Pt] pg/g	error (pg/g)	[Os]/[Ir]	[Pt]/[Ir]
379.80	65.713	0.4342	0.0015	19.0	0.0						
379.60	65.727	0.4443	0.0031	16.0	0.1						
379.40	65.742	0.4589	0.0018	16.5	0.0	11.2	0.3	112.8	1.5	1.47	10.05
379.20	65.756	0.5047	0.0031	13.6	0.1	7.2	0.1	122.9	3.0	1.88	16.97
379.20	65.756	0.4780	0.0040	13.5	0.1	7.5	0.3	121.8	1.5	1.81	16.29
379.00	65.771	0.4833	0.0019	18.1	0.0	11.3	0.2	146.0	2.1	1.60	12.88
378.80	65.785	0.4973	0.0014	15.7	0.0	11.4	0.1	120.4	2.3	1.38	10.58
378.40	65.814	0.5324	0.0023	13.6	0.0						
378.40	65.814					8.4	0.1	94.1	2.7		11.27
378.20	65.829	0.5448	0.0016	14.1	0.0	8.3	0.2	90.4	4.3	1.68	10.83
378.20	65.829					8.6	0.2	91.2	1.5		10.58
378.00	65.843	0.5546	0.0021	14.7	0.0	12.7	0.2	112.7	1.9	1.15	8.87
377.80	65.903	0.5742	0.0025	14.6	0.0	9.8	0.2	91.2	2.9	1.49	9.32
377.50	65.992	0.5789	0.0019	14.9	0.0	10.3	0.3	122.6	3.5	1.44	11.88
377.20	66.082	0.5840	0.0030	23.8	0.1	19.6	0.2	257.2	1.2	1.21	13.14
376.90	66.172	0.6068	0.0019	15.8	0.0	7.7	0.2	105.4	3.1	2.04	13.61
376.30	66.351	0.6126	0.0025	14.0	0.0	8.4	0.2	88.2	2.7	1.66	10.45
376.30	66.351	0.6126	0.0034	14.8	0.0	8.7	0.3	93.7	4.3	1.69	10.71
376.10	66.411	0.6094	0.0023	13.1	0.0						

Table A6: Os isotope and PGE data from the Bottaccione Section, Gubbio, Italy.

Height (m)	Age (Ma)	$^{187}Os/^{188}Os$	error (2σ)	[Os] pg/g	error (pg/g)	[Ir] pg/g	error (pg/g)	[Pt] pg/g	error (pg/g)	[Os]/[Ir]	[Pt]/[Ir]
376.10	66.411	0.6254	0.0057	13.3	0.1	7.9	0.1	85.7	1.5	1.68	10.87
375.80	66.500	0.6023	0.0042	13.8	0.1	7.5	0.2	92.6	1.7	1.84	12.38
375.50	66.590	0.6087	0.0023	13.0	0.0	7.6	0.2	93.8	3.8	1.71	12.40
375.50	66.590	0.6107	0.0036	13.8	0.0	7.9	0.1	96.0	2.0	1.75	12.18
375.20	66.680	0.6119	0.0021	13.4	0.0	8.5	0.3	95.7	2.2	1.58	11.26
374.90	66.769	0.5967	0.0017	17.2	0.0						
374.60	66.859	0.5944	0.0018	15.8	0.0	10.7	0.4	101.9	2.3	1.48	9.50
374.30	66.949	0.6146	0.0021	15.6	0.1	9.3	0.3	120.3	4.5	1.67	12.92
374.30	66.949	0.6004	0.0013	15.8	0.1	9.8	0.5	124.8	4.9	1.61	12.72
374.00	67.038	0.6118	0.0030	13.5	0.1	7.0	0.3	60.7	2.2	1.92	8.61
374.00	67.038	0.6185	0.0040	13.1	0.1	7.2	0.2	69.2	2.8	1.81	9.59
373.80	67.098	0.6386	0.0070	14.9	0.1	8.3	0.2	84.0	3.9	1.79	10.06
373.50	67.188	0.6258	0.0076	12.6	0.1						
373.20	67.277	0.6303	0.0087	12.3	0.1	7.6	0.2	98.3	0.9	1.61	12.91
373.00	67.337	0.6074	0.0024	12.4	0.0						
372.80	67.397	0.6018	0.0019	13.4	0.0	8.1	0.2	109.6	4.3	1.65	13.46
372.80	67.397	0.6038	0.0036	13.1	0.1	6.9	0.3	107.8	4.5	1.90	15.68
372.50	67.487	0.6028	0.0027	14.7	0.0						
372.20	67.576	0.5823	0.0030	15.9	0.0	9.9	0.1	100.2	3.4	1.60	10.13

Table A6: Os isotope and PGE data from the Bottaccione Section, Gubbio, Italy.

Height (m)	Age (Ma)	$^{187}Os/^{188}Os$	error (2σ)	[Os] pg/g	error (pg/g)	[Ir] pg/g	error (pg/g)	[Pt] pg/g	error (pg/g)	[Os]/[Ir]	[Pt]/[Ir]
372.00	67.636	0.6084	0.0017	14.8	0.0						
372.00	67.636	0.6105	0.0027	14.8	0.0	8.0	0.2	92.9	4.9	1.86	11.67
371.95	67.651	0.6218	0.0080	13.6	0.1	7.9	0.1	70.2	2.2	1.71	8.85
371.90	67.666	0.6095	0.0026	16.4	0.0						
371.70	67.726	0.6020	0.0037	12.3	0.1	10.0	0.5	75.2	2.7	1.23	7.51
371.50	67.785	0.5946	0.0033	12.8	0.0	6.5	0.3	80.5	1.6	1.99	12.48
371.45	67.800	0.5875	0.0022	15.0	0.0	7.9	0.3	86.1	2.8	1.89	10.84
371.40	67.815	0.5888	0.0027	14.1	0.0	8.0	0.1	88.1	1.3	1.77	11.00
371.35	67.830	0.5803	0.0045	15.3	0.1	8.0	0.2	95.2	3.2	1.91	11.90
371.20	67.875	0.5919	0.0021	17.0	0.1	12.8	0.4	120.9	3.7	1.32	9.42
370.95	67.901	0.5620	0.0031	15.9	0.0	7.8	0.3	85.9	3.6	2.04	10.99
370.90	67.906	0.5817	0.0038	15.3	0.0	7.3	0.2	118.7	1.6	2.10	16.23
370.90	67.906	0.5794	0.0028	16.2	0.1	8.0	0.1	107.3	2.9	2.02	13.37
370.75	67.922	0.5831	0.0026	21.0	0.1	9.4	0.2	130.2	4.1	2.24	13.91
370.75	67.922	0.5840	0.0022	20.8	0.0						
370.70	67.927	0.5890	0.0049	16.4	0.2	8.1	0.2	89.3	1.3	2.02	11.00
370.70	67.927	0.5904	0.0038	16.2	0.1						
370.60	67.938	0.5953	0.0063	15.4	0.1	6.7	0.2	74.5	1.1	2.30	11.17
370.60	67.938	0.5677	0.0014	16.8	0.0						

Table A6: Os isotope and PGE data from the Bottaccione Section, Gubbio, Italy.

Height (m)	Age (Ma)	$^{187}Os/^{188}Os$	error (2σ)	[Os] pg/g	error (pg/g)	[Ir] pg/g	error (pg/g)	[Pt] pg/g	error (pg/g)	[Os]/[Ir]	[Pt]/[Ir]
370.60	67.938	0.5704	0.0028	18.0	0.0	8.3	0.2	118.5	3.8	2.17	14.26
370.40	67.958	0.5666	0.0028	19.2	0.1	7.4	0.2	141.2	1.1	2.58	19.03
370.20	67.979	0.5670	0.0022	18.4	0.1	8.6	0.4	102.2	3.6	2.15	11.95
370.00	68.000	0.5696	0.0018	19.8	0.0	11.5	0.1	103.3	0.6	1.72	9.00
370.00	68.000	0.5593	0.0015	20.2	0.0	12.1	0.2	107.4	2.3	1.67	8.90

Table A7: Os isotope and PGE data from DSDP Leg 74 Site 525A.

Sample*	Depth (mbsf)	Age	$^{187}Os/^{188}Os$*	error* (2σ)	[Os] pg/g*	[Ir] pg/g#	[Pt] pg/g#	[Os]/[Ir] #	[Pt]/[Ir] #
525A-40R-02 97-100cm	452.57	65.57	0.3880	0.0080	46	26	432	1.76	16.55
525A-40R-02 97-100cm	452.57	65.57	0.4150	0.0100	42	22	354	1.92	16.20
525A-40R-03 120-123cm	454.30	65.68	0.4002	0.0027	39	24	367	1.61	15.19
525A-40R-04 62-64cm	455.12	65.74	0.4300	0.0050	25	13	401	1.95	31.27
525A-40R-04 62-64cm	455.12	65.74	0.4170	0.0060	27	14	413	1.91	29.21
525A-40R-05 87-90cm	456.87	65.86	0.4580	0.0060	27	11	297	2.56	28.18
525A-40R-06 5-9cm	457.55	65.94	0.4829	0.0021	74	20	437	3.67	21.65
525A-41R-01 21-24cm	459.81	66.19	0.5462	0.0023	57	21	436	2.78	21.25
525A-41R-03 131-134cm	463.91	66.64	0.5570	0.0060	49	22	504	2.27	23.34
525A-41R-03 131-134cm	463.91	66.64	0.5520	0.0060	52	17	433	3.08	25.63
525A-41R-07 29-32cm	468.58	67.15	0.562	0.0052	45	21	369	2.12	17.55
525A-43R-101 130-133cm	479.90	68.27	0.636	0.0136	38	19	426	1.98	22.55

*Previously published data from Ravizza and Peucker-Ehrenbrink, 2003.

#Previously unpublished data

Table A8: Re-Os analyses of sediment leaches and associated age corrections.

Sample	Depth (mbsf)	Age (Ma)	bulk $^{187}Os/^{188}Os$	error (2σ)	[Os] pg/g	error	[Re] pg/g	$^{187}Os/^{188}Os$ corrected	correction magnitude
690C 015 04W 60-65	248.00	65.525	0.3484	0.0023	32.7	0.27	4.6	0.3477	0.21%
690C 015 04W 120-125cm	248.60	65.570	0.4043	0.0029	22.6	0.21	6.2	0.4029	0.36%
690C 015 CCW 0-7cm	252.26	65.843	0.4720	0.0480	10.9	0.48	4.4	0.4699	0.45%
690C 016 01W 15-19cm	252.65	66.124	0.6085	0.0078	10.0	0.20	4.0	0.6063	0.35%
690C 016 01W 146-149	253.96	67.102	0.6087	0.0065	10.3	0.20	4.0	0.6066	0.35%
690C 016 03W 60-65cm	256.10	67.948	0.5798	0.0064	10.5	0.22	2.6	0.5785	0.23%
690C 016 CCW 15-20cm	258.05	68.077	0.5412	0.0044	19.4	0.18	4.1	0.5400	0.22%
BTT 382.40m	382.40	65.524	0.2844	0.0044	19.4	0.21	2.5	0.2837	0.23%
BTT 381.80m	381.80	65.568	0.5525	0.0470	2.0	0.28	1.4	0.5487	0.70%
BTT 378.00m	378.00	65.843	0.5519	0.0094	6.5	0.20	3.1	0.5494	0.46%
BTT 376.90m	376.90	66.172	0.5968	0.0104	7.1	0.23	2.6	0.5948	0.33%
BTT 373.80m	373.80	67.098	0.6016	0.0117	5.5	0.22	2.8	0.5989	0.45%
BTT 370.00m	370.00	68.000	0.5599	0.0088	8.2	0.21	2.5	0.5582	0.31%
577A 013H 03W 126-130cm	118.16	67.124	0.5884	0.0149	4.3	0.20	2.9	0.5847	0.64%
525A 40R-2 97-100cm	452.57	65.570	0.3866	0.0051	13.9	0.23	6.5	0.3842	0.63%
525A 40R-5 87-90cm	456.87	65.860	0.4099	0.0059	12.7	0.16	4.0	0.4083	0.40%
525A 41R-1 21-24cm	459.81	66.190	0.5564	0.0076	7.6	0.23	19.1	0.5429	2.42%
525A 41R-7 29-32cm	468.58	67.150	0.5889	0.0117	12.0	0.24	100.3	0.5432	7.76%

Figure A1: Comparison of $^{187}Os/^{188}Os$ with $\delta^{18}O$ of benthic foraminiferaComparison of $^{187}Os/^{188}Os$ with $\delta^{18}O$ planktic (○) and benthic (▼) foraminifera for study sites. Stable isotope data for DSDP Site 525 (○ = R. rugosa; ▼=A.acuta) is from Li and Keller, 1998; DSDP Site 577 (▼=N.truempyi) is unpublished data from Norris; ODP Site 690 (○ = A. australis & H. globulosa; ▼= N. truempyi & G. beccariformis) is from Huber & Barrera, 1990 and Barrera and Savin, 1999. Barrera, E., Huber, B., 1990. Evolution of Antarctic waters during the Maastrichtian: Foraminifer oxygen and carbon isotope ratios, Leg 113. Proc. Ocean Drill. Prog. Sci. Results 113, 813–828. Barrera, E., Savin, S.,1999. Evolution of late Campanian–Maastrichtian marine climates and oceans. In: Evolution of the Cretaceous Ocean-Climate System. Geol. Soc. Am. Spec. Pap. 332, 245–282.

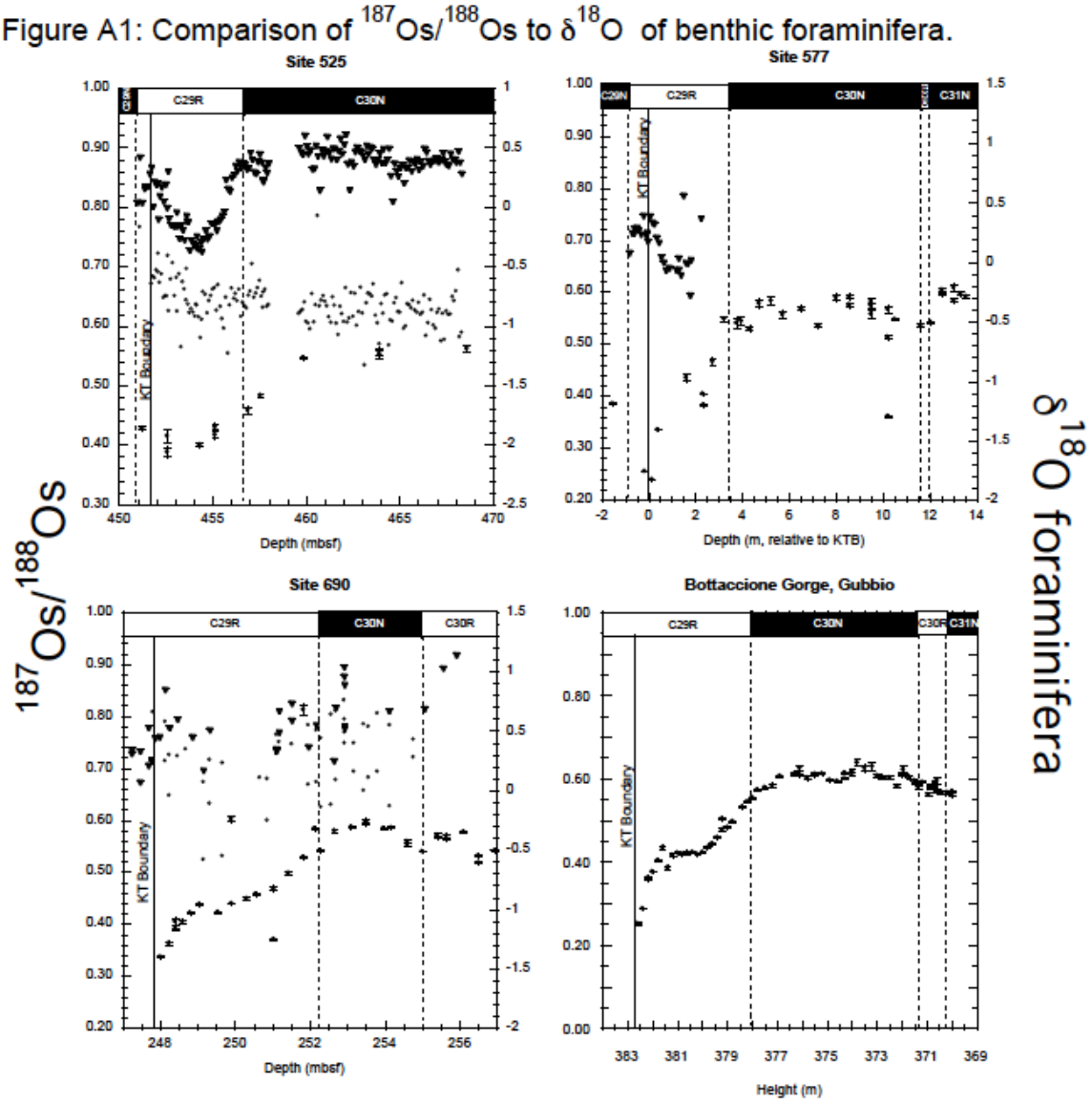

APPENDIX B

Supplementary data from Robinson et al. (2009) presented with revised age model

Note: Appendix A contains the supplemental material that originally accompanied Robinson et al. (2009). Appendix B presents the same data with revised ages after Gradstein et al. (2012).

Table B1: Calculated fractional contributions of lithogenic and cosmic Os to the total Os inventory of pelagic carbonates using age model from Gradstein et al., 2012.

	f_{lith}[1] *from [Al]*	f_{lith} *from $CaC0_3$*	$f_{lith}Os$[2] *from [Al]*	$f_{lith}Os$[2] *from $CaCO_3$*	Sed MAR[3] *(g/cm^2*kyr)*	$f_{ET}Os$[4] *Os_{ET} burial flux = 1.5 pg/cm^2ky*	$f_{ET}Os$[4] *Os_{ET} burial flux = 3.5 pg/cm^2ky*
Site 525	0.27 to 0.51[5]	0.24 to 0.45[8]	0.159 to 0.393	0.139 to 0.432	0.34 to 2.29	0.016 to 0.096	0.036 to 0.225
Site 577	0.006 to 0.036[6]	0.005 to 0.074[9]	0.003 to 0.096	0.006 to 0.251	0.52 to 1.11	0.025 to 0.414	0.058 to 0.966
Site 690	0.04 to 0.17[7]	0.03 to 0.19[10]	0.03 to 0.45	0.04 to 0.62	0.276 to 2.95	0.008 to 0.304	0.019 to 0.710
Bottacione	-	0.028 to 0.084[11]	-	0.019 to 0.137	1.02 to 3.47	0.009 to 0.1	0.020 to 0.2

[1] $[Al]_{UCC}$ = 8wt%, Taylor & McLennan, 1995

[2] $f_{lith}Os = (f_{lith} * [Os]_{UCC}]/[Os]_{total})$; $[Os]_{UCC}$ = 30 pg/g, from Peucker-Ehrenbrink & Jahn 2001

[3] Sediment mass accumuluation rate (MAR) = dry bulk density (DBD)* sedimentation rate

[4] $f_{ET}Os = Os_{ET}$ burial flux / Os_{total} burial flux; Os_{total} burial flux = $[Os]_{total}$ * Sed Rate * DBD

[5] [Al] calculated from Maillot & Robert DSDP Initial Reports vol. 74

[6] [Al] calculated from Michel et al. DSDP Initial Reports vol. 86 (year)

[7] [Al] from this study, see supplemental data table 2

[8] $CaCO_3$ from Kucera et al., 1997

[9] $CaCO_3$ is previously unpublished data from WHOI (see supplemental data table 2).

[10] $CaCO_3$ from this study (see supp. data table 2). When available EA values used otherwise calculated from XRF assuming $CaCO_3$ = LOI

[11] $CaCO_3$ from Crockett et al. 1988

Table B2: Age model datums using Gradstein et al., 2012

	Age (Ma)	Site 525 (mbsf)	Site 577 (m, below KPB)	Site 690 (mbsf)	Bottaccione (height)
KPB	66.04	451.71	0	247.82	382.60
C30n top	66.398	456.69	3.46	252.28	378.00
C30n bottom	68.196	475.15	11.55	255.00	371.20
C31n top	68.37	476.5	12.02	*missing*	370.20
reference	*a*	*b*	*c,d*	*e*	*f*

[a]*Gradstein et al (2012)*
[b]*Shackleton, 1984*
[c]*Bleil, 1985*
[d]*Michel et al., 1985*
[e]*Hamilton, 1990*
[f]*Coccioni et al., 2004*

Table B3: Os isotope and PGE data from DSDP Leg 86 Sites 577A and 577B using age model from Gradstein et al., 2012.

Sample		Depth (mcd)	Depth relative to KTB (m)	Age (Ma)	$^{187}Os/^{188}Os$	error (2σ)	[Os] pg/g	error (pg/g)	[Ir] pg/g	error (pg/g)	[Pt] pg/g	error (pg/g)	[Os] / [Ir]	[Pt] / [Ir]
577B-001-04 85-86cm	*	109.73	0.13	66.05	0.240	0.001	54.0		348		726		0.16	2.09
577B-001-04 109-110cm	*	109.97	0.37	66.08	0.336	0.001	26.0		46		165		0.57	3.59
577A-012-05 73-76cm	*	111.20	1.60	66.21	0.436	0.006	13.0		34		1303		0.38	37.81
577A-012-06 1-3cm	*	111.90	2.30	66.28	0.405	0.001	15.0		20		255		0.77	13.01
577B-001-06 2-4cm	*	111.91	2.31	66.28	0.383	0.002	15.0		29		249		0.52	8.65
577A-012-06 42-46cm	#	112.32	2.72	66.32	0.467	0.006	9.0		16		231		0.57	14.55
577A-012-06 90-95cm	#	112.81	3.21	66.37	0.549	0.004	7.0		7		110		0.94	14.66
577A-012-06 144-147cm	#	113.34	3.74	66.46	0.541	0.010	7.0		22		173		0.31	7.74
577A-012-07 13-16cm	#	113.54	3.94	66.50	0.545	0.007	9.0		9		143		0.95	15.07
577A-013-01 0-3cm	#	113.90	4.30	66.58	0.530	0.004	14.0		15		312		0.91	20.20
577A-013-01 40-43cm	#	114.30	4.70	66.67	0.579	0.008	8.0		5		640		1.65	132.20
577A-013-01 90-94cm	#	114.81	5.21	66.79	0.584	0.007	8.0		7		163		1.20	24.38
577A-013-01 140-145cm	#	115.31	5.71	66.90	0.557	0.006	10.0		5		57		1.92	10.94
577A-013-02 70-75cm	#	116.11	6.51	67.08	0.569	0.004	10.0		8		92		1.33	12.20
577A-013-02 143-147cm		116.83	7.23	67.24	0.5360	0.0033	8.3	0.03	9	0.65	123	3.33	0.98	14.46
577A-013-03 69-72cm	#	117.59	7.99	67.96	0.590	0.005	10.0		6		122		1.75	21.36
577A-013-03 126-130cm		118.16	8.56	67.53	0.5757	0.0030	8.4	0.02	7	0.50	126	2.50	1.11	16.78
577A-013-03 126-130cm		118.16	8.56	67.53	0.5915	0.0035	8.1	0.02	7	0.67	90	10.07	1.12	12.54
577A-013-03 126-130cm		118.16	8.56	67.53	0.5756	0.0035	8.1	0.03	6	0.24	86	12.68	1.29	13.78
577A-013-04 70-74cm		119.10	9.50	67.74	0.5743	0.0047	8.0	0.06	6	0.66	113	5.08	1.28	18.12
577A-013-04 70-74cm		119.10	9.50	67.74	0.5581	0.0079	8.9	0.06	6	0.60	91	15.95	1.40	14.37
577A-013-04 70-74cm		119.10	9.50	67.74	0.5825	0.0048	8.6	0.05	5	0.61	112	14.12	1.73	22.51
577A-013-04 141-145cm		119.81	10.21	67.90	0.5140	0.0029	9.0	0.02	10	0.26	120	3.31	0.86	11.46

Table B3: Os isotope and PGE data from DSDP Leg 86 Sites 577A and 577B using age model from Gradstein et al., 2012.

Sample		Depth (mcd)	Depth relative to KTB (m)	Age (Ma)	$^{187}Os/^{188}Os$	error (2σ)	[Os] pg/g	error (pg/g)	[Ir] pg/g	error (pg/g)	[Pt] pg/g	error (pg/g)	[Os] / [Ir]	[Pt] / [Ir]
577A-013-04 141-145cm		119.81	10.21	67.90	0.5672	0.0061	7.8	0.04	6	0.60	99	16.67	1.37	17.33
577A-013-04 141-145cm		119.81	10.21	67.90	0.3618	0.0014	14.8	0.17	13	0.64	115	13.08	1.13	8.73
577A-013-05 84-86cm	*	120.1	10.50	67.96	0.548	0.001	14.0		7		111		2.06	16.32
577A-013-05 131-135cm		121.21	11.61	68.22	0.5366	0.0029	9.0	0.02	9.7	1.87	99.7	5.32	0.93	10.30
577A-013-06 24-27cm		121.64	12.04	68.38	0.5423	0.0019	9.2	0.02	12.8	0.86	194.7	8.23	0.71	15.17
577A-013-06 72-76cm		122.12	12.52	68.55	0.5960	0.0022	9.7	0.02	7.0	0.29	81.0	2.07	1.38	11.62
577A-013-06 72-76cm		122.12	12.52	68.55	0.6048	0.0024	10.2	0.02	7.3	0.74	84.8	10.90	1.38	11.54
577A-013-06 123-127cm		122.63	13.03	68.74	0.5844	0.0037	9.0	0.04	7.1	1.09	652.6	8.43	1.27	91.96
577A-013-06 123-127cm		122.63	13.03	68.74	0.6088	0.0056	8.6	0.03						
577A-013-07 1-5cm		122.91	13.31	68.84	0.5977	0.0030	9.9	0.02	6.2	0.47	109.3	2.13	1.59	17.51
577A-013-CC 16-20cm		123.14	13.54	68.93	0.5919	0.0025	9.0	0.02	9.6	2.18	122.9	1.14	0.93	12.79

*Previously published Os data (Ravizza and Peucker-Ehrenbrink, 2003), except for [Pt] and some [Ir] which is previously unreported data from WHOI

#This study. Analyses at WHOI

Table B4: Os isotope and PGE data from ODP Leg 113 Site 690C using age model from Gradstein et al., 2012.

Sample	Depth (mbsf)	Age (Ma)	$^{187}Os/^{188}Os$	error (2σ)	[Os] pg/g	error (pg/g)	[Ir] pg/g	error (pg/g)	[Pt] pg/g	error (pg/g)	[Os] [Ir]	[Pt] [Ir]
690C-015 04W 60-65cm	248.00	66.04	0.3374	0.0014	49.9	1.1	117.6	0.9	526.2	3.3	0.42	4.48
690C-015 04W 83-88cm	248.23	66.07	0.3635	0.0030	43.0	0.2	98.0	1.6	583.2	2.3	0.44	5.95
690C-015 04W 100-105cm	248.40	66.09	0.4055	0.0069	40.3	0.4	35.3	0.7	409.9	5.2	1.14	11.61
	248.40	66.09	0.3905	0.0015	41.1	0.1	33.6	0.6	372.3	3.7	1.22	11.08
690C-015 04W 120-125cm	248.60	66.10	0.4052	0.0028	34.9	0.1	30.5	0.6	470.9	9.4	1.14	15.42
690C-015 04W 140-145cm	248.80	66.12	0.4220	0.0014	31.1	0.2	36.4	0.4	484.2	3.0	0.85	13.29
690C-015 05W 15-20cm	249.05	66.14	0.4386	0.0021	30.7	0.1	28.3	0.3	510.1	2.5	1.09	18.03
690C-015 05W 64-66cm	249.54	66.18	0.4234	0.0014	30.6	0.1	19.9	0.3	357.3	3.8	1.54	17.97
690C-015 05W 100-105cm	249.90	66.21	0.6022	0.0048	31.1	0.1	15.0	0.3	275.5	8.4	2.08	18.37
	249.90	66.21	0.4399	0.0014	30.7	0.1	19.0	0.0	286.9	0.0	1.61	15.11
690C-015 05W 140-145cm	250.30	66.24	0.4499	0.0020	32.9	0.1	23.5	0.4	440.8	3.3	1.40	18.77
690C-015 06W 15-18cm	250.55	66.26	0.4582	0.0022	25.9	0.1	23.6	1.1	450.2	6.4	1.10	19.07
690C-015 06W 63-67cm	251.03	66.30	0.3716	0.0016	27.7	0.1	32.5	0.7	418.9	1.8	0.85	12.88
	251.03	66.30	0.4693	0.0031	19.9	0.1	24.7	1.2	424.1	6.0	0.81	17.20
690C-015 06W 102-105cm	251.42	66.33	0.4982	0.0025	15.7	0.0	17.3	0.3	274.7	1.5	0.90	15.88
690C-015 06W 142-145cm	251.82	66.36	0.5294	0.0022	15.1	0.1	12.9	0.3	216.9	2.4	1.17	16.81
	251.82	66.36	0.8126	0.0093	6.4	0.0	12.1	0.5	205.0	3.5	0.53	16.98
690C-015 07W 22-25cm	252.12	66.39	0.5842	0.0026	13.1	0.0	11.7	0.4	181.3	0.9	1.12	15.45
690C-015 CCW 0-7cm	252.26	66.40	0.5418	0.0029	15.2	0.0	15.6	0.4	240.7	2.8	0.97	15.43
690C-016 01W 15-19cm	252.65	66.64	0.5796	0.0023	18.5	0.1	12.9	0.2	197.2	1.2	1.43	15.25
690C-016 01W 60-65cm	253.10	66.94	0.5872	0.0025	19.7	0.0	8.7	0.3	163.3	2.6	2.28	18.88
690C-016 01W 100-103cm	253.50	67.20	0.5942	0.0017	22.1	0.0	17.3	0.4	244.9	2.9	1.28	14.16
	253.50	67.20	0.5968	0.0063	22.2	0.3	9.6	0.4	169.4	5.0	2.32	17.66

Table B4: Os isotope and PGE data from ODP Leg 113 Site 690C using age model from Gradstein et al., 2012.

Sample	Depth (mbsf)	Age (Ma)	$^{187}Os/^{188}Os$	error (2σ)	[Os] pg/g	error (pg/g)	[Ir] pg/g	error (pg/g)	[Pt] pg/g	error (pg/g)	[Os] [Ir]	[Pt] [Ir]
690C-016 01W 146-149m	253.96	67.51	0.5850	0.0019	19.6	0.1	8.9	0.2	149.0	1.9	2.21	16.77
690C-016 02W 16-20cm	254.16	67.64	0.5858	0.0019	19.4	0.0	8.9	0.1	147.1	1.2	2.17	16.48
690C-016 02W 60-65cm	254.60	67.93	0.5539	0.0025	18.0	0.1	11.9	0.1	209.9	1.3	1.51	17.68
	254.60	67.93	0.5594	0.0030	17.9	0.1	12.0	0.2	215.0	5.4	1.49	17.91
690C-016 02W 100-105cm	255.00	68.20	0.5401	0.0017	28.6	0.1	16.3	0.4	504.0	4.3	1.75	30.83
690C-016 02W 140-145cm	255.40	68.22	0.5678	0.0022	19.3	0.0	7.1	0.2	266.5	2.9	2.73	37.70
	255.40	68.22	0.5718	0.0029	19.1	0.0	7.1	0.2	264.4	6.3	2.69	37.27
690C-016 03W 15-20cm	255.65	68.24	0.5640	0.0020	20.4	0.0	7.4	0.4	315.1	2.2	2.74	42.36
	255.65	68.24	0.5704	0.0024	19.8	0.1	7.4	0.2	321.6	2.5	2.68	43.54
690C-016 03W 60-65cm	256.10	68.26	0.5777	0.0017	21.6	0.0	8.5	0.3	322.3	1.5	2.54	37.84
690C-016 03W 100-105cm	256.50	68.29	0.5187	0.0013	31.9	0.0	9.9	0.3	2296.9	57.3	3.23	232.31
	256.50	68.29	0.5318	0.0022	41.2	0.2	11.1	0.3	2350.8	9.2	3.70	210.93
690C-016 03W 144-145cm	256.94	68.32	0.5422	0.0020	22.4	0.1	11.0	0.2	375.2	1.6	2.04	34.05
690C-016 04W 36-40cm	257.36	68.34	0.5369	0.0023	18.5	0.0	11.2	0.3	192.7	2.7	1.65	17.16
	257.36	68.34	0.5434	0.0030	18.1	0.1	10.0	0.1	206.1	1.7	1.82	20.66
690C-016 04W 80-85cm	257.80	68.37	0.5634	0.0020	21.4	0.1	9.6	0.4	240.4	2.2	2.24	25.15
690C-016 CCW 15-20cm	258.05	68.38	0.5181	0.0014	54.6	0.1	8.8	0.1	266.6	1.7	6.19	30.22
	258.05	68.38	0.5181	0.0014	54.6	0.1	8.4	0.0	248.5	0.0	6.47	29.43
	258.05	68.38	0.5187	0.0011	55.6	0.1	9.7	0.2	296.7	4.7	5.72	30.49
690C-017 01W 16-20cm	261.96	68.63	0.5350	0.0017	42.2	0.1	8.0	0.1	214.3	0.9	5.28	26.80
690C-017 01W 62-65cm	262.42	68.66	0.5447	0.0021	46.0	0.2	8.0	0.3	328.4	1.9	5.77	41.24
690C-017 01W 100-104cm	262.80	68.68	0.5490	0.0021	39.7	0.4	8.3	0.2	228.4	3.8	4.78	27.50
	262.80	68.68					16.0	0.8	224.7	6.3		14.00

Table B4: Os isotope and PGE data from ODP Leg 113 Site 690C using age model from Gradstein et al., 2012.

Sample	Depth (mbsf)	Age (Ma)	$^{187}Os/^{188}Os$	error (2σ)	[Os] pg/g	error (pg/g)	[Ir] pg/g	error (pg/g)	[Pt] pg/g	error (pg/g)	[Os] [Ir]	[Pt] [Ir]
690C-017 01W 142-144cm	263.22	68.70	0.5404	0.0052	54.3	0.5	9.4	0.2	232.2	2.9	5.78	24.72
690C-017 02W 16-20cm	263.46	68.72	0.5284	0.0016	61.6	0.2	12.0	0.3	218.3	2.1	5.15	18.26
	263.46	68.72	0.5309	0.0033	61.5	1.2	11.0	0.3	203.6	3.2	5.58	18.49
690C-017 02W 60-65cm	263.90	68.75	0.5404	0.0014	60.5	0.2	11.1	0.2	562.6	1.8	5.45	50.67
690C-017 02W 100-104cm	264.30	68.77	0.5430	0.0015	64.1	0.1	8.9	0.2	248.6	1.7	7.22	28.01

s

Table B5: Os isotope and PGE data from the Bottaccione Section, Gubbio, Italy using age model from Gradstein et al., 2012.

Height (m)	Age (Ma)	$^{187}Os/^{188}Os$	error (2σ)	[Os] pg/g	error (pg/g)	[Ir] pg/g	error (pg/g)	[Pt] pg/g	error (pg/g)	[Os]/[Ir]	[Pt]/[Ir]
382.60	66.040	0.2505	0.0010	59.0	0.5	106.5	1.3	375.1	8.5	0.55	3.52
382.60	66.040	0.2519	0.0017	49.5	0.5	85.0	1.6	356.9	5.2	0.58	4.20
382.40	66.056	0.2881	0.0012	34.5	0.1	95.7	0.9	305.6	7.5	0.36	3.19
382.20	66.071	0.3610	0.0041	28.9	0.3	24.1	0.5	258.9	3.5	1.20	10.76
382.20	66.071	0.3588	0.0008	28.8	0.0	23.8	0.2	259.3	4.9	1.21	10.87
382.00	66.087	0.3763	0.0011	26.1	0.1	23.5	0.4	152.3	2.4	1.11	6.47
381.80	66.102	0.4034	0.0013	19.8	0.0	14.9	0.3	88.3	3.9	1.33	5.92
381.60	66.118	0.4345	0.0037	24.5	0.2	19.9	0.2	160.6	3.9	1.23	8.09
381.40	66.133	0.3860	0.0034	24.6	0.1	14.4	0.7	119.7	3.2	1.71	8.29
381.20	66.149	0.4164	0.0029	20.0	0.1	13.5	0.1	185.0	2.8	1.48	13.70
381.00	66.165	0.4217	0.0014	22.2	0.1	18.9	0.3	181.4	2.6	1.17	9.59
380.80	66.180	0.4181	0.0019	18.9	0.1	11.5	0.4	135.8	3.5	1.64	11.79
380.60	66.196	0.4223	0.0041	18.2	0.1						
380.60	66.196					10.6	0.2	97.8	0.8		
380.60	66.196	0.4215	0.0015	17.6	0.0						
380.40	66.211	0.4232	0.0016	18.4	0.0	17.6	0.8	139.6	2.7	1.05	7.94
380.20	66.227	0.4183	0.0020	19.2	0.0	12.0	0.3	127.1	1.4	1.60	10.59
380.00	66.242	0.4234	0.0019	20.3	0.1	17.6	0.6	163.4	4.1	1.15	9.26
380.00	66.242					12.4	0.2	151.9	2.8		12.24

Table B5: Os isotope and PGE data from the Bottaccione Section, Gubbio, Italy using age model from Gradstein et al., 2012.

Height (m)	Age (Ma)	$^{187}Os/^{188}Os$	error (2σ)	[Os] pg/g	error (pg/g)	[Ir] pg/g	error (pg/g)	[Pt] pg/g	error (pg/g)	[Os]/[Ir]	[Pt]/[Ir]
379.80	66.258	0.4342	0.0015	19.0	0.0						
379.60	66.273	0.4443	0.0031	16.0	0.1						
379.40	66.289	0.4589	0.0018	16.5	0.0	11.2	0.3	112.8	1.5	1.47	10.05
379.20	66.305	0.5047	0.0031	13.6	0.1	7.2	0.1	122.9	3.0	1.88	16.97
379.20	66.305	0.4780	0.0040	13.5	0.1	7.5	0.3	121.8	1.5	1.81	16.29
379.00	66.320	0.4833	0.0019	18.1	0.0	11.3	0.2	146.0	2.1	1.60	12.88
378.80	66.336	0.4973	0.0014	15.7	0.0	11.4	0.1	120.4	2.3	1.38	10.58
378.40	66.367	0.5324	0.0023	13.6	0.0						
378.40	66.367					8.4	0.1	94.1	2.7		11.27
378.20	66.382	0.5448	0.0016	14.1	0.0	8.3	0.2	90.4	4.3	1.68	10.83
378.20	66.382					8.6	0.2	91.2	1.5		10.58
378.00	66.398	0.5546	0.0021	14.7	0.0	12.7	0.2	112.7	1.9	1.15	8.87
377.80	66.451	0.5742	0.0025	14.6	0.0	9.8	0.2	91.2	2.9	1.49	9.32
377.50	66.530	0.5789	0.0019	14.9	0.0	10.3	0.3	122.6	3.5	1.44	11.88
377.20	66.610	0.5840	0.0030	23.8	0.1	19.6	0.2	257.2	1.2	1.21	13.14
376.90	66.689	0.6068	0.0019	15.8	0.0	7.7	0.2	105.4	3.1	2.04	13.61
376.30	66.848	0.6126	0.0025	14.0	0.0	8.4	0.2	88.2	2.7	1.66	10.45
376.30	66.848	0.6126	0.0034	14.8	0.0	8.7	0.3	93.7	4.3	1.69	10.71
376.10	66.900	0.6094	0.0023	13.1	0.0						

Table B5: Os isotope and PGE data from the Bottaccione Section, Gubbio, Italy using age model from Gradstein et al., 2012.

Height (m)	Age (Ma)	$^{187}Os/^{188}Os$	error (2σ)	[Os] pg/g	error (pg/g)	[Ir] pg/g	error (pg/g)	[Pt] pg/g	error (pg/g)	[Os]/[Ir]	[Pt]/[Ir]
376.10	66.900	0.6254	0.0057	13.3	0.1	7.9	0.1	85.7	1.5	1.68	10.87
375.80	66.980	0.6023	0.0042	13.8	0.1	7.5	0.2	92.6	1.7	1.84	12.38
375.50	67.059	0.6087	0.0023	13.0	0.0	7.6	0.2	93.8	3.8	1.71	12.40
375.50	67.059	0.6107	0.0036	13.8	0.0	7.9	0.1	96.0	2.0	1.75	12.18
375.20	67.138	0.6119	0.0021	13.4	0.0	8.5	0.3	95.7	2.2	1.58	11.26
374.90	67.218	0.5967	0.0017	17.2	0.0						
374.60	67.297	0.5944	0.0018	15.8	0.0	10.7	0.4	101.9	2.3	1.48	9.50
374.30	67.376	0.6146	0.0021	15.6	0.1	9.3	0.3	120.3	4.5	1.67	12.92
374.30	67.376	0.6004	0.0013	15.8	0.1	9.8	0.5	124.8	4.9	1.61	12.72
374.00	67.456	0.6118	0.0030	13.5	0.1	7.0	0.3	60.7	2.2	1.92	8.61
374.00	67.456	0.6185	0.0040	13.1	0.1	7.2	0.2	69.2	2.8	1.81	9.59
373.80	67.509	0.6386	0.0070	14.9	0.1	8.3	0.2	84.0	3.9	1.79	10.06
373.50	67.588	0.6258	0.0076	12.6	0.1						
373.20	67.667	0.6303	0.0087	12.3	0.1	7.6	0.2	98.3	0.9	1.61	12.91
373.00	67.720	0.6074	0.0024	12.4	0.0						
372.80	67.773	0.6018	0.0019	13.4	0.0	8.1	0.2	109.6	4.3	1.65	13.46
372.80	67.773	0.6038	0.0036	13.1	0.1	6.9	0.3	107.8	4.5	1.90	15.68
372.50	67.852	0.6028	0.0027	14.7	0.0						
372.20	67.932	0.5823	0.0030	15.9	0.0	9.9	0.1	100.2	3.4	1.60	10.13

Table B5: Os isotope and PGE data from the Bottaccione Section, Gubbio, Italy using age model from Gradstein et al., 2012.

Height (m)	Age (Ma)	$^{187}Os/^{188}Os$	error (2σ)	[Os] pg/g	error (pg/g)	[Ir] pg/g	error (pg/g)	[Pt] pg/g	error (pg/g)	[Os]/[Ir]	[Pt]/[Ir]
372.00	67.984	0.6084	0.0017	14.8	0.0						
372.00	67.984	0.6105	0.0027	14.8	0.0	8.0	0.2	92.9	4.9	1.86	11.67
371.95	67.998	0.6218	0.0080	13.6	0.1	7.9	0.1	70.2	2.2	1.71	8.85
371.90	68.011	0.6095	0.0026	16.4	0.0						
371.70	68.064	0.6020	0.0037	12.3	0.1	10.0	0.5	75.2	2.7	1.23	7.51
371.50	68.117	0.5946	0.0033	12.8	0.0	6.5	0.3	80.5	1.6	1.99	12.48
371.45	68.130	0.5875	0.0022	15.0	0.0	7.9	0.3	86.1	2.8	1.89	10.84
371.40	68.143	0.5888	0.0027	14.1	0.0	8.0	0.1	88.1	1.3	1.77	11.00
371.35	68.156	0.5803	0.0045	15.3	0.1	8.0	0.2	95.2	3.2	1.91	11.90
371.20	68.196	0.5919	0.0021	17.0	0.1	12.8	0.4	120.9	3.7	1.32	9.42
370.95	68.232	0.5620	0.0031	15.9	0.0	7.8	0.3	85.9	3.6	2.04	10.99
370.90	68.239	0.5817	0.0038	15.3	0.0	7.3	0.2	118.7	1.6	2.10	16.23
370.90	68.239	0.5794	0.0028	16.2	0.1	8.0	0.1	107.3	2.9	2.02	13.37
370.75	68.261	0.5831	0.0026	21.0	0.1	9.4	0.2	130.2	4.1	2.24	13.91
370.75	68.261	0.5840	0.0022	20.8	0.0						
370.70	68.268	0.5890	0.0049	16.4	0.2	8.1	0.2	89.3	1.3	2.02	11.00
370.70	68.268	0.5904	0.0038	16.2	0.1						
370.60	68.283	0.5953	0.0063	15.4	0.1	6.7	0.2	74.5	1.1	2.30	11.17
370.60	68.283	0.5677	0.0014	16.8	0.0						

Table B5: Os isotope and PGE data from the Bottaccione Section, Gubbio, Italy using age model from Gradstein et al., 2012.

Height (m)	Age (Ma)	$^{187}Os/^{188}Os$	error (2σ)	[Os] pg/g	error (pg/g)	[Ir] pg/g	error (pg/g)	[Pt] pg/g	error (pg/g)	[Os]/[Ir]	[Pt]/[Ir]
370.60	68.283	0.5704	0.0028	18.0	0.0	8.3	0.2	118.5	3.8	2.17	14.26
370.40	68.311	0.5666	0.0028	19.2	0.1	7.4	0.2	141.2	1.1	2.58	19.03
370.20	68.340	0.5670	0.0022	18.4	0.1	8.6	0.4	102.2	3.6	2.15	11.95
370.00	68.369	0.5696	0.0018	19.8	0.0	11.5	0.1	103.3	0.6	1.72	9.00
370.00	68.369	0.5593	0.0015	20.2	0.0	12.1	0.2	107.4	2.3	1.67	8.90

Table B6: Os isotope and PGE data from DSDP Leg 74 Site 525A using age model from Gradstein et al., 2012.

Sample*	Depth (mbsf)	Age	$^{187}Os/^{188}Os$*	error* (2σ)	[Os] pg/g*	[Ir] pg/g#	[Pt] pg/g#	[Os]/[Ir] #	[Pt]/[Ir] #
525A-40R-02 97-100cm	452.57	66.10	0.3880	0.0080	46	26	432	1.76	16.55
525A-40R-02 97-100cm	452.57	66.10	0.4150	0.0100	42	22	354	1.92	16.20
525A-40R-03 120-123cm	454.30	66.23	0.4002	0.0027	39	24	367	1.61	15.19
525A-40R-04 62-64cm	455.12	66.29	0.4300	0.0050	25	13	401	1.95	31.27
525A-40R-04 62-64cm	455.12	66.29	0.4170	0.0060	27	14	413	1.91	29.21
525A-40R-05 87-90cm	456.87	66.42	0.4580	0.0060	27	11	297	2.56	28.18
525A-40R-06 5-9cm	457.55	66.48	0.4829	0.0021	74	20	437	3.67	21.65
525A-41R-01 21-24cm	459.81	66.70	0.5462	0.0023	57	21	436	2.78	21.25
525A-41R-03 131-134cm	463.91	67.10	0.5570	0.0060	49	22	504	2.27	23.34
525A-41R-03 131-134cm	463.91	67.10	0.5520	0.0060	52	17	433	3.08	25.63
525A-41R-07 29-32cm	468.58	67.56	0.562	0.0052	45	21	369	2.12	17.55
525A-43R-101 130-133cm	479.90	68.80	0.636	0.0136	38	19	426	1.98	22.55

*Previously published data from Ravizza and Peucker-Ehrenbrink, 2003.

#Previously unpublished data

Table B7: Re-Os analyses of sediment leaches and associated age corrections using age model from Gradstein et al., 2012.

Sample	Depth (mbsf)	Age (Ma)	bulk $^{187}Os/^{188}Os$	error (2σ)	[Os] pg/g	error	[Re] pg/g	$^{187}Os/^{188}Os$ corrected	correction magnitude
690C 015 04W 60-65	248.00	66.054	0.3484	0.0023	32.7	0.27	4.6	0.3477	0.21%
690C 015 04W 120-125cm	248.60	66.103	0.4043	0.0029	22.6	0.21	6.2	0.4029	0.36%
690C 015 CCW 0-7cm	252.26	66.396	0.4720	0.0480	10.9	0.48	4.4	0.4699	0.45%
690C 016 01W 15-19cm	252.65	66.643	0.6085	0.0078	10.0	0.20	4.0	0.6063	0.35%
690C 016 01W 146-149	253.96	67.509	0.6087	0.0065	10.3	0.20	4.0	0.6066	0.35%
690C 016 03W 60-65cm	256.10	68.264	0.5798	0.0064	10.5	0.22	2.6	0.5785	0.23%
690C 016 CCW 15-20cm	258.05	68.384	0.5412	0.0044	19.4	0.18	4.1	0.5400	0.22%
BTT 382.40m	382.40	66.056	0.2844	0.0044	19.4	0.21	2.5	0.2837	0.23%
BTT 381.80m	381.80	66.102	0.5525	0.0470	2.0	0.28	1.4	0.5487	0.70%
BTT 378.00m	378.00	66.398	0.5519	0.0094	6.5	0.20	3.1	0.5494	0.46%
BTT 376.90m	376.90	66.698	0.5968	0.0104	7.1	0.23	2.6	0.5948	0.33%
BTT 373.80m	373.80	67.509	0.6016	0.0117	5.5	0.22	2.8	0.5989	0.45%
BTT 370.00m	370.00	68.369	0.5599	0.0088	8.2	0.21	2.5	0.5582	0.31%
577A 013H 03W 126-130cm	118.16	67.530	0.5884	0.0149	4.3	0.20	2.9	0.5847	0.64%
525A 40R-2 97-100cm	452.57	66.100	0.3866	0.0051	13.9	0.23	6.5	0.3842	0.63%
525A 40R-5 87-90cm	456.87	66.420	0.4099	0.0059	12.7	0.16	4.0	0.4083	0.40%
525A 41R-1 21-24cm	459.81	66.700	0.5564	0.0076	7.6	0.23	19.1	0.5429	2.42%
525A 41R-7 29-32cm	468.58	67.560	0.5889	0.0117	12.0	0.24	100.3	0.5432	7.76%

APPENDIX C

A complete marine Os isotope record for the Maastrichtian (66.04 – 71.68 Ma) from Leg 113 Site 690C

Figure C1: $^{187}Os/^{188}Os$ record of ODP Site 690C for the complete Maastrichtian

$^{187}Os/^{188}Os$ from ODP Site 690C vs depth (mbsf) for the Maastrichtian. Arrow indicates data point that plots above axis limit. The C30r/C31n reversal boundary was not recovered in this core so placement of C30r is approximate. In most case error bars are smaller than the symbols used.

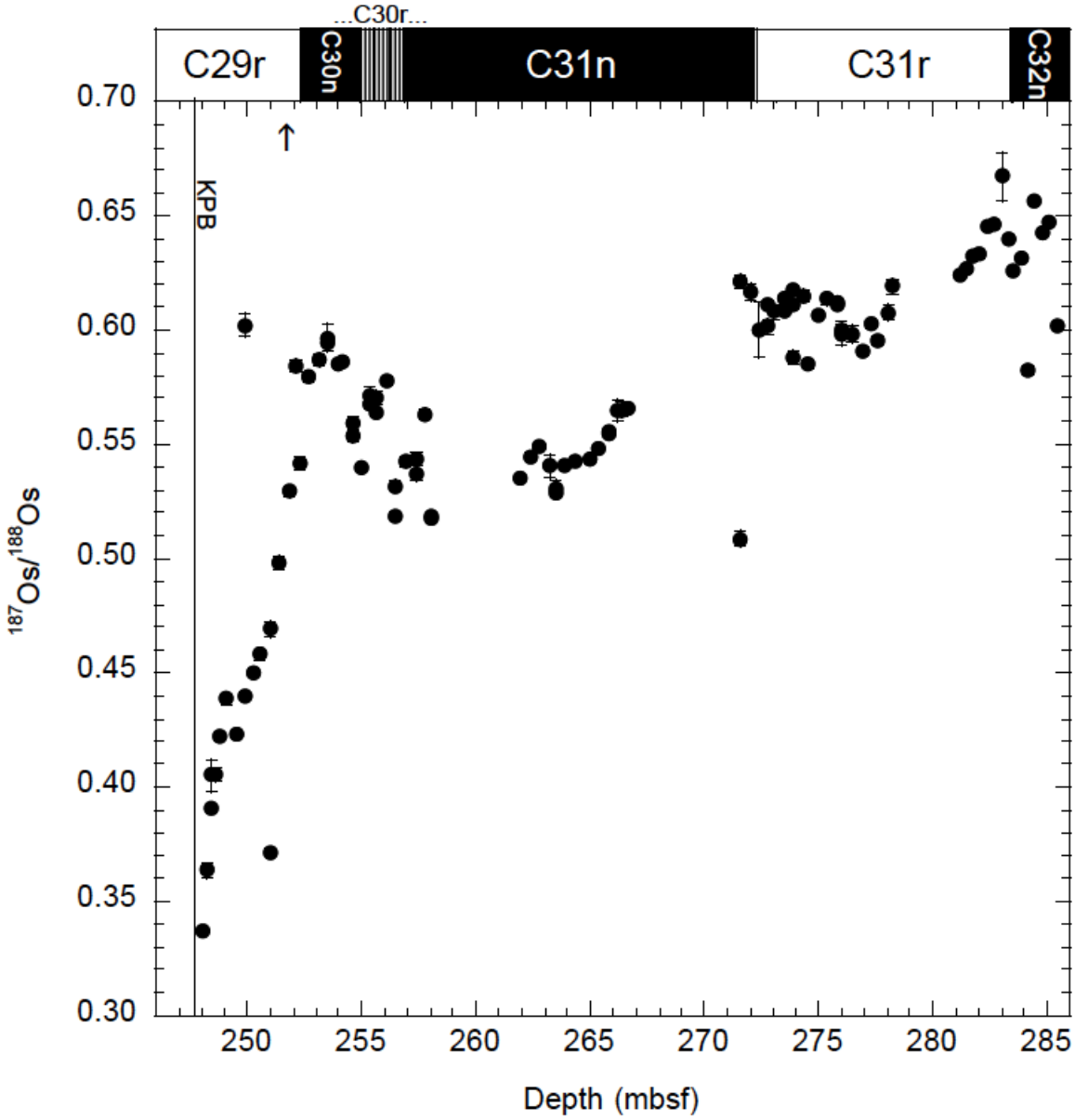

Table C1:
Age model for 690C for the Maastrichtian (66.04 - 73.65)

Depth	Event	Date
247.82	K-Pg	66.04
252.28	C29r/C30n	66.40
255.00	C30n/C30r	68.20
272.25	C31n/C31r	69.27
283.39	C31r/C32n	71.45
302.78	C32n/C32r	73.65

Dates from Gradstein et al., 2012.

Depths of age datum from Hamilton, 1990.

Table C2: Os isotope and PGE data from ODP Leg 113 Site 690C

Sample	Depth (mbsf)	Age (Ma)	$^{187}Os/^{188}Os$	error (2σ)	[Os] (ppt)	2σ error (ppt)	[Ir] ppt	2σ error (ppt)	[Pt] ppt	2σ error (ppt)	[Os] / [Ir]	[Pt] / [Ir]
690C-015 04W 60-65cm	248.00	66.05	0.3374	0.0014	49.91	1.08	117.57	0.91	526.24	3.28	0.42	4.48
690C-015 04W 83-88cm	248.23	66.07	0.3635	0.0030	43.04	0.19	97.95	1.61	583.21	2.31	0.44	5.95
690C-015 04W 100-105cm	248.40	66.09	0.4055	0.0069	40.25	0.42	35.30	0.66	409.91	5.23	1.14	11.61
	248.40	66.09	0.3905	0.0015	41.05	0.10	33.60	0.61	372.30	3.74	1.22	11.08
690C-015 04W 120-125cm	248.60	66.10	0.4052	0.0028	34.85	0.13	30.54	0.62	470.86	9.43	1.14	15.42
690C-015 04W 140-145cm	248.80	66.12	0.4220	0.0014	31.11	0.17	36.42	0.45	484.17	3.03	0.85	13.29
690C-015 05W 15-20cm	249.05	66.14	0.4386	0.0021	30.71	0.11	28.29	0.32	510.11	2.53	1.09	18.03
690C-015 05W 64-66cm	249.54	66.18	0.4234	0.0014	30.60	0.05	19.89	0.33	357.34	3.84	1.54	17.97
690C-015 05W 100-105cm	249.90	66.21	0.6022	0.0048	31.14	0.13	15.00	0.32	275.53	8.40	2.08	18.37
	249.90	66.21	0.4399	0.0014	30.66	0.07	18.99	0.00	286.95	0.00	1.61	15.11
690C-015 05W 140-145cm	250.30	66.24	0.4499	0.0020	32.93	0.09	23.49	0.36	440.82	3.26	1.40	18.77
690C-015 06W 15-18cm	250.55	66.26	0.4582	0.0022	25.89	0.08	23.61	1.15	450.20	6.38	1.10	19.07
690C-015 06W 63-67cm	251.03	66.30	0.3716	0.0016	27.65	0.06	32.52	0.69	418.88	1.82	0.85	12.88
	251.03	66.30	0.4693	0.0031	19.90	0.07	24.65	1.21	424.14	5.97	0.81	17.20
690C-015 06W 102-105cm	251.42	66.33	0.4982	0.0025	15.66	0.05	17.30	0.29	274.73	1.46	0.90	15.88
690C-015 06W 142-145cm	251.82	66.36	0.5294	0.0022	15.07	0.12	12.91	0.27	216.92	2.40	1.17	16.81
	251.82	66.36	0.8126	0.0093	6.43	0.05	12.07	0.55	205.01	3.49	0.53	16.98
690C-015 07W 22-25cm	252.12	66.39	0.5842	0.0026	13.10	0.03	11.73	0.42	181.33	0.88	1.12	15.45
690C-015 CCW 0-7cm	252.26	66.40	0.5418	0.0029	15.20	0.04	15.60	0.38	240.71	2.80	0.97	15.43
690C-016 01W 15-19cm	252.65	66.64	0.5796	0.0023	18.50	0.06	12.93	0.17	197.17	1.15	1.43	15.25
690C-016 01W 60-65cm	253.10	66.94	0.5872	0.0025	19.72	0.04	8.65	0.31	163.33	2.61	2.28	18.88
690C-016 01W 100-103cm	253.50	67.20	0.5942	0.0017	22.08	0.04	17.29	0.36	244.88	2.88	1.28	14.16

Table C2: Os isotope and PGE data from ODP Leg 113 Site 690C

Sample	Depth (mbsf)	Age (Ma)	$^{187}Os/^{188}Os$	error (2σ)	[Os] (ppt)	2σ error (ppt)	[Ir] ppt	2σ error (ppt)	[Pt] ppt	2σ error (ppt)	[Os] / [Ir]	[Pt] / [Ir]
	253.50	67.20	0.5968	0.0063	22.23	0.29	9.59	0.41	169.42	5.05	2.32	17.66
690C-016 01W 146-149m	253.96	67.51	0.5850	0.0019	19.62	0.05	8.89	0.21	149.00	1.94	2.21	16.77
690C-016 02W 16-20cm	254.16	67.64	0.5858	0.0019	19.35	0.04	8.92	0.13	147.06	1.20	2.17	16.48
690C-016 02W 60-65cm	254.60	67.93	0.5539	0.0025	17.96	0.06	11.87	0.14	209.94	1.27	1.51	17.68
	254.60	67.93	0.5594	0.0030	17.89	0.07	12.01	0.25	215.01	5.35	1.49	17.91
690C-016 02W 100-105cm	255.00	68.20	0.5401	0.0017	28.60	0.06	16.35	0.36	504.03	4.33	1.75	30.83
690C-016 02W 140-145cm	255.40	68.22	0.5678	0.0022	19.28	0.04	7.07	0.24	266.47	2.91	2.73	37.70
	255.40	68.22	0.5718	0.0029	19.10	0.05	7.09	0.19	264.37	6.34	2.69	37.27
690C-016 03W 15-20cm	255.65	68.24	0.5640	0.0020	20.42	0.04	7.44	0.40	315.12	2.21	2.74	42.36
	255.65	68.24	0.5704	0.0024	19.80	0.07	7.39	0.24	321.60	2.45	2.68	43.54
690C-016 03W 60-65cm	256.10	68.26	0.5777	0.0017	21.59	0.04	8.52	0.33	322.29	1.51	2.54	37.84
690C-016 03W 100-105cm	256.50	68.29	0.5187	0.0013	31.91	0.04	9.89	0.34	2296.94	57.33	3.23	232.31
	256.50	68.29	0.5318	0.0022	41.19	0.17	11.14	0.30	2350.82	9.19	3.70	210.93
690C-016 03W 144-145cm	256.94	68.32	0.5422	0.0020	22.44	0.05	11.02	0.23	375.15	1.56	2.04	34.05
690C-016 04W 36-40cm	257.36	68.34	0.5369	0.0023	18.50	0.04	11.23	0.25	192.74	2.69	1.65	17.16
	257.36	68.34	0.5434	0.0030	18.10	0.06	9.97	0.10	206.07	1.71	1.82	20.66
690C-016 04W 80-85cm	257.80	68.37	0.5634	0.0020	21.38	0.05	9.56	0.36	240.37	2.21	2.24	25.15
690C-016 CCW 15-20cm	258.05	68.39	0.5181	0.0014	54.62	0.14	8.82	0.11	266.58	1.66	6.19	30.22
	258.05	68.39	0.5181	0.0014	54.62	0.14	8.45	0.00	248.54	0.00	6.47	29.43
	258.05	68.39	0.5187	0.0011	55.64	0.09	9.73	0.22	296.70	4.65	5.72	30.49
690C-017 01W 16-20cm	261.96	68.63	0.5350	0.0017	42.21	0.13	7.99	0.15	214.26	0.86	5.28	26.80
690C-017 01W 62-65cm	262.42	68.66	0.5447	0.0021	45.99	0.16	7.96	0.26	328.40	1.94	5.77	41.24

Table C2: Os isotope and PGE data from ODP Leg 113 Site 690C

Sample	Depth (mbsf)	Age (Ma)	$^{187}Os/^{188}Os$	error (2σ)	[Os] (ppt)	2σ error (ppt)	[Ir] ppt	2σ error (ppt)	[Pt] ppt	2σ error (ppt)	[Os] / [Ir]	[Pt] / [Ir]
690C-017 01W 100-104cm	262.80	68.68	0.5490	0.0021	39.69	0.39	8.31	0.23	228.40	3.76	4.78	27.50
	262.80	68.68					16.05	0.76	224.67	6.28		14.00
690C-017 01W 142-144cm	263.22	68.71	0.5404	0.0052	54.29	0.46	9.39	0.24	232.17	2.92	5.78	24.72
690C-017 02W 16-20cm	263.46	68.72	0.5284	0.0016	61.61	0.18	11.95	0.27	218.27	2.10	5.15	18.26
	263.46	68.72	0.5309	0.0033	61.47	1.20	11.01	0.27	203.58	3.20	5.58	18.49
690C-017 02W 60-65cm	263.90	68.75	0.5404	0.0014	60.50	0.18	11.10	0.16	562.62	1.76	5.45	50.67
690C-017 02W 100-104cm	264.30	68.77	0.5430	0.0015	64.06	0.15	8.88	0.24	248.65	1.73	7.22	28.01
690C-017 03W 15-18cm	264.95	68.81	0.5434	0.0014	46.29	0.09	9.59	0.34	223.99	2.38	4.83	23.36
690C-017 03W 60-65cm	265.40	68.84	0.5486	0.0013	54.69	0.11	11.70	0.27	300.46	2.97	4.68	25.68
690C-017 03W 100-105cm	265.80	68.87	0.5560	0.0015	54.10	0.55	10.66	0.26	268.74	3.75	5.07	25.21
	265.80	68.87	0.5548	0.0014	53.74	0.13	11.03	0.29	220.89	4.86	4.87	20.04
690C-017 03W 140-145cm	266.20	68.89	0.5650	0.0047	45.62	0.29	12.10	0.35	584.84	2.42	3.77	48.32
690C-017 04W 5-10cm	266.35	68.90	0.5653	0.0031	43.48	0.19	13.13	0.32	243.91	2.92	3.31	18.58
690C-017 CCW 15-20cm	266.66	68.92	0.5660	0.0021	43.73	0.11	10.45	0.32	208.11	2.54	4.19	19.92
	266.66	68.92					9.80	0.18	201.09	2.41		20.53
	266.66	68.92					10.49	0.40	183.69	2.59		17.51
690C-018 01W 15-20cm	271.55	69.23	0.6215	0.0026	27.40	0.10	10.03	0.12	176.02	3.25	2.73	17.56
	271.55	69.23	0.5088	0.0034	38.02	0.33	19.71	0.71	215.06	1.43	1.93	10.91
690C-018 01W 60-65cm	272.00	69.25	0.6168	0.0034	26.06	0.11	11.02	0.35	234.72	3.77	2.37	21.31
690C-018 01W 100-105cm	272.40	69.30	0.6002	0.0118	30.77	0.33	11.64	0.47	278.18	2.89	2.64	23.91
690C-018 01W 140-145cm	272.80	69.38	0.6115	0.0018	33.51	0.07	12.04	0.41	387.95	4.76	2.78	32.23
	272.80	69.38	0.6018	0.0032	32.95	0.10	11.29	0.24	361.63	3.71	2.92	32.04

Table C2: Os isotope and PGE data from ODP Leg 113 Site 690C

Sample	Depth (mbsf)	Age (Ma)	$^{187}Os/^{188}Os$	error (2σ)	[Os] (ppt)	2σ error (ppt)	[Ir] ppt	2σ error (ppt)	[Pt] ppt	2σ error (ppt)	[Os] / [Ir]	[Pt] / [Ir]
690C-018 02W 16-19cm	273.06	69.43	0.6081	0.0032	29.95	0.08	10.24	0.32	205.13	3.37	2.92	20.03
690C-018 02W 60-64cm	273.50	69.51	0.6139	0.0022	30.78	0.11	13.08	0.20	333.43	2.54	2.35	25.49
	273.50	69.51	0.6084	0.0023	31.69	0.10	15.22	0.42	331.30	4.41	2.08	21.77
690C-018 02W 100-105cm	273.90	69.59	0.6115	0.0019	31.81	0.05	14.90	0.18	279.64	2.62	2.13	18.76
	273.90	69.59	0.5878	0.0026	32.80	0.09	16.07	0.31	287.24	1.08	2.04	17.87
	273.90	69.59	0.6175	0.0023	31.21	0.09	13.90	0.26	320.88	4.31	2.25	23.09
690C-018 02W 140-145m	274.30	69.67	0.6152	0.0028	31.50	0.09	20.06	0.29	374.03	1.93	1.57	18.64
690C-018 03W 15-20cm	274.55	69.72	0.5852	0.0015	41.77	0.42	26.80	0.38	489.52	3.27	1.56	18.27
	274.55	69.72	0.5853	0.0015	40.41	0.09	26.42	0.76	483.32	7.96	1.53	18.29
690C-018 03W 60-65cm	275.00	69.81	0.6069	0.0017	36.16	0.19	17.69	0.39	681.69	4.53	2.04	38.53
690C-018 03W 100-105cm	275.40	69.89	0.6136	0.0020	35.03	0.07	15.50	0.19	533.22	4.20	2.26	34.40
690C-018 03W 142-144cm	275.82	69.97	0.6121	0.0015	41.71	0.08	15.03	0.51	592.67	3.83	2.78	39.44
	275.82	69.97	0.6112	0.0012	41.31	0.09	15.01	0.17	524.86	8.32	2.75	34.96
690C-018 04W 15-20cm	276.05	70.01	0.5981	0.0044	31.71	0.13	11.66	0.31	324.93	3.38	2.72	27.88
	276.05	70.01	0.6005	0.0028	33.23	0.10	10.68	0.12	346.40	4.71	3.11	32.43
690C-018 04W 60-65cm	276.50	70.10	0.5984	0.0036	34.34	0.12	11.40	0.26	288.72	3.41	3.01	25.33
690C-018 04W 100-105cm	276.90	70.18	0.5908	0.0017	40.22	0.06	13.01	0.43	481.41	1.12	3.09	37.00
690C-018 04W 140-142cm	277.30	70.26	0.6024	0.0014	41.10	0.07	13.83	0.17	752.71	4.62	2.97	54.42
690C-018 05W 15-20cm	277.55	70.31	0.5955	0.0018	34.92	0.08	12.90	0.09	360.66	3.88	2.71	27.97
	277.55	70.31					12.51	0.37	310.58	4.42		24.82
690C-018 05W 60-65cm	278.00	70.39	0.6078	0.0029	40.04	0.14	15.68	0.16	487.40	2.91	2.55	31.08
690C-018 CCW 5-10cm	278.20	70.43	0.6192	0.0032	42.15	0.27	17.15	0.25	502.05	2.13	2.46	29.28

Table C2: Os isotope and PGE data from ODP Leg 113 Site 690C

Sample	Depth (mbsf)	Age (Ma)	$^{187}Os/^{188}Os$	error (2σ)	[Os] (ppt)	2σ error (ppt)	[Ir] ppt	2σ error (ppt)	[Pt] ppt	2σ error (ppt)	[Os] / [Ir]	[Pt] / [Ir]
690C-019 01X 8-10cm	281.18	71.02	0.6238	0.0014	77.32	0.19	27.59	0.54	631.36	10.63	2.80	22.89
690C-019 01X 34-36cm	281.44	71.07	0.6271	0.0011	74.34	0.14	26.62	0.30	525.84	4.57	2.79	19.75
690C-019 01X 66-69cm	281.76	71.13	0.6325	0.0013	81.19	0.32	28.90	0.38	613.23	7.79	2.81	21.22
690C-019 01X 96-98cm	282.06	71.19	0.6331	0.0017	82.27	0.27	29.29	0.53	649.85	3.34	2.81	22.19
690C-019 01X 125-127cm	282.35	71.25	0.6450	0.0012	63.55	0.13	22.52	0.75	436.23	1.46	2.82	19.37
690C-019 02X 9-11cm	282.69	71.31	0.6459	0.0014	78.04	0.12	138.56	2.93	595.45	11.42	0.56	4.30
690C-019 02X 41-43cm	283.01	71.37	0.6673	0.0104	66.57	0.20	23.79	0.41	493.86	3.39	2.80	20.76
690C-019 02X 68-70cm	283.28	71.43	0.6403	0.0012	63.20	0.10	25.80	0.24	474.90	8.21	2.45	18.40
690C-019 02X 94-96cm	283.54	71.47	0.6259	0.0013	66.80	0.10	25.62	0.26	435.57	1.45	2.61	17.00
690C-019 02X 123-125cm	283.83	71.50	0.6311	0.0016	74.59	0.23	30.24	0.73	517.26	1.62	2.47	17.11
690C-019 03X 8-10cm	284.18	71.54	0.5825	0.0022	85.47	0.56	36.80	0.76	767.61	2.09	2.32	20.86
690C-019 03X 35-37cm	284.45	71.57	0.6566	0.0009	145.73	0.31	49.05	0.97	1587.95	29.16	2.97	32.37
690C-019 03X 68-70cm	284.78	71.61	0.6431	0.0014	129.89	0.74	35.91	1.16	768.51	9.60	3.62	21.40
690C-019 03X 95-97cm	285.05	71.64	0.6475	0.0013	126.52	0.22	45.84	0.94	845.62	11.32	2.76	18.45
690C-019 03X 133.5-135.5	285.44	71.68	0.6021	0.0010	114.31	0.18	47.27	0.91	624.33	4.16	2.42	13.21

Table C3: Leachates and Re concentrations for ODP Site 690C

	Depth (mbsf)	Age (Ma)	$^{187}Os/^{188}Os$ measured	[Os] ppt	$^{185}Re/^{187}Re$	[Re] ppt	$^{187}Os/^{188}Os$ corrected
690C 015 04W 60-66	248.00	65.53	0.3484	32.69	11.78	4.58	0.3477
690C 015 04W 120-125cm	248.60	65.57	0.4043	22.56	10.69	6.25	0.4029
690C 015 CCW 0-7cm	252.26	65.84	0.4720	10.85	11.95	4.38	0.4699
690C 016 01W 15-19cm	252.65	66.12	0.6085	9.97	12.31	3.98	0.6063
690C 016 01W 146-150	253.96	67.10	0.6087	10.29	12.34	4.01	0.6066
690C 016 03W 60-65cm	256.10	67.95	0.5798	10.49	13.66	2.56	0.5785
690C 016 CCW 15-20cm	258.05	68.08	0.5412	19.37	12.23	4.14	0.5400
690C 017 02W 100-104cm	264.30	68.49	0.5646	26.06	11.22	5.32	0.5635
690C 017 03W 140-145cm	266.20	68.61	0.5763	17.49	12.11	4.33	0.5749
690C 018 03W 15-20cm	274.55	69.31	0.5853*	40.41*	11.11	5.52	0.5845
690C 018 04W 15-20cm	276.05	69.50	0.5981*	31.71*	9.87	7.44	0.5968
690C 019 01X 125-127cm	282.35	70.31	0.6459	23.44	1.44	172.79	0.6034
690C 019 02X 94-96cm	283.54	70.46	0.6342	20.77	1.54	159.68	0.5898
690C 019 03X 35-37cm	284.45	70.58	0.7136	78.07	0.71	1377.20	0.6106
690C 019 03X 133.5-135.6	285.44	70.70	0.6021*	114.31*	0.62	6718.67	0.2631

*bulk analysis data

APPENDIX D

Mixing model for marine Os

Mass balance equation

(After Ravizza & Peuchker-Ehrenbrink, 2003).

Mass balance equation demonstrating how the "paving" affect of radiogenic continental crust with unradiogenic Deccan basalt would be responsible for the observed decrease in $^{187}Os/^{188}Os$ in the late Maastrichtian.

Post-eruption steady state

Equation 1:

$$R_{SW} = R_D F + R_O(1 - F)$$

Pre-eruption steady state

Equation 2:

$$R_{SW} = R_D F + R_O(1 - F)$$

where $R_{SW} = {}^{187}Os/^{188}Os$ ratio of seawater, $R_D = {}^{187}Os/^{188}Os$ ratio of Deccan, and $R_O = {}^{187}Os/^{188}Os$ ratio of other (non-Deccan) sources, F = steady state mole fraction of ^{188}Os supplied by Deccan sources to the ocean. "Deccan sources" refers to sources located in the geographical extent of Deccan. In pre-eruption steady state, the source is the portion of the Indian craton that will be covered by Deccan lavas. In post-eruption steady state, the source is Deccan basalt.

We assume F remains unchanged by Deccan volcanism. In other words, the mole fraction of ^{188}Os of the oceans from the geographical extent of Deccan remains the same before and after volcanism.

Subtracting Equation 2 from Equation 1 =

$$\Delta R_{SW} = \Delta R_D F$$

where the change in the $^{187}Os/^{188}Os$ ratio of seawater from pre- to post- eruption Deccan is equal to the change in the $^{187}Os/^{188}Os$ ratio of Deccan sources, multiplied by the mole fraction of ^{188}Os supplied by Deccan sources to the ocean.

Post steady state Deccan $R_{SW} = 0.4$

Pre steady state Deccan $R_{SW} = 0.6$

So $\Delta R_{SW} = -0.2$

Assume R_D of pre-eruption Deccan = 1.8 and R_D of post-eruption Deccan = 0.13. These assumptions are reasonable if Deccan volcanism replaces a radiogenic source of continental Os of $^{187}Os/^{188}Os = 1.8$ with an unradiogenic source of mantle-like Os of $^{187}Os/^{188}Os = 0.13$ (see Table 1.1).

Now $\Delta R_D = 0.13 - 1.8 = -1.7$.

$F = \Delta R_{SW} / \Delta R_D = -0.2 / -1.7 = 0.118$

In other words, these assumptions require that ~12% of $^{188}Os_{SW}$ is from Deccan sources. Deccan covered ~1.5% of the Earth's surface (10^6 km^2, Jay & Widdowson, 2008). While it is plausible that freshly erupted basalts weathered more rapidly than other sources of Os, this scenario requires that Deccan provided 7x that amount of Os than other areas of comparable size. Even factoring in the equatorial location of Deccan with the assumed increase in the hydrologic cycle that resulted from volcanism induced warming, this suggests some of the assumptions made here are incorrect.

This suggests that the "paving affect" of covering a radiogenic sources of Os with an unradiogenic source is probably only responsible for part of the decrease in $^{187}Os/^{188}Os_{SW}$ from 0.6 to 0.4. It is possible that there was another source of unradiogenic Os to the oceans (ie increased seafloor hydrothermal input) such that the assumption that F remains constant is incorrect, or that the Indian craton contained a lithology characterized by a much higher $^{187}Os/^{188}Os$ than average continental crust (R_D pre-eruption > 1.8).

References

Allègre, C., Birck, J.L., Capmus, F., Courtillot, V., 1999. Age of Deccan traps using ^{187}Re–^{187}Os systematics. Earth and Planetary Science Letters 170, 197–204.

Alvarez, W., Asaro, F., Montanari, A., 1990. Iridium profile for 10 million years across the Cretaceous-Tertiary Boundary at Gubbio (Italy). Science 250, 1700-1702.

Anbar, A.D., Creaser, R.A., Papanastassiou, D.A., Wasserburg, G.J., 1992. Rhenium in seawater: confirmation of generally conservative behavior. Geochimica et Cosmochimica Acta 56, 4099–4103.

Barrera, E., Huber, B., 1990. Evolution of Antarctic waters during the Maastrichtian: Foraminifer oxygen and carbon isotope ratios, Leg 113. Proceedings of the Ocean Drilling Program Scientific Results 113, 813-828.

Barrera, E., Savin, S., 1999. Evolution of late Campanian-Maastrichtian marine climates, and oceans in Evolution of the Cretaceous Ocean-Climate System. Geological Society of America Special Paper 332, 245-282.

Begemann, F., Ludwig, K.R., Lugmair, G.W., Min, K., Nyquist, L.E., Patchett P.J., Renne, P.R., Shih, C.Y., Villa, I.M., Walker, R.J., 2001. Call for an improved set of decay constants for geochronological use. Geochimica et Cosmochimica Acta, 65 111-121.

Berner, R., Beerling, D. 2007. Volcanic degassing necessary to produce a $CaCO_3$ undersaturated ocean at the Triassic-Jurassic boundary. Palaeogeography, Palaeoclimatology, Paleoecology 244, 368-373.

Blackburn, J., Olsen, P., Bowring, S., McLean, N., Kent, D., Puffer, J., McHone, G., Rasbury, T., Et-Touhami, M., 2013. Zircon U-Pb geochronology links the end-Triassic extinction with the Central Atlantic Magmatic Province. Science 304, 941-945.

Bond, D., Wignall, P., 2014. Large igneous provinces and mass extinctions: An update. Geological Society of America Special Paper 505.

Bottini, C., Cohen, A., Erba, E., Jenkyns, H., Coe, A., 2012. Osmium-isotope evidence for volcanism, weathering, and ocean mixing during the early Aptian OAE 1a. Geology 40, 583-586.

Broecker,W., Peng, T., 1982. *Tracers in the sea*. Lamont-Doherty Geological Observatory, Palisades, NY.

Burnham, O.M., Rogers, N.W., Pearson, D.G., van Calsternen, P.W., Hawkesworth, C.J., 1998. The petrogenesis of the eastern Pyrenean peridotites: An integrated study of their whole-rock geochemistry and Re-Os isotope composition. Geochimica et Cosmochimica Acta, 62 2293-2310.

Burton, K.W., 2006. Global weathering variations inferred from marine radiogenic isotope records. Journal of Geochemical Exploration 88, 262-265.

Burton, K., Gannoun, A., Parkinson, I., 2010. Climate driven glacial-interglacial variations in the osmium isotope composition of seawater recorded by planktic foraminifera. Earth and Planetary Science Letters 295, 58-68.

Caldeira, K., Rampino, M., 1990. Carbon dioxide emissions from Deccan volcanism and a K/T boundary greenhouse effect, Geophysical Research Letters 17, 1299-1302.

Carlson, R., 2005. Application of the Pt-Re-Os isotopic systems to mantle geochemistry and geochronology. Lithos 82, 249-272.

Chamley, H., Maillot, H., Duee, G., Robert, C., 1984. Paleoenvironmental history of the Walvis Ridge at the Cretaceous-Tertiary transition, from mineralogical and geochemical investigations. Initial Reports Deep Sea Drilling Program, 74, 685-695.

Chen, C. and Sharma, M., 2009. High precision and high sensitivity measurements of osmium in seawater. Analytical Chemistry 81, 5400–5406.

Chenet, A.L., Quidelleur, X., Fluteau, F., Courtillot, V., Bajpai, S., 2007. ^{40}K-^{40}Ar dating of the Main Deccan large igneous province: Further evidence of the KTB age and short duration. Earth and Planetary Science Letters 263, 1-15.

Chenet, A.L., Fluteau, F., Courtillot, V., Gerard, M., Subbarao, K., 2008. Determination of rapid Deccan eruptions across the KTB using paleomagnetic secular variations: 1. Results from a 1200-m-thick section in the Mahabaleshwar escarpment. Journal of Geophysical Research 113, B04101, doi:10.1029/2006JB004635.

Coccioni, R., Ferraro, E., Giusberti, L., Lirer, F., Luciani, V., Marsili, A., Spezzaferri, S., 2004. New insights on the late Cretaceous-Eocene foraminiferal record from the classical Bottaccione and Contessa pelagic Tethyan sections (Gubbio, central Italy): results from high resolution study and a new sample preparation technique. 32nd IGC, p. 340.

Cohen, A., Coe, A., 2002. New geochemical evidence for the onset of volcanism in the Central Atlantic magmatic province and the environmental change at the Triassic-Jurassic boundary. Geology 30, 267-270.

Cohen, A., Coe, A., 2007. The impact of the Central Atlantic Magmatic Province on climate and on the Sr- and Os-isotope evolution of seawater. Palaeogeography, Palaeoclimatology, Paleoecology 244, 374-390.

Colodner, D., Sachs, J., Ravizza, G., Turekian, K., Edmond, J., Boyle, E., 1993. The geochemical cycle of rhenium: a reconnaissance. Earth and Planetary Science Letters 117, 205-211.

Crocket, J., Officer, C., Wezel, F., Johnson, G., 1988. Distribution of noble metals across the Cretaceous/Tertiary boundary at Gubbio, Italy: Iridium variation as a constraint of the duration and nature of Cretaceous/Tertiary boundary events. Geology 16, 77-80.

Crocket, J. H., Paul, D. K., 2004. Platinum-group elements in Deccan mafic rocks: a comparison of suites differentiated by Ir content. Chemical Geology 208, 273– 291.

Courtillot, V., Renne, P., 2003. On the ages of flood basalts. Comptes Rendus Geoscience 333, 113-140.

Dalai, T. Ravizza, G., 2006. Estimation of sediment accumulation rates using iridium concentrations of marine sediments: An assessment from Os isotope and platinum group element records from the Ontong-Java Plateau. Geochimica et Cosmochimica Acta 70, 3928-3942.

Dalai, T., Ravizza, G., Peucker-Ehrenbrink, B., 2006. The Late Eocene $^{187}Os/^{188}Os$ excursion: Chemostratigraphy, cosmic dust flux and the Early Oligocene glaciation. Earth and Planetary Science Letters 241, 477-492.

D'Hondt, S., Pilson, M., Sigurdsson, H. Hanson, A., Carey, S., 1994. Surface-water acidification and extinction at the Cretaceous-Tertiary boundary. Geology 22, 983-986.

Dickson, A., Cohen, A., Coe, A., Davies, M., Shcherbinina, E., Gavrilov, Y., 2015. Evidence for weathering and volcanism during the PETM from Arctic Ocean and Peri-Tethys osmium isotopes records. Palaeogeography, Palaeoclimatology, Palaeoecology 438, 300-307.

Dubin, A., Peucker-Ehrenbrink, B., 2015. The importance of organic-rich shales to the geochemical cycles of rhenium and osmium. Chemical Geology 403, 111-120.

Duvivier, A., Selby, D., Sageman, B., Jarvis, I., Gröcke, D., Voigt, S., 2014. Marine $^{187}Os/^{188}Os$ isotope stratigraphy reveals the interaction of volcanism and ocean circulation during Oceanic Anoxic Event 2. Earth and Planetary Science Letters 389, 23-33.

Duvivier, A., Selby, D., Condon, D.J., Takashima, R., Nishi, H., 2015. Pacific $^{187}Os/^{188}Os$ isotope chemistry and U-Pb geochronology: Synchroneity of global Os isotope change across OAE2. Earth and Planetary Science Letters 428, 204-216.

Esser, B., Turekian, K., 1988. Accretion rate of extraterrestrial particles determined from osmium isotope systematics of Pacific Pelagic clay and manganese nodules. Geochimica et Cosmochimica Acta 52, 1383-1388.

Esser, B.K., Turekian, K., 1993. The osmium isotopic composition of the continental crust. Geochimica et Cosmochimica Acta 57, 3093-3104.

Evans, N., Chai, C., 1997. The distribution and geochemistry of platinum-group elements as event markers in the Phanerozoic. Palaeogeography, Palaeoclimatology, Paleoecology 132, 373-390.

Farley, K.A., Love, S.G., Patterson, D.B., 1997. Atmospheric entry heating and helium retentivity of interplanetary dust particles. Geochimica et Cosmochimica Acta 61, 2309-2316.

Farley, K.A., Vokrouhlicky, D., Bottke, W., Nesvorny, D., 2006. A late Miocene dust shower from the break-up of an asteroid in the main belt. Nature 439, 295-297.

Gannoun, A., Vlastelic, I., Schiano, P., 2015. Escape of unraiogenic osmium during sub-aerial lava degassing: Evidence from fumarolic deposits, Piton de la Fournaise, Reunion Island. Geochimica et Cosmochimica Acta 166, 312-326.

Georgiev, S., Stein, H., Hannah, J., Weiss, H., Bingen, B., Xu, G., Rein, E., Hatlø, V., Løseth, H., Nali, M., Piasecki, S., 2012. Chemical signals for oxidative weathering predict Re-Os isochroneity in black shales, East Greenland. Chemical Geology 324-325, 108-121.

Gradstein, F.M., Ogg, J.G., Schmitz, M., Ogg, G., 2012. The Geologic Time Scale 2012. Amsterdam, Elsevier, 1176 p.

Hamilton, N., 1990. Mesozoic magnetostratigraphy of Maud Rise, Antarctica, Proc. Ocean Drilling Program Scientific Results 113. 255-259.

Hannah, J., Stein, H., Re-Os isotope geochemistry. In: H.V.A. Melezhik et al. (eds.), *Reading the Archive of Earth's Oxygenation, Volume 3: Global Events and the Fennoscandian* 1500

Arctic Russia - Drilling Early Earth Project, Springer-Verlag Berlin Heidelberg 2013, pp 1506-1514.

Hassler, D., Peucker-Ehrenbrink, B., Ravizza, G., 2000. Rapid determination of Os isotopic composition by sparging OsO_4 into a magnetic-sector ICP-MS. Chemical Geology 166, 1-14.

Henehan, M.J., Hull, P.M., Penman, D.E., Rae, J.W.B., Schmidt, D.N., 2016 Biogeochemical significance of pelagic ecosystem function: an end-Cretaceous case study. Philosophical Transactions B, Royal Society Publishing 371: 20150510

Hicks, J., Johnson, K., Obradovich, J., Tauxe, L., Clark, D., 2002. Magnetostratigraphy and geochronology of the Hell Creek and basal Fort Union Formations of southwestern North Dakota and a recalibration of the age of the Cretaceous-Tertiary boundary. Geological Society of America Special Paper 361, 35-55.

Horan, M.F., Walker, R.J., Morgan, J.W., Grossman, J.N., Rubin, A.E., 2003. Highly siderophile elements in chondrites. Chemical Geology 196, 5–20.

Husson, D., Galbrun, B., Laskar, J., Hinnov, L., Thibault, N., Gardin, S., Locklair, R., 2011. Astronomical calibration of the Maastrichtian (Late Cretaceous). Earth and Planetary Science Letters 305, 328–340.

Jay, A.E., Mac Niocaill, C., Widdowson, M., Turner, W., 2008. New palaeomagnetic data from the Mahabaleshwar Plateau, Deccan Flood Basalt Province, India: implications for the volcanostratigraphic architecture of continental flood basalt provinces. Journal of the Geological Society of London, 166,13–24.

Jenkyns, H., 2010. Geochemistry of oceanic anoxic events. Geochemistry Geophysics Geosystems 11, Q03004.

Jerram, D., Widdowson, M., 2005. The anatomy of Continental Flood Basalt Provinces: geological constraints on the processes and products of flood volcanism. Lithos 79, 385-405.

Keller, G., Adatte, T., Gardin, S., Bartolini, A., Bajpai, S., 2008. Main Deccan volcanism phase ends near the K-T boundary: Evidence from the Krishna-Godavari Basin, SE India. Earth and Planetary Science Letters 268, 293-311.

Kerr, A.C., 1998. Oceanic plateau formation: a cause of mass extinction and black shale deposition around the Cenomanian–Turonian boundary, Journal of the Geological Society of London 155, 619–626.

Klemm, V., Levasseur, S., Frank, M., Hein, J., Halliday, A., 2005.Osmium isotope stratigraphy of a marine ferromanganese crust. Earth and Planetary Science Letters 238, 42-48.

Koeberl, C., Shirey, S., 1997. Re-Os isotope systematics as a diagnostic tool for the study of impact craters and distal ejecta, Palaeogeography, Palaeoclimatology, Paleoecology 132, 25-46.

Kucera, M., Malmgren, B.A., Sturesson, U.,1997. Foraminiferal dissolution at shallow depths of the Walvis Ridge and Rio Grande Rise during the latest Cretaceous: Inferences for deep-water circulation in the South Atlantic. Palaeogeography, Palaeoclimatology, Paleoecology 129, 195-212.

Kuiper, K. F., Deino, A., Hilgen, F. J., Krijgsman, W., Renne, P. R., Wijbrans, J. R., 2008. Synchronizing Rock Clocks of Earth History Science 320, 500-504.

Kuroda, J., Hori, R., Suzuki, K., Gröcke, D., Ohkouchi, N., 2010. Marine osmium isotope record across the Triassic-Jurassic boundary from a Pacific pelagic site. Geology 38, 1095-1098.

Kyte, F., Leinen, M., Heath, G.R., Zhou, L., 1993. Cenozoic sedimentation history of the central North Pacific: Inferences in the elemental geochemistry of core LL44-GPC3. Geochimica et Cosmochimica Acta 57, 1719-1740.

Lee, C.T., Wasserburg, G., Kyte, F. 2003. Platinum-group element (PGE) and rhenium in marine sediments across the Cretaceous-Tertiary boundary: Constraints on Re-PGE transport in the marine environment. Geochimica et Cosmochimica Acta 67, 655-670.

Levasseur, S., Birck, J-L., Allegre, C.J., 1999. The osmium riverine flux and the oceanic mass balance of osmium. Earth and Planetary Science Letters 174, 7-23.

Li, L., Keller, G., 1999. Variability in Late Cretaceous climate and deep waters: evidence from stable isotopes. Marine Geology 161, 171-190.

Luck, J.M., Turekian, K.K., 1983. Os^{187}/Os^{186} in manganese nodules and the Cretaceous-Tertiary boundary. Science 222, 613-615.

Luck, J.M., Allegre, C., 1991. Osmium isotopes in ophiolites. Earth and Planetary Science Letters 107, 406-415.

McDonough, W.F., Sun, S.S., 1995. Composition of the earth. Chemical Geology 120, 223–253.

MacLennan, J., Jones, S., 2006. Regional uplift, gas hydrate dissociation and the origins of the Paleocene-Eocene Thermal Maximum. Earth and Planetary Science Letters 245, 65-80.

McLennan S. M., Sediments and soils: chemistry and abundances. In: Rock physics and phase relations, A handbook of physical constants, AGU Reference Shelf 3, (1995), T. J. Aherns (ed.) American Geophysical Union, p. 8-19

Meisel, T, Walker, R.J., Morgan, J.W., 1996. The osmium isotopic composition of the Earth's primitive upper mantle. Nature 383, 517-520.

Michel, H., Asaro, F., Alvarez, W., Alvarez, L., 1985. Elemental profile of iridium and other elements near the Cretaceous/Tertiary boundary in Hole 577B. Initial Report, Deep Sea Drilling Project 86, 533-538.

Michel, H., Asaro, F., Alvarez, W., Alvarez, L., 1990. Geochemical studies of the Cretaceous-Tertiary boundary in ODP Holes 689B and 690C. Proceedings of the Ocean Drilling Program Scientific Results 113, 159-168.

Miller, C., Peucker-Ehrenbrink, B., Walker, B., Marcantonio, F., 2011. Re-assessing the surface cycling of molybdenum and rhenium. Geochimica et Cosmochimica Acta 75, 7146-7179.

Morgan J. W., 1986. Ultramafic xenoliths: Clues to Earth's late accretionary history. Journal of Geophysical Research 91, 12375–12387.

Nomade, S., Knight, K.B., Beutel, E., Renne, P.R., Verati, C., Féraud, G., Marzoli, A., Youbi, N., Bertrand, H., 2007. Chronology of the Central Atlantic magmatic province: Implications for the Central Atlantic rifting processes and the Triassic-Jurassic biotic crisis. Palaeogeography, Palaeoclimatology, Palaeoecology 244, 326–344.

Nordt, L., Atchley, S., Dworkin, S., 2003. Terrestrial evidence for two greenhouse events in the latest Cretaceous. GSA Today 13, Issue12: 4-9.

Olsson, R., Wright, J., Miller, K., 2001. Paleobiogeography of Pseudotextularia elegans during the latest Maastrichtian global warming event, Journal of Foraminiferal Research 31, 275-282.

Oxburgh, R., 1998. Variations in the osmium isotopic composition of sea water over the past 200,000 years. Earth and Planetary Science Letters 159, 183-191.

Oxburgh, R., Pierson-Wickmann, A.C., Reisberg, L., Hemming, S., 2007. Climate-correlated variations in seawater $^{187}Os/^{188}Os$ over the past 200,000 yr: Evidence from the Cariaco Basin, Venezuela. Earth and Planetary Science Letters 263, 246-258.

Palme, H., O'Neill, H., 2003. Cosmochemical estimates of mantle composition. In: Holland, H., Turekian, K.K., eds. *Treatise on Geochemistry, Vol. 2.* Elsevier Science, p. 1-38.

Paquay, F., Ravizza, G., Dalai, T., Peucker-Ehrenbrink, B., 2008. Determining chondritic impactor size from the marine osmium isotope record. Science 320. 214-218.

Paquay, F., Ravizza, G., 2012. Heterogeneous seawater $^{187}Os/^{188}Os$ during the Late Pleistocene glaciations. Earth and Planetary Science 349-350, 126-138.

Paquay, F., Ravizza, G., Coccioni, R., 2014. The influence of extraterrestrial material on the late Eocene marine Os isotope record. Geochimica et Cosmochimica Acta 144, 238-257.

Pegram, W., Krishnaswami, S., Ravizza, G., 1992. The record of seawater $^{187}Os/^{188}Os$ variations though the Cenozoic. Earth and Planetary Science 113, 569-576.

Pegram, W., Turekian, K., 1999. The osmium isotope composition change of Cenozoic seawater inferred from a deep-sea core corrected for meteoritic contributions. Geochimica et Cosmochimica Acta 63, 4053-4058.

Peucker-Ehrenbrink, B., Blum, J., 1998. Re-Os isotopic systematics and weathering of Precambrian crustal rocks: implications for the marine Os isotopic record. Geochimica et Cosmochimica Acta 62, 3193-3203.

Peucker-Ehrenbrink, B., Hannigan, R., 2000. Effects of black shale weathering on the mobility of rhenium and platinum group elements. Geology 28, 475-478.

Peucker-Ehrinbrink, B., Jahn, B., 1999. Platinum-group-element concentrations and osmium-isotopic ratios in loess: A proxy for the eroding upper continental crust? In: *Ninth Annual V.M. Goldschmidt Conference, LPI Contribution No. 971*, LPI, Houston, pp.224-225.

Peucker-Ehrenbrink, B., Jahn, B., 2001. Rhenium–osmium isotope systematics and platinum group element concentrations: loess and the upper continental crust. Geochemistry, Geophysics, Geosystems 2. doi:10.1029/2001GC000172.

Peucker-Ehrinbrink, B., Ravizza, G., 2000. The marine osmium isotopic record. Terra Nova 12, 205-219.

Peucker-Ehrinbrink, B., Ravizza, G., 2012. Osmium isotope stratigraphy. In Gradstein, F., Ogg, J., Schmitz, M., Ogg, G. (Eds.), *The Geologic Time Scale 2012*. (pp. 145-166). Amsterdam, Elsevier.

Peucker-Ehrenbrink, B., Ravizza, G., Hofmann, A., 1995. The marine $^{187}Os/^{186}Os$ record of the past 80 million years. Earth and Planetary Science Letters 130, 155-167.

Premoli Silva, I., Sliter, W., 1995. Cretaceous planktonic foraminiferal biostratigraphy and evolutionary trends from the Bottaccione section, Gubbio, Italy. Palaeontographia Italica 82, 1-89.

Ravizza, G., 1993. Variations of the $^{187}Os/^{188}Os$ ratio of seawater over the past 28 millions years as inferred from metalliferous carbonates. Earth and Planetary Science Letters 118, 335-348.

Ravizza, G., Pyle, D., 1997. PGE and Os isotopic analyses of single sample aliquots with NiS fire assay preconcentration. Chemical Geology 141, 251-268.

Ravizza G., 2001. The distribution of the platinum group elements and their isotopes. In: The Encyclopedia of Ocean Sciences. Academic Press p. 2208-2217.

Ravizza, G., Norris, R., Blusztajn, J., 2001. An osmium isotope excursion associated with the late Paleocene thermal maximum: Evidence of intensified chemical weathering. Paleoceanography 16, 155-163.

Ravizza, G., Peucker-Ehrenbrink, B., 2003. Chemostratigraphic evidence of Deccan volcanism from the marine osmium isotope record. Science 302, 1392-1395.

Ravizza, G., 2007. Reconstructing the marine $^{187}Os/^{188}Os$ record and the particulate flux of meteoritic osmium during the late Cretaceous from ODP 886C. Geochimica et Cosmochimica Acta 71, 1355-1369.

Ravizza, G., Paquay, F., 2008. Osmium isotope chemostratigraphy applied to organic-rich marine sediments from the Eocene-Oligocene transition on the West African margin (ODP Site 959). Paleoceanography 23, doi:10.1029/2007PA001460.

Ravizza, G., Vonderhaar, D., 2012. A geochemical clock in earliest Paleogene pelagic carbonates based on the impact-induced Os isotope excursion at the Cretaceous-Paleogene boundary. Paleoceanography 27, PA3219.

Renne, P., Deino, A., Hilgen, F., Kuiper, K., Mark, D., Mitchell, W., Morgan, L., Mundil, R., Smit, J., 2013. Time scales of critical events around the Cretaceous-Paleogene boundary. Science 339, 684-687.

Renne, P., Sprain, C., Richards, M., Self, S., Vanderkluysen, L., Pande, K., 2015. State shift in Deccan volcanism at the Cretaceous-Paleogene boundary, possibly induced by impact. Science 350, 76-78.

Reusch, D., Ravizza, G., Maasch, K., Wright, J., 1998. Miocene seawater $^{187}Os/^{188}Os$ ratios inferred from metalliferous carbonates. Earth and Planetary Science Letters 160, 163-178.

Robinson, N., Ravizza, G., Coccioni, R., Peucker-Ehrenbrink, B., Norris, R., 2009. A high-resolution marine $^{187}Os/^{188}Os$ record for the late Maastrichtian: Distinguishing the chemical fingerprints of Deccan volcanism and the KP impact event. Earth and Planetary Science Letters 281, 159-168.

Rocchia, R., Boclet, D., Bonte, P., Jehanno, C., Chen, Y., Courtillot, V., Mary, C., Wezel, F., 1990. The Cretaceous-Tertiary boundary at Gubbio revisited: vertical extent of the Ir anomaly. Earth and Planetary Science Letters 99, 206-219.

Roy-Barnum, M., Wasserburg, G., Papanastassiou, D., Chaussidon, M., 1998. Osmium isotopic compositions and Re-Os concentrations in sulfide globules from basaltic glasses. Earth and Planetary Science Letters 154, 331-347.

Schoene, B., Samperton, M., Eddy, M., Keller, G., Adatte, T., Bowring, S., Khadri, S., Gertsch, B., 2015. U-Pb geochronology of the Deccan Traps and relation to the end-Cretaceous mass extinction. Science 347, 182-184.

Selby, D., Creaser, R., Stein, H., Markey, R., Hannah, J., 2007. Assessment of the ^{187}Re decay constant by cross calibration of Re-Os molybdenite and U-Pb zircon chronometers in magmatic ore systems. Geochimica et Cosmochimica Acta 71, 1999-2013.

Self, S., Widdowson, M., Thordarson, T., Jay, A., 2006. Volatile fluxes during flood basalt eruptions and potential effects on the global environment. Earth and Planetary Science Letters 248, 518-532.

Self, S., Blake, S., Sharma, K., Widdowson, M., Sephton, S., 2008. Sulfur and chlorine in late Cretaceous Deccan magmas and eruptive gas release. Science 319, 1654-1657.

Sharma, M., Rosenberg, E., Butterfield, D., 2007. Search for the proverbial mantle osmium sources to the oceans: Hydrothermal alteration of mid-ocean ridge basalt. Geochimica et Cosmochimica Acta 71, 4655-4667.

Sharma, M., 2011. Applications of osmium and iridium as biogeochemical tracers in the environment. In: Baskaran, M. editor. *Handbook of environmental isotope geochemistry*. Berlin Heidelberg: Springer-Verlag p. 205-227.

Shirey, S., Walker, R., 1998. The Re-Os isotopic system in cosmochemistry and high-temperature geochemistry. Annual Review of Earth and Planetary Sciences 26, 423-500.

Sinton, C.W., Duncan, R.A., 1997. Potential links between ocean plateau volcanism and global ocean anoxia at the Cenomanian-Turonian boundary. Economic Geology and the Bulletin of the Society of Economic Geologists 92, 836–842.

Snow, L., Duncan, R., 2005. Trace element abundances in the Rock Canyon Anticline, Pueblo Colorado, marine sedimentary section and their relationship to Caribbean plateau construction and oxygen anoxic event 2. Paleoceanography 20, PA2005.

Sohsuke, O., Sujita, S., 2006. Rapid fall of the K/T sulfuric acid aerosols and oceanic pH reduction. 37th Lunar and planetary science conference, LPI, Houston, TX.

Sprain, C.J., Renne, P.R., Wilson, G.P., Clemens, W.A., 2015. High-resolution chronostratigraphy of the terrestrial Cretaceous-Paleogene transition and recovery interval in the Hell Creek region, Montana. Geological Society of America Bulletin 127, 393–409.

Stanley, S., Luczaj, J. *Earth System History* (W.H. Freeman, New York, ed. 4, 2015), pp.174.

Storey, M., Duncan, R., Tegner, C., 2007. Timing and duration of volcanism in the North Atlantic Igneous Province: Implications for geodynamics and links to the Iceland hotspot. Chemical Geology 241, 264-281.

Storey, M., Duncan, R., Swisher, C., 2007. Paleocene-Eocene Thermal Maximum and the opening of the Northeast Atlantic. Science 316, 587-589.

Stott, L.D., Kennett, J.P., 1990. The paleoceanographic and paleoclimatic signature of the Cretaceous/Paleogene boundary in the Antarctic: Stable isotopic results from ODP Leg 113. Proceeding of the Ocean Drilling Program Scientific Results 113, 829-848.

Tejada, M., Suzuki, K., Sakamoto, T., Coccioni, R., Kuroda, J., Tatsumi, Y., Mahoney, J.J., 2006. Ontong Java plateau and OAE1: Is there really a link? Geochimica et Cosmochimica Acta 70, A642.

Tejada, M., Suzuki, K., Kuroda, J., Coccioni, R., Mahoney, J., Ohkouchi, N., Sakamoto, T., Tatsumi, Y., 2009. Ontong Java Plateau eruption as a trigger for the early Aptian oceanic anoxic event. Geology 37, 855-858.

Tejada, M., Ravizza, G., Suzuki, K., Paquay, F., 2012. An extraterrestrial trigger for the early Cretaceous massive volcanism? Evidence from the paleo-Tethys Ocean. Scientific Reports 2, 268.

Thibault, N., Gardin, S., 2007. The late Maastrichtian nannofossil record of climate change in the South Atlantic DSDP Hole 525A. Marine Micropaleontology 65, 163-184.

Thibault, N., Husson, D., 2016. Climatic fluctuations and sea-surface water circulation patterns at the end of the Cretaceous era: Calcareous nannofossil evidence. Palaeogeography, Palaeoclimatology, Paleoecology 441, 152-164.

Turgeon, S.C, Creaser, R.A., 2008. Cretaceous anoxic event 2 triggered by a massive magmatic episode. Nature 454, 323-326.

Widdowson, M., Kelley, S., (2008). Dating the Deccan: Determining the Timing and Duration of the Indian KTB-Spanning CFB Eruptions. (Abs.) American Geophysical Union Fall Meeting, V23H-04.

Wilf, P., Johnson, K., Huber, B., 2003. Correlated terrestrial and marine evidence for global climate change before mass extinction at the Cretaceous-Paleogene boundary. Proceedings of the National Academy of Science 100, 599-604.

Wimpenny, J., Gannoun, A., Burton, K., Widdowson, M., James, R., Gislason, S., 2007. Rhenium and osmium isotope and elemental behaviours accompanying laterite formation the Deccan region of India. Earth and Planetary Science Letters 261, 239-258.

Yamashita, Y., Takahashi, Y., Haba, H., Enomoto, S., Shizuma, H., 2007. Comparison of reductive accumulation of Re and Os in seawater-sediment systems. Geochimica et Cosmochimica Acta 71, 3458-3475.

Zachos, J.C., Arthur, M.A., Thunell, R.C., Williams, D.F., Tappa, E.J., 1985. Stable isotope and trace element geochemistry of carbonate sediments across the Cretaceous-Tertiary boundary at Deep Sea Drilling Project Hole 577, Leg 86. Initial Report. DSDP 86, 513-532.

Zachos, J.C., Röhl, U., Schellenberg, S.A., Sluijs, A., Hodell, D.A., Kelly, D.C., Thomas, E., Nicolo, M., Raffi, I., Lourens, L.J., McCarren, H., Kroon, D., 2005. Rapid acidification of the ocean during the Paleocene–Eocene Thermal Maximum. Science 308, 1611-1616.

Zeebe, R., Zachos, J.C., 2007. Reversed deep-sea carbonate ion basin-gradient during Paleeocene-Eocene Thermal Maximum. Paleoceanography 22, PA3201, doi:10.1029/ 2006PA001395.

Zoller, W., Parrington, J., Kotra, J., Phelan, M., 1993. Iridium enrichment in airborne particles from Kilauea Volcano. Science 222, 1118-1121.